Chem Soc Rev

Chemical Society Reviews

rsc.li/chem-soc-rev

ROYAL SOCIETY
OF **CHEMISTRY**

REVIEW ARTICLE
Dong Ha Kim, Yijiang Liu, Zhiqun Lin *et al.*
Zn-based batteries for sustainable energy storage:
strategies and mechanisms

Check for updates

Zn-based batteries for sustainable energy storage: strategies and mechanisms

Lei Tang,†[a] Haojia Peng,†[a] Jiarui Kang,[a] Han Chen,[a] Mingyue Zhang,[a] Yan Liu,[c] Dong Ha Kim, ✉*[b] Yijiang Liu*[d] and Zhiqun Lin ✉*[ab]

Batteries play a pivotal role in various electrochemical energy storage systems, functioning as essential components to enhance energy utilization efficiency and expedite the realization of energy and environmental sustainability. Zn-based batteries have attracted increasing attention as a promising alternative to lithium-ion batteries owing to their cost effectiveness, enhanced intrinsic safety, and favorable electrochemical performance. In this context, substantial endeavors have been dedicated to crafting and advancing high-performance Zn-based batteries. However, some challenges, including limited discharging capacity, low operating voltage, low energy density, short cycle life, and complicated energy storage mechanism, need to be addressed in order to render large-scale practical applications. In this review, we comprehensively present recent advances in designing high-performance Zn-based batteries and in elucidating energy storage mechanisms. First, various redox mechanisms in Zn-based batteries are systematically summarized, including insertion-type, conversion-type, coordination-type, and catalysis-type mechanisms. Subsequently, the design strategies aiming at enhancing the electrochemical performance of Zn-based batteries are underscored, focusing on several aspects, including output voltage, capacity, energy density, and cycle life. Finally, challenges and future prospects of Zn-based batteries are discussed.

1. Introduction

The increasing use of fossil fuels and growing environmental concerns have placed a great demand for efficient and sustainable energy storage systems capable of harnessing energy from renewable and clean sources such as wind, solar, and tidal power.[1-9] This surge in demand has played a major role in driving the widespread adoption of electrification and rechargeable batteries. Lithium-ion batteries have prominently featured in various secondary battery applications across industries, including communication (mobile phones), portable electronic devices (smartwatches), and transportation (automotive vehicles), owing to their high energy density, well-established manufacturing technology, and low weight.[10-15] Between 2020 and 2021, the

[a] *Department of Chemical and Biomolecular Engineering, National University of Singapore, 4 Engineering Drive 4, Singapore, 117585, Singapore. E-mail: z.lin@nus.edu.sg*

[b] *Department of Chemistry and Nano Science, Ewha Womans University, 52 Ewhayeodae-gil, Seodaemun-gu, Seoul 03760, Republic of Korea. E-mail: dhkim@ewha.ac.kr*

[c] *Institute of Sustainability for Chemicals, Energy and Environment (ISCE²), Agency for Science, Technology and Research (A*STAR), 1 Pesek Road, Jurong Island, Singapore 627833, Republic of Singapore*

[d] *College of Chemistry, Key Lab of Environment-Friendly Chemistry and Application in Ministry of Education, Xiangtan University, Xiangtan 411105, Hunan Province, P. R. China. E-mail: liuyijiang84@xtu.edu.cn*

† L Tang and H Peng contributed equally.

worldwide demand for batteries amounted to approximately 960 GW h, with battery production reaching a range of 7 to 10 million tons (Fig. 1a).[16] The anticipated growth in market demand over the upcoming years will continue to hinge on batteries, with projections indicating a surpassing of 3200 GW h by 2030 (Fig. 1a). The escalating demand cannot be solely addressed by Li-ion batteries, given the projected depletion of the world's lithium resources within the span of a century. The diminishing availability of economically extractable lithium reserves has prompted increasing concerns regarding global energy security, emphasizing the critical urgency for battery technologies rooted in abundant earth metals. Furthermore, the utilization of Li-ion batteries for large-scale energy storages faces impediments due to their elevated costs, as well as apprehensions related to safety and environmental considerations.[17] Therefore, the urgency to explore alternative battery systems beyond lithium-ion batteries is paramount in order to effectively meet the rising requirements for affordable, safe, and high-performance energy storage systems.

Battery chemistries employing abundant elements like sodium, potassium, zinc, magnesium, aluminum, and calcium as the anode have attracted considerable attention as alternative options.[18-31] Within the realm of "beyond Li-ion" battery technologies, rechargeable Zn-based batteries show considerable promise for large-scale energy storage applications due to distinct advantages associated with metallic zinc. These advantages encompass a high theoretical capacity (820 mA h g⁻¹ or 5854 mA h cm⁻³) as illustrated in Fig. 1b,

This journal is © The Royal Society of Chemistry 2024

Chem. Soc. Rev., 2024, **53**, 4877–4925 | **4877**

a lower cost of zinc ($\sim$US\$2 kg^{-1}) compared to alkali metals (*e.g.*, lithium $\sim$US\$19 kg^{-1}; potassium $\sim$US\$13 kg^{-1}; sodium $\sim$US\$3 kg^{-1}), stability and reversibility in aqueous electrolytes, non-toxicity, and ease of material processing and battery fabrication.[32–36] In addition, the low anodic potential (-0.763 V *vs.* standard hydrogen electrode) and the two-electron transfer during
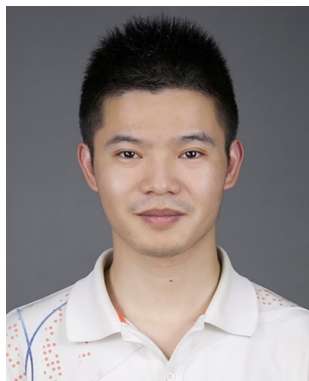
Lei Tang

Lei Tang received his bachelor's degree in Bioengineering from Sichuan University in 2014, and his master's degree in Chemical Engineering and Technology from Tianjin University in 2017. He received his PhD in Physical Chemistry from the University of Chinese Academy of Sciences in 2022, under the supervision of Prof. Dehui Deng. He is currently a postdoctoral research associate in the Department of Chemical and Biomolecular Engineering at National University of Singapore under the supervision of Prof. Zhiqun Lin. His current research focuses on energy electrocatalysis and Zn-based batteries.

Haojia Peng

Haojia Peng received his BS degree in Material Science and Engineering from Beijing Institute of Technology in 2023. He is currently working toward his master's degree in Energy Systems in the Department of Chemical and Biomolecular Engineering at National University of Singapore. His research interests include electrocatalysis for alkaline HER and cathode materials for lithium-ion batteries.

Jiarui Kang

Jiarui Kang is a PhD student in the Department of Chemical and Biomolecular Engineering at National University of Singapore. She conducts her research under the mentorship of Professor Zhiqun Lin. Her scholarly pursuits are twofold: one project focuses on the development of polymer hydrogel electrolytes, while the other examines the anode interface in zinc-ion batteries. Each project aims to expand the frontiers of knowledge in energy storage technology.

Han Chen

Han Chen is currently a PhD student in the Department of Chemical and Biomolecular Engineering at National University of Singapore. His research mainly focuses on the rational design of advanced electrolytes for high energy density lithium–metal batteries.

Mingyue Zhang

Mingyue Zhang received his BS, master's, and PhD degrees in Materials Science and Engineering from the Pennsylvania State University, University of Pennsylvania, and Georgia Institute of Technology in 2016, 2018, and 2022 respectively. He is now a research fellow in the Department of Chemical and Biomolecular Engineering at National University of Singapore. His research interests include non-linear polymers, chiral polymers, functional nanocrystals, self-assembly, and nanotechnologies for energy related applications.

Yan Liu

Dr Yan Liu is a principal scientist at the Institute of Sustainability for Chemicals, Energy and Environment (ISCE^2), Agency for Science, Technology and Research (A*STAR), Singapore. Her research interests include the development of multifunctional materials for thermal catalysis, electrocatalysis, and sonocatalysis for CO$_2$ utilization and green hydrogen production.

4878 | *Chem. Soc. Rev.*, 2024, **53**, 4877–4925

This journal is © The Royal Society of Chemistry 2024

the battery operation contribute to elevated energy densities.[37–43] Additional benefits of Zn-based batteries include the affordability, safety, and high ionic conductivity (up to 1 S cm^{-1}) of commonly used aqueous electrolytes, in contrast to flammable organic electrolytes employed in lithium-ion batteries ($\sim$1–10 mS cm^{-1}).[37,44–48] The projected cost of a Zn-based battery utilizing a Zn anode and a MnO$_2$ cathode is anticipated to be less than \$100 per kW h, representing approximately half the cost of contemporary lithium-ion batteries ($\sim$\$200 per kW h) (Fig. 1c).[49] Notably, the anticipated cost of Zn–air batteries, estimated at approximately \$100 per kW h and possessing significantly higher energy density than Li-ion batteries, is markedly lower than that of Li-ion batteries. Given these advantageous attributes (Fig. 1d), Zn-based batteries demonstrate significant potential for practical applications.

Historically, metal zinc served as the initial anode material for batteries, specifically in the Volta Pile, dating back to 1799.[50] Currently, zinc finds extensive application in diverse battery technologies, including the Zn-ion battery, Zn–air battery, Zn–CO$_2$ battery, Zn-based flow battery, and Zn-based flexible battery. Compared to Li-based batteries, Zn-based batteries have distinct advantages in price and safety, yet their performance needs to be further improved to ensure large-scale practical applications (Fig. 1d).[21,51–59] For battery performance, energy density and cycle life are the two most important evaluation indicators. Essentially, energy density is derived from the product of a battery's specific capacity and voltage (energy density = capacity $\times$ voltage).[60] Consequently, four primary design strategies are employed to attain high-performance Zn-based batteries, focusing on advancements in high capacity, increased voltage, enhanced energy density, and prolonged cycle life. Design strategies for achieving high capacity in Zn-based batteries center primarily on cathode materials and electrodes,[61–63] and the design strategies for enhancing voltage in Zn-based batteries primarily involve the optimization of the electrolyte to facilitate high-potential reactions.[57,64,65] Particularly, exploring innovative battery configurations and optimizing the energy storage mechanism stand out as crucial strategies for achieving high energy density in Zn-based batteries.[66–69] In addition, the design strategies for long-cycle-life Zn-based batteries focus mainly on the Zn anode and its interface with the electrolyte.[70–78] Influenced by these strategies, Zn-based batteries have achieved notable advancements, wherein the metrics of output voltage, capacity, and energy density attain levels of 2.92 V, 2000 mA h g^{-1}, and 2372 W h kg^{-1}, respectively (as determined by the mass of active materials), as depicted in Table 1. Simultaneously, Zn-based batteries display a prolonged cycle life, surpassing 1000 hours.

For Zn-based batteries, beyond the pursuit of high-performance batteries, understanding energy storage mechanisms and exploring new reaction mechanisms have also emerged as the key research areas.[52,79–83] The reaction mechanism of Zn-based batteries diverges from the established energy storage chemistry reliant on Li/Na ions (including intercalation, conversion, and alloying reactions), remaining enigmatic and subject to frequent
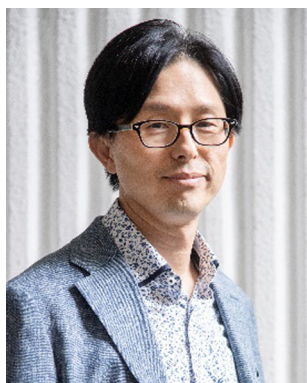
Dong Ha Kim

Dr Dong Ha Kim is a professor of the Department of Chemistry and Nanoscience at Ewha Womans University. He received his PhD degree from the Department of Fiber and Polymer Science of Seoul National University (2000). He conducted postdoctoral research at the University of Massachusetts at Amherst and the Max Planck Institute for Polymer Research. In 2006, he joined the faculty of the Division of Nanoscience at Ewha Womans University. His research focuses on the development of hybrid nanostructures for energy, catalysis, memory, display, and theragnosis. Currently, he is a Fellow of Royal Society of Chemistry and Associate Editor of Nanoscale.

Yijiang Liu

Dr Yijiang Liu is a professor in the College of Chemistry at Xiangtan University, China. She received her MS degree from Xiangtan University in 2009 and PhD from the Institute of Chemistry, Chinese Academy of Sciences, in 2015. She was a visiting scholar at Georgia Institute of Technology during 2017–2018. Her research work focuses on the design and preparation of advanced functional materials: porous carbon materials for efficient and durable electrocatalysts in energy conversion and storage devices; the crafting of highly stable perovskite nanocrystals by using functional polymers as nanoreactors; and Janus materials for concurrent catalysis and emulsification.

Zhiqun Lin
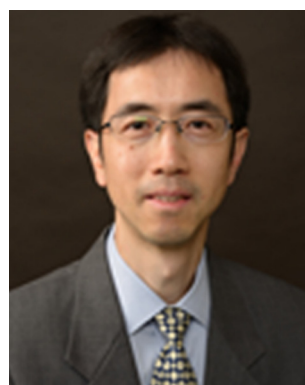
Dr Zhiqun Lin is a Professor in the Department of Chemical and Biomolecular Engineering at the National University of Singapore. His research interests include electrocatalysis, batteries, solar energy conversion, photocatalysis, semiconductor organic–inorganic nanocomposites, multifunctional nanocrystals, conjugated polymers, block copolymers, hierarchical structure formation and assembly, and surface and interfacial properties.
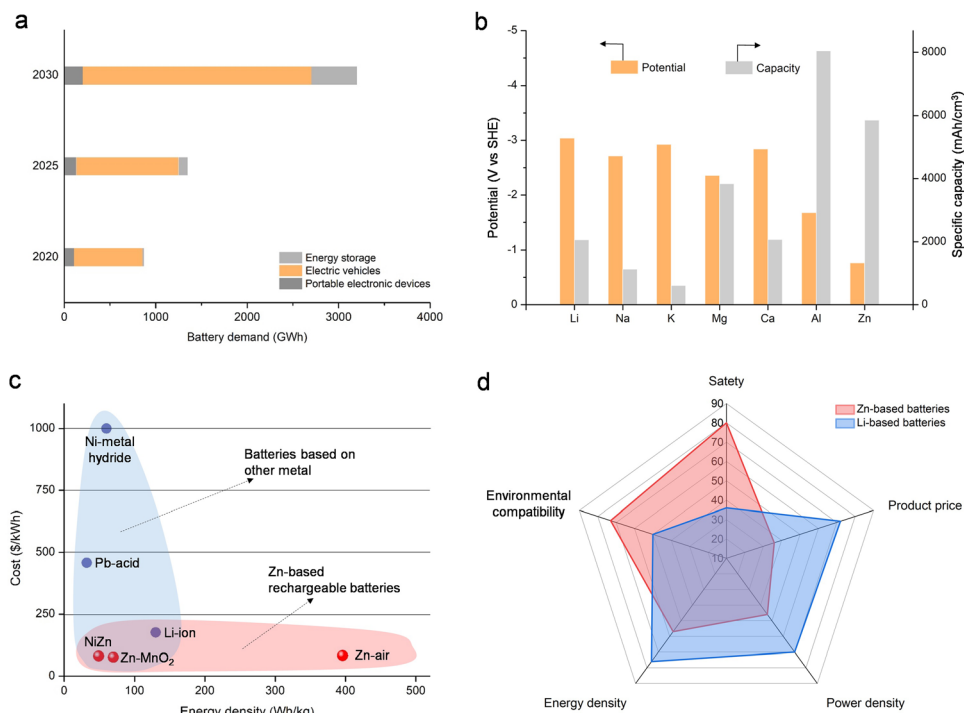
This journal is © The Royal Society of Chemistry 2024

Chem. Soc. Rev., 2024, **53**, 4877–4925 | **4879**

Fig. 1 Motivation to study Zn-based batteries. (a) Projected battery demand (GW h) for portable electronic devices, electric vehicles, and energy storage systems spanning the period 2020 to 2030. (b) Redox potential and specific capacity of various metals. (c) Energy density and price of various batteries. (d) Comparison of Zn-based batteries and Li-based batteries from multiple metrics.

debate. Using the Zn–MnO$_2$ battery as an example, three distinct energy storage mechanisms have been proposed, encompassing (1) Zn^{2+} insertion/extraction reaction, (2) H$^+$/Zn^{2+} co-insertion reaction, and (3) conversion reaction. To deepen our comprehension of the reaction mechanism in Zn-based batteries and advance the design of higher-performance counterparts, ongoing efforts involve the use of diverse electrochemical methods, advanced characterization techniques (both *in situ* and *ex situ*), and theoretical calculations. Since battery performance is affected by multiple factors such as the electrolyte, electrodes, and the energy storage mechanism, more efforts are required to reveal the reaction mechanism underlying the overall battery device.

This review surveys the latest efforts in designing high-performance Zn-based batteries and elucidating energy storage mechanisms (Fig. 2). We will discuss the four types of redox mechanisms (*i.e.*, insertion-type, conversion-type, coordination-type and catalysis-type mechanisms), highlight the design strategies employed in enhancing the performance of Zn-based batteries while concurrently presenting challenges encountered and providing insights into the future outlook of these batteries. It is imperative to acknowledge that the references discussed in this review are not meant to be exhaustive; instead, they serve as initial literature for more in-depth studies. Additionally, this review leverages valuable insights from numerous outstanding reviews on the Zn-ion battery, Zn–air battery, and flexible battery, enhancing our understanding of reaction mechanisms and design strategies for high-performance Zn-based batteries.[45,84–99] Furthermore, our discussion extends beyond the scope of Zn-based batteries, as the strategies and mechanisms delineated herein are applicable to a wider array of battery systems.

2. Mechanisms of Zn-based batteries

The energy storage mechanism of Zn-based batteries is presently in its nascent research phase, contributing to controversy and misunderstanding in comprehending the reaction process and mechanism. In addition, the intricate nature of battery devices adds complexity to the exploration and comprehension of the reaction mechanism in Zn-based batteries. Various configurations of Zn-based battery devices share a common structure, predominantly featuring Zn anode, electrolyte, and cathode. Irrespective of their classification, the anodes in all Zn-based batteries function based on the Zn^{2+}/Zn redox couple. Nevertheless, diverse electrochemistry can be achieved on the cathode side owing to variations in electrolyte and cathode materials. Therefore, in this review, we mainly discuss various redox mechanisms on the cathode side. In this section, four types of redox mechanisms based on the different electrochemical behaviors of the cathode will be introduced: (1) insertion-type mechanisms, (2) conversion-type mechanisms, (3) coordination-type mechanisms, and (4) catalysis-type mechanisms. Among the four reaction mechanisms, the insertion-type mechanism is predominantly observed in Zn-ion batteries featuring inorganic materials (such as Mn-based oxide or V-based oxide) as the

4880 | *Chem. Soc. Rev.*, 2024, **53**, 4877–4925

This journal is © The Royal Society of Chemistry 2024

Table 1 Summary of high performance and mechanism in diverse Zn-based batteries

Types of Zn-based batteries	Cathode material	Electrolyte	Capacity (mA h g^{-1})/ working voltage (V)	Energy density (W h kg^{-1})/cycle life (h or cycles)	Mechanism	Ref.
Zn-ion battery	V_6O_{13}/carbon cloth	3 M $ZnSO_4$	520/0.98	511/1000 cycles	Insertion-type mechanisms	191
	MnVO	3 M $Zn(CF_3SO_3)_2$	610.2/0.77	469/4000 cycles		192
	La–Ca co-doped MnO_2	1 M $ZnSO_4$ + 0.4 M $MnSO_4$	297/1.35	401/200 cycles		215
	MnO_2	1 M $(NH_4)_2SO_4$ + 0.1 M $MnSO_4$	365/1.35	493/4000 cycles		234
	$CoFe(CN)_6$	4 M $Zn(CF_3SO_3)_2$	173.4/1.75	303/2200 cycles		66
	$LiVPO_4F$	21 M LiTFSI + 2 M $Zn(OTf)_2$	140/1.65	230/600 cycles		242
	$Co_{0.247}V_2O_5$	20 M LiTFSI + 1 M Zn (TFSI)$_2$	432/1.15	497/7500 cycles		67
	α-MnO_2	1 M $Al(CF_3SO_3)_3$ + 1 M $Zn(CF_3SO_3)_2$	265/1.5	395/1000 cycles		245
	CuHCF	WIG-NaCl/ZnSO$_4$/SA	260/1.7	440/450 cycles		116
	S@C	Gelatin/CuSO$_4$//gelatin/ZnSO$_4$	2063/1.15	2372/100 cycles	Conversion-type mechanisms	204
	S/KB	0.5 M CuSO$_4$//0.5 M Na$_2$SO$_4$//0.5 M ZnSO$_4$	2000/1.15	2300/100 cycles		201
	S@CNTs-50	1 M $Zn(CH_3COO)_2$ + 0.05 wt% I_2	1105/0.455	502/50 cycles		203
	PbO_2	4 M H_2SO_4 + 0.5 M K_2SO_4//6 M KOH + 0.8 M $Zn(CH_3COO)_2$	86/2.92	252.4/250 cycles		64
	SeS$_{5.76}$@3D-NPCF	3 M $ZnSO_4$ + 0.1 wt% I_2	1222/0.71	867.6/500 cycles		205
	Se/CMK-3	2 M ZnTFSI/PEG/water	611/1.01	751/500 cycles		206
	PAC/I$_2$	$ZnCl_2$ + LiCl + CH_3CN	594/1.26	750/6000 cycles		236
	Co_3O_4	2 M $ZnSO_4$ + 0.2 M $CoSO_4$	200/1.8	361/5000 cycles		241
	MnO_2	1 M $MnSO_4$ + 1 M $ZnSO_4$ + 0.1 M H_2SO_4	570/1.95	1100/1800 cycles		246
	MnO_2	0.5 M Mn(Ac)$_2$ + 0.5 M Zn(Ac)$_2$ + 2 M KCl	616/1.58	973/400 cycles		253
	BQ-NCC	3 M $ZnSO_4$	489/1.1	538/500 cycles	Coordination-type mechanisms	233
	C4Q	3 M $Zn(CF_3SO_3)_2$	335/1	335/1000 cycles		147
	HAQ-COF	2 M $ZnSO_4$	344/0.84	289/10 000 cycles		199
Zn–air battery	F–Ni$_{27}$Fe$_{10}$-LDH(charge cathode)//FeNC (discharge cathode)	6 M KOH + 0.2 M Zn(Ac)$_2$	786.6/1.2	959.6/5220 h	Catalysis-type mechanisms	456
	HESA	6 M KOH + 0.2 M Zn(Ac)$_2$	779/0.96	748/200 h		411
	NPMC foam	6 M KOH	735/1.14	835/240 h		386
	XC72R	1 M $Zn(OTf)_2$	684/1	684/1600 h		502
	Pt/C + Co_3O_4	Gel electrolyte	742/1.3	964/200 h		513
	Pt/C + IrO_2	ZnSO$_4$ + LiTFSI//H$_2$SO$_4$ + LiTFSI	802.3/1.5	1243.6/2000 h		481
	Fe$_3$C-NG/Ni foam	6 M KOH + 0.2 M Zn(Ac)$_2$	810/0.87	706.4/1000 h		492
	NiCo$_2$S$_4$/N-CNT	6 M KOH + 0.2 $ZnCl_2$	431.1/1.29	554.6/150 cycles		504
Zn–CO$_2$ battery	CHF	The ionic liquid	340/0.85	288.3/192 h		518
Zn–C$_2$H$_2$ battery	Cu dendrites	1 M KOH	786/0.27	213.8/40 h		521
Zn–NO$_2^-$ battery	C/Co$_3$O$_4$	1 M KOH//0.5 M K$_2$SO$_4$ + 50 mM NO$_2^-$	764.3/0.67	512.1/24 h		519

Fig. 2 Overview of energy storage mechanisms and design strategies employed in Zn-based battery systems.

cathode electrode, while the conversion-type mechanism is primarily evident in Zn-ion batteries and Zn-based redox flow batteries. In particular, the coordination-type mechanism mainly appears in Zn-ion batteries with organic materials as the cathode electrode (Zn–organic batteries). In addition, the catalysis-type mechanism is predominantly present in Zn-based batteries wherein the cathode relies on a catalyst to facilitate redox reactions, exemplified by Zn–air batteries and Zn–CO$_2$ batteries.

2.1. Insertion-type mechanisms

2.1.1. Zn^{2+} insertion–extraction mechanism. Zinc ions possess an ionic radius (0.074 nm) comparable to that of lithium ions (0.076 nm).[81,100] Simultaneously, the hydrated zinc ions exhibit an ionic radius size (0.412–0.430 nm) close to that of hydrated lithium ions (0.340–0.382 nm), facilitating the insertion and extraction process of Zn^{2+} ions in the crystal structure of the cathode material. Given that the insertion-type mechanism is predominantly observed in Zn-ion batteries employing inorganic materials as the cathode, Zn-ion batteries are employed as exemplars to elucidate the mechanism of insertion and extraction of zinc ions. Cathode materials typically involve the use of metal oxides or other compounds distinguished by layered structures or tunnel-type configurations.[101,102] These structural features are essential, ensuring reversible insertion and extraction of Zn^{2+} ions within the crystal lattice of the cathode material. In recent years, considerable endeavors have been directed toward this domain. For example, Kim *et al.* employed various *in situ* characterization techniques, such as *in situ* X-ray diffraction (XRD) and *in situ* X-ray near-edge absorption spectrum, to clarify the insertion/extraction mechanism of zinc ions in tunnel-type γ-MnO$_2$ cathode materials.[103] Fig. 3 illustrates the complete

This journal is © The Royal Society of Chemistry 2024

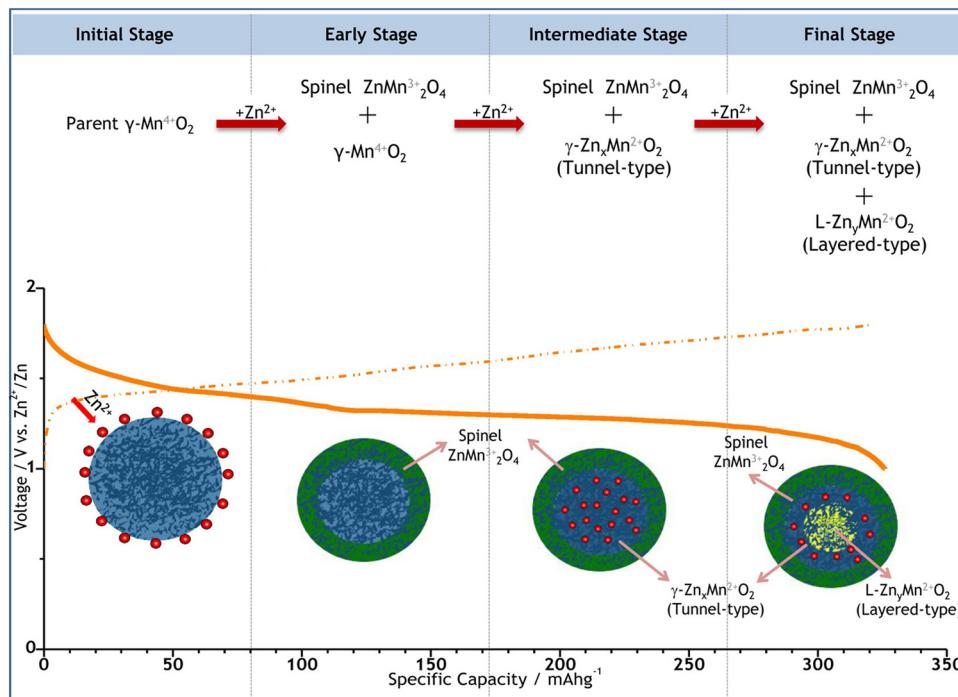*Chem. Soc. Rev.*, 2024, **53**, 4877–4925 | **4881**

Fig. 3 Schematic depiction of the electrochemically induced multi-step phase transition and the corresponding Zn^{2+} insertion process in the γ-MnO_2 cathode. Reproduced with permission from ref. 103. Copyright 2015 American Chemical Society.

insertion process of Zn ions in γ-MnO_2, corresponding to the discharge process. During the initial discharge state, a segment of γ-MnO_2 undergoes structural transformation into $ZnMn_2O_4$ with spinel type phase, leading to the conversion of Mn^{4+} to Mn^{3+}. Upon further discharge, zinc ions are progressively inserted into the tunnels of γ-MnO_2, resulting in the gradual formation of a new γ-Zn_xMnO_2 (Mn^{2+}) with a tunnel structure. Subsequently, with an increasing influx of zinc ions into the tunnel structure of γ-Zn_xMnO_2, certain fully occupied tunnels undergo expansion and collapse, giving rise to a layered structure of L-Zn_yMnO_2 (Mn^{2+}). In the fully discharged state, three discharge products with distinct crystal structures and varying Mn valence states coexist. Following the charging process, the structure of the product obtained during discharge can be restored to the initial γ-MnO_2 structure, signifying a reversible insertion/extraction mechanism.

Apart from the aforementioned Mn-based active materials, the exploration of electroactive cathode host materials for reversible zinc ion insertion/extraction has extended to include other substances with layered or tunnel-type structures, such as V-based oxides.[84,88,104–107] Illustratively, Mai *et al.* employed layered $Na_{0.33}V_2O_5$ nanowires as cathode materials for Zn-ion batteries, utilizing X-ray photoelectron spectroscopy (XPS), XRD, scanning electron microscopy (SEM), and transmission electron microscopy (TEM), to unveil the reversible insertion/extraction mechanism of zinc ions in cathode materials.[108] The schematic diagram in Fig. 4 depicts the complete charge and discharge process. During discharge, a segment of the $Na_{0.33}V_2O_5$ nanowire undergoes a phase change, transforming into a novel $Zn_xNa_{0.33}V_2O_5$ phase. This structural transformation is due to the crystal distortion caused by the insertion of Zn^{2+}. In contrast, during

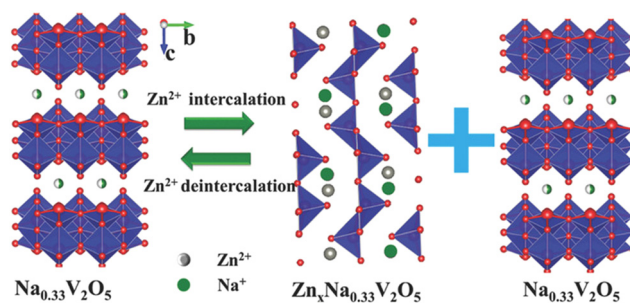**Fig. 4** Schematic depiction of the Zn^{2+} insertion mechanism in the $Na_{0.33}V_2O_5$ cathode. Reproduced with permission from ref. 108. Copyright 2018 John Wiley & Sons.

the charging phase, the new phase formed during the discharge process gradually dissipates owing to the progressive deintercalation of Zn^{2+}, underscoring the high reversibility of the phase change and structural alteration in $Na_{0.33}V_2O_5$.

2.1.2. Co-insertion mechanism. Beyond the reversible insertion and extraction mechanism observed for individual zinc ions, recent electrochemical analyses and structural characterization have substantiated the existence of a concurrent co-insertion mechanism involving zinc ions alongside either H^+ ions or H_2O molecules within the cathode host material.[109,110] Illustratively, Wang and collaborators validated the MnO_2 cathode's sequential co-insertion/extraction processes involving H^+ and Zn^{2+}, demonstrating notable reversibility and cycling stability.[111] Following a comprehensive characterization regimen involving the discharge galvanostatic intermittent titration technique (GITT), impedance spectroscopy, and XRD testing, the
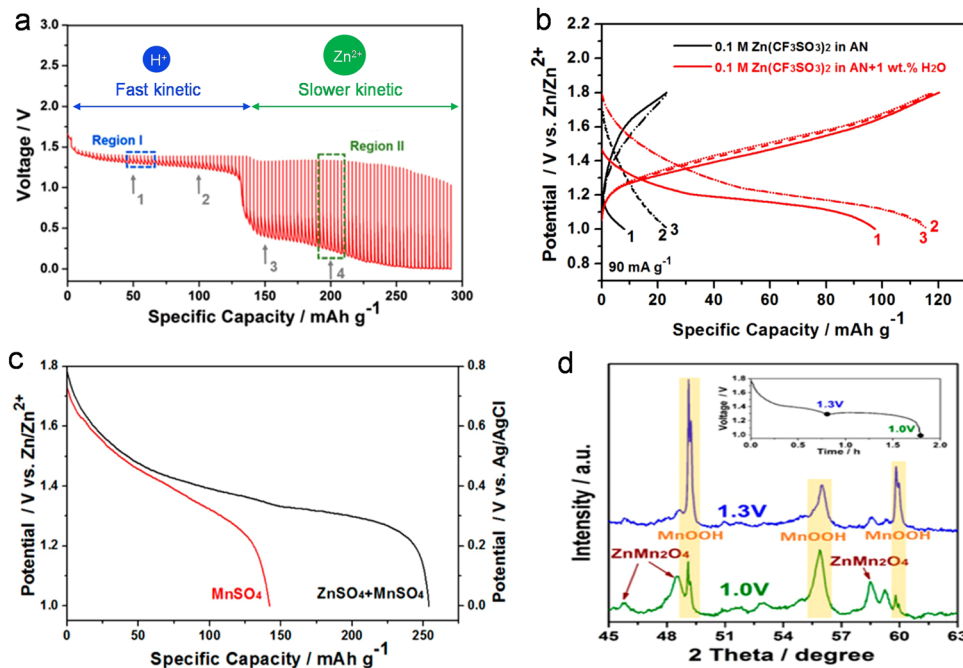
4882 | *Chem. Soc. Rev.*, 2024, **53**, 4877–4925

This journal is © The Royal Society of Chemistry 2024

Fig. 5 Co-insertion mechanism of H^+ and Zn^{2+} ions. (a) GITT curve depicting the behavior of Zn/MnO_2 batteries. (b) Galvanostatic charge–discharge curves of Zn/MnO_2 batteries in an organic Zn-based electrolyte, with and without H_2O addition. (c) Discharge curve of the MnO_2 cathode in a $MnSO_4$ solution, with or without $ZnSO_4$ as the electrolyte. (d) XRD patterns depicting the MnO_2 cathode post-discharge at 1.0 V and 1.3 V. Reproduced with permission from ref. 111. Copyright 2017 American Chemical Society.

authors substantiated the insertability of both Zn^{2+} and H^+ into MnO_2, as previously documented. The initial discharge plateau (Region I) in the discharge curve corresponds to H^+ ion insertion, while the subsequent plateau (Region II) signifies Zn^{2+} insertion (Fig. 5). To validate the co-insertion mechanism, the authors systematically controlled the presence or absence of H^+ or Zn^{2+} ions in the electrolyte, observing a significant impact on region I or II, respectively. This manipulation confirms the involvement of both H^+ and Zn^{2+} in the battery's charging/discharging process. Additionally, XRD results reveal the presence of MnOOH and $ZnMn_2O_4$ phases in the discharge products (Fig. 5), providing robust experimental support for the co-insertion mechanism of H^+ and Zn^{2+} ions into MnO_2.

The co-insertion reaction mechanism involving Zn^{2+} and H_2O has garnered considerable attention and scrutiny within various Zn-ion battery systems. Notably, Naza and her colleagues recently conducted an investigation into the co-insertion mechanism of H_2O and Zn ions in Zn/V_2O_5 batteries (Fig. 6).[112] After a series of electrochemical characterization and structural characterization (XRD, TEM and XPS), the authors revealed the specific evolution process of Zn^{2+} and H_2O insertion and extraction in layered V_2O_5. Throughout the discharge process, as Zn^{2+} and H_2O were gradually inserted, the initially layered V_2O_5 underwent a transformation into the layered $Zn_xV_2O_5 \cdot nH_2O$ phase, incorporating water. Concurrently, the interlayer spacing expanded from the original 4.4 Å to 13.4 Å, owing to the co-insertion of H_2O molecules and hydrated Zn^{2+} ions. In the subsequent charging process, the newly formed phase from the discharge gradually dissipated as the hydrated Zn ions

detached from the lattice of the cathode material. Because the crystal structure of the cathode host material usually has charge repulsion with Zn^{2+} ions, the co-insertion of water can effectively slow down this charge repulsion. When only organic electrolytes were used without water, the battery exhibited very limited capacity, demonstrating that water co-insertion can reduce charge repulsion.

2.1.3. Hybrid insertion–extraction mechanism involving alkali metal ions. While the insertion of Zn ions into the lattice of the host material is feasible, achieving reversible and rapid insertion and extraction of Zn ions typically poses a challenge.[113] This problem also greatly limits the reversibility and output voltage of Zn-ion batteries. Recently, a new type of hybrid battery was constructed by coupling the alkali metal ion-inserted cathode with the zinc anode.[114–121] This new type of hybrid battery can overcome the problems faced in traditional Zn-ion batteries. Simultaneously, the operational principle of this hybrid battery diverges from that of the conventional Zn-ion batteries (Fig. 7). Throughout the charge and discharge cycle, the anode undergoes the dissolution/deposition process of zinc. However, the conventional insertion and extraction of Zn ions at the cathode are substituted with processes involving alkali metal ions (Li^+, K^+, Na^+, Al^{3+}, and Mg^{2+}). The electrolyte in this hybrid battery serves as a conduit for conductive ions, collaborating with the cathode in energy storage. These innovative hybrid configurations significantly diversify rechargeable battery chemistries, offering fresh avenues for the subsequent design of high-performance Zn-based batteries.

For a more comprehensive comprehension of the hybrid insertion mechanism, the $LiMn_2O_4//Zn$ battery serves as an
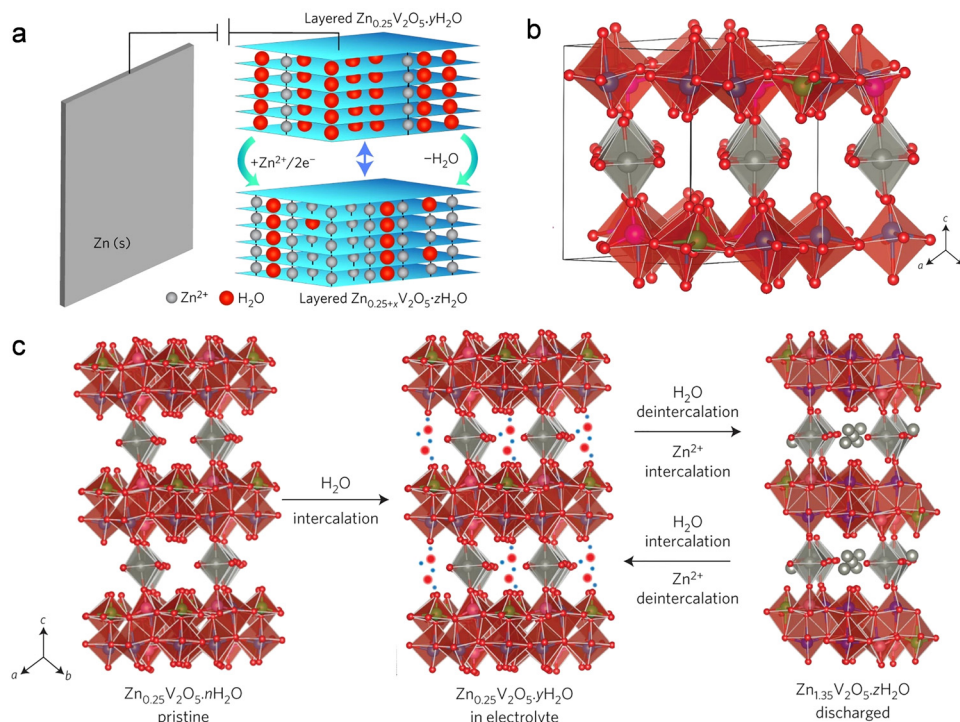
This journal is © The Royal Society of Chemistry 2024

Chem. Soc. Rev., 2024, **53**, 4877–4925 | **4883**

Fig. 6 Co-insertion mechanism of H_2O and Zn^{2+}. (a) Schematic representation illustrating the co-insertion of H_2O and Zn^{2+} during discharge. (b) Crystal structure depiction of $Zn_{0.25}V_2O_5$. (c) Schematic diagram delineating the reversible co-insertion/extraction process of H_2O and Zn ions in $Zn_{0.25}V_2O_5 \cdot nH_2O$. Reproduced with permission from ref. 112. Copyright 2016 Springer Science & Business Media.
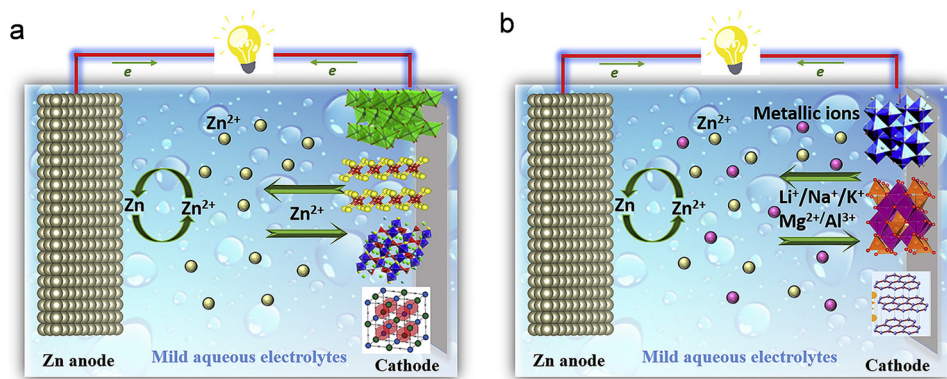

Fig. 7 Comparing the operational principles of Zn-ion batteries. (a) Zn-ion battery (Zn^{2+} insertion/extraction mechanism). (b) Hybrid Zn-ion battery (Li/Na/K/Mg/Al insertion/extraction mechanism). Reproduced with permission from ref. 114. Copyright 2019 Elsevier.

illustrative example to delineate the cathode and anode evolution throughout the charge and discharge processes.[122] The electrolyte for this battery comprises a blended aqueous solution containing $LiCl$ and $ZnCl_2$. By using XRD to monitor the evolution of spinel $LiMn_2O_4$ and Zn anodes during battery charge and discharge, the hybrid insertion–extraction mechanism is revealed. Concerning spinel $LiMn_2O_4$, as the charging process unfolds, the characteristic peaks associated with the (111), (311), and (400) planes of spinel $LiMn_2O_4$ progressively shift to higher angles. This shift indicates both the desorption of Li^+ ions and the formation of the Mn_2O_4 phase during

charging.[123] Conversely, throughout the discharge process, these characteristic peaks exhibit a gradual shift towards lower angles, ultimately returning to their original positions. This pattern reflects the reversible insertion/extraction process of Li ions in the $LiMn_2O_4$ material. For zinc anodes, XRD results also confirmed the reversible deposition/dissolution process of zinc during charge and discharge. Preceding the charging process, only the characteristic peaks of the carrier are discernible in the XRD spectrum. Post-charging, the emergence of characteristic peaks corresponding to (002), (010), and (011) of Zn in the XRD spectrum substantiates the deposition of zinc ions from the

4884 | Chem. Soc. Rev., 2024, **53**, 4877–4925

This journal is © The Royal Society of Chemistry 2024

mixed electrolyte onto the carrier. In this hybrid insertion–extraction mechanism, the cathode experiences an intercalation/deintercalation process involving alkali metal ions, while the anode undergoes a reversible Zn deposition/dissolution process.

2.2. Conversion-type mechanisms

2.2.1. Protonation/deprotonation mechanism. In mild electrolytes, it was found that some Zn-ion batteries operate based on the protonation/deprotonation mechanism. Diverging from the conventional Zn^{2+} insertion/extraction mechanism, this mechanism relies on protonation/deprotonation, entailing a conversion reaction between protons (H^+) and the electrode material in Zn-ion batteries (Fig. 8a).[124] As illustrated by Pan *et al.*, the superior performance of a Zn–MnO_2 battery system primarily stems from the conversion reaction between H^+ and α-MnO_2.[125] During the discharge process of the battery, α-MnO_2 undergoes a reaction with H^+ from the aqueous electrolyte, leading to the formation of a new MnOOH phase (H^+ + MnO_2 + e^- ↔ MnOOH). Concurrently, the OH^- ions present in the electrolyte will combine with $ZnSO_4$ and H_2O to produce a Zn salt compound ($ZnSO_4[Zn(OH)_2]_3\cdot xH_2O$), ensuring charge balance within the entire electrolyte system. The authors validated this chemical transformation mechanism through various structural characterization techniques, including TEM, XRD, and STEM-EDS. TEM analysis showed that after discharge, α-MnO_2 transformed into two discharge products with different lattice distances. This was further confirmed by XRD characterization (Fig. 8b), affirming that the discharge product is MnOOH rather than Zn_xMnO_2 or $ZnMn_2O_4$, as observed in the traditional Zn^{2+} insertion mechanism. Additionally, STEM-EDS elucidated the element distribution of the discharge products, indicating that Mn is primarily distributed on short nanorods and nanoparticles, while Zn predominantly resides in sheet-like materials derived from the electrolyte. These results confirm the occurrence of the conversion reaction mechanism.

Beyond the charge/discharge processes observed in mild Zn-ion batteries, governed by the deprotonation/protonation mechanism, certain alkaline Zn-ion batteries (*e.g.*, Ni–Zn, Co–Zn batteries) also follow the deprotonation/protonation mechanism. Due to this mechanism, these alkaline Zn-ion batteries typically achieve higher operating voltages, approximately in the range of 1.7–1.8 V, in comparison to other aqueous rechargeable batteries. In alkaline electrolytes, materials such as Co or Ni-based oxides/hydroxides, sulfides, and phosphides interact with OH^- under voltage-driven conditions.[126] Charge storage is achieved through deprotonation/protonation conversion reactions during charge and discharge. Illustrating the deprotonation/protonation mechanism of Ni or Co-based hydroxides, the process can be succinctly represented by the equation $A(OH)_2 + OH^- \leftrightarrow AOOH + H_2O + e^-$, where A denotes metal cations like Co or Ni.

Lu *et al.* employed the deprotonation/protonation reaction mechanism to fabricate a high-performance Zn-ion battery, utilizing 2D nickel cobaltite ($NiCo_2O_4$) nanosheets endowed with abundant O defects as the active material.[127] In the charging process, $NiCo_2O_4$ nanosheets undergo an oxidation reaction with OH^-, transforming into NiOOH and CoO_2. Simultaneously, $[Zn(OH)_4]^{2-}$ in the electrolyte is also reduced to Zn. Conversely, in the discharge process, both CoO_2 and NiOOH are reduced to lower valence oxides, and Zn undergoes oxidation with the hydroxide anion in the electrolytes, resulting in the formation of $[Zn(OH)_4]^{2-}$. This deprotonation/protonation reaction mechanism is succinctly represented by the following equation:

$$\text{Cathode: } NiCo_2O_4 + H_2O + OH^- \leftrightarrow 2CoOOH + NiOOH + e^- \tag{1}$$

$$CoOOH + OH^- \leftrightarrow H_2O + CoO_2 + e^- \tag{2}$$

$$\text{Anode: } Zn(OH)_4^{2-} + 2e^- \leftrightarrow 4OH^- + Zn \tag{3}$$
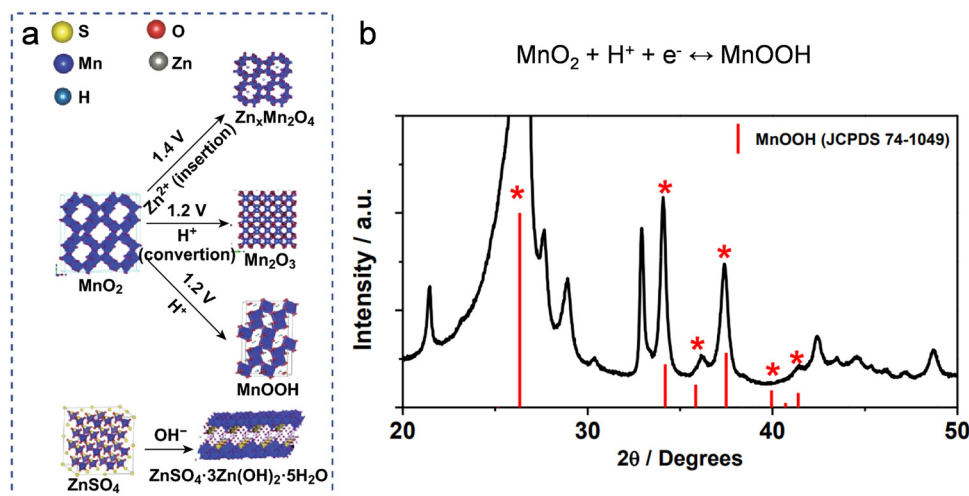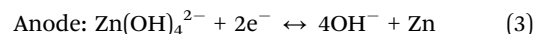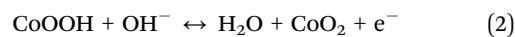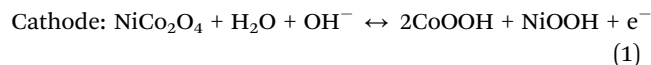
Fig. 8 Conversion mechanism based on protonation/deprotonation. (a) Schematic diagram of phase evolution during discharge. Reproduced with permission from ref. 124. Copyright 2019 Springer Science & Business Media. (b) The XRD pattern of α-MnO_2 in its fully discharged state unequivocally validates the generation of MnOOH. Reproduced with permission from ref. 125. Copyright 2016 Springer Science & Business Media.

This journal is © The Royal Society of Chemistry 2024

Chem. Soc. Rev., 2024, **53**, 4877–4925 | **4885**

$$3Zn(OH)_4^{2-} + 2NiCo_2O_4 \leftrightarrow 2NiOOH + 4CoO_2 + 6OH^- + 2H_2O + 3Zn \quad (4)$$
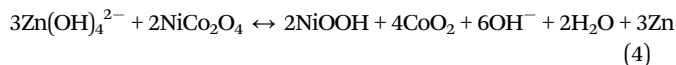
In addition to transition metal hydroxides, nickel- or cobalt-based sulfides and phosphides are also used in alkaline Zn-ion batteries, and their charge and discharge processes are also based on the deprotonation/protonation conversion mechanism. Concurrently, batteries employing cathode materials based on nickel or cobalt sulfides and phosphides exhibit enhanced performance owing to their conductivity and more suitable electronic structure in comparison to transition metal oxides.[128] Transition metal sulfides and phosphides participate in reversible redox reactions with OH^- in aqueous electrolytes during charge and discharge processes, facilitating charge storage. Exemplifying this with transition metal sulfides, the reaction mechanism in alkaline Zn-ion batteries is succinctly represented by the equation $AS + OH^- \leftrightarrow ASOH + e^-$, where A denotes the metal cation.

2.2.2. Redox-couple conversion mechanism. The redox-couple conversion mechanism mainly exists in Zn-based redox flow batteries. Due to the obvious advantages of flow batteries in theoretical energy density and recyclability,[129] Zn-based flow batteries have witnessed significant advancements in recent years. Presently, a variety of Zn-based redox flow batteries featuring

diverse redox couples have been established, encompassing Zn–halogen (e.g., I_2, Cl_2, Br_2), Zn–Ce, Zn–organic, and Zn–Fe flow batteries (Fig. 9a).[130–132] Despite achieving notable breakthroughs, Zn-based flow batteries require further enhancement in performance to realize widespread and practical large-scale applications. Current efforts are devoted to exploring new redox couples and optimizing electrolytes, membranes, and electrodes.[133–135] In order to acquire a more profound understanding of the mechanism underlying Zn-based flow batteries, we will delve into the Zn–I_2 flow battery as an illustrative example and scrutinize its energy storage mechanism. Iodide, known for its high solubility (exceeding 8 mol L^{-1}) in aqueous electrolytes, emerges as a promising cathodic redox candidate capable of delivering high energy density. In traditional Zn–I_2 flow batteries, the working principle is succinctly described by the following equation:

$$Zn + I_3^- \leftrightarrow Zn^{2+} + 3I^-, \quad E = 1.299 \text{ V}. \quad (5)$$
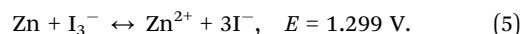
From the results of the above equation, it can be seen that the theoretical electrode voltage of the traditional Zn–I_2 flow battery is only 1.299 V. Therefore, it is necessary to innovate on the basis of the traditional Zn–I_2 flow battery to increase its voltage. In this context, the electrolyte decoupling strategy emerges as an effective
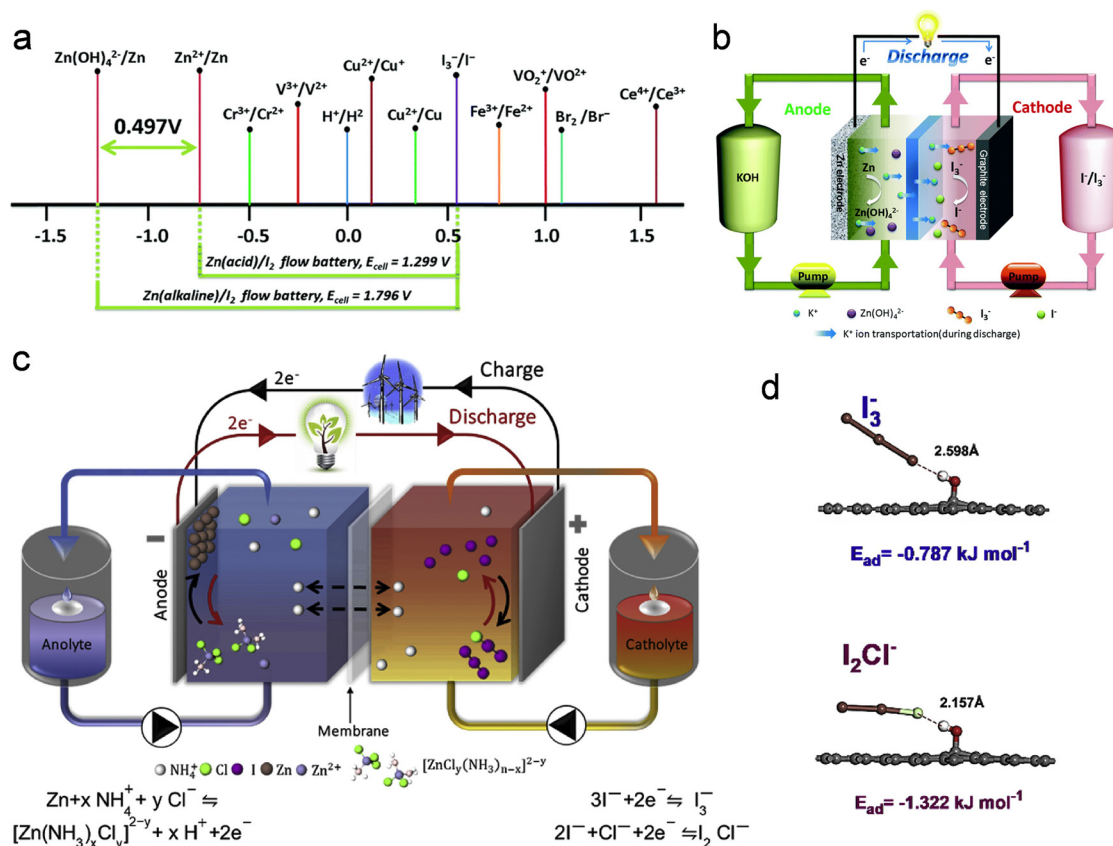
Fig. 9 Zn–I_2 battery based on the redox-couple conversion mechanism. (a) Standard redox potentials for various candidate redox couples. (b) Illustration outlining the operational mechanism during the discharge phase of an alkaline Zn–I_2 redox flow battery. Reproduced with permission from ref. 136. Copyright 2018 Royal Society of Chemistry. (c) Illustrative depiction elucidating the operational principles of a Zn–I_2 redox flow battery utilizing an electrolyte containing NH_4Cl. (d) DFT optimized molecular structure, and anions on the cathode surface. Reproduced with permission from ref. 137. Copyright 2020 Elsevier.

4886 | Chem. Soc. Rev., 2024, **53**, 4877–4925

This journal is © The Royal Society of Chemistry 2024

approach to elevate the voltage of Zn–I$_2$ flow batteries. A case in point is the design by Chen and colleagues, who implemented a hybrid alkaline Zn–I$_2$ redox flow battery by transitioning the anolyte from acidic to alkaline conditions (Fig. 9b).[136] This hybrid Zn–I$_2$ flow battery exhibits an elevated electrode voltage, marked by a potential enhancement of 0.497 V compared to the conventional Zn–I$_2$ flow batteries. The redox mechanism of this hybrid system can be succinctly captured by the following equation:

$$Zn + 4OH^- + I_3^- \leftrightarrow 3I^- + Zn(OH)_4^{2-}, \quad E = 1.796\ V \quad (6)$$
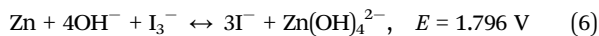
In Zn–I$_2$ flow batteries, the challenges of zinc dendrite formation and the precipitation of insoluble iodine (I$_2$) are primary contributors to their compromised cycle stability and low energy efficiency. These issues significantly impede the large-scale practical applications of Zn–I$_2$ flow batteries. Recently, Chen et al. successfully addressed both challenges by incorporating ammonium chloride (NH$_4$Cl) into the electrolyte of Zn–I$_2$ flow batteries (Fig. 9c).[137] The addition of NH$_4$Cl serves a dual purpose in enhancing Zn–I$_2$ flow battery performance. Firstly, it effectively modulates the chemical composition of the electrolyte, suppressing both the formation of Zn dendrites and the generation of insoluble iodine. Secondly, NH$_4$Cl not only accelerates the reaction kinetics at the cathode and anode but also involves Cl$^-$ in the formation of I$_2$Cl, contributing to additional capacity release (Fig. 9d). This

mechanism-guided design proves instrumental in effectively ameliorating Zn–I$_2$ flow battery performance.

2.3. Coordination-type mechanisms

Coordination-type mechanisms are primarily characteristic of Zn–organic batteries. In recent years, investigations have revealed that numerous organic compounds, including caliquinone, p-tetrachlorobenzoquinone, and tetrachloro-1, among others, serve as effective cathode materials in reversible Zn-ion batteries.[90,138–146] Through coordination with Zn^{2+}, the organic compounds undergo alterations in their charge states during the redox processes. This evolution in the charge state of the electroactive group serves as a valuable indicator for elucidating the redox mechanism in Zn–organic batteries. To pinpoint the specific sites within organic compounds that engage in coordination with Zn^{2+}, Chen and collaborators conducted a meticulous analysis, determining the active sites by comparing electrostatic potentials (ESP) across various locations within organic compounds (Fig. 10a–e). ESP, a widely employed metric in organic chemistry, proves instrumental in assessing electrophilic or nucleophilic reactions.[147] Because the cathode will involve the absorption of Zn^{2+} during battery discharge, sites with more negative ESP in organic compounds are beneficial to the discharge reaction. By comparing the ESP of each site in the calix[4]quinone (C4Q) molecule, it can be seen that the carbonyl groups on the molecule and below the molecule show a lower
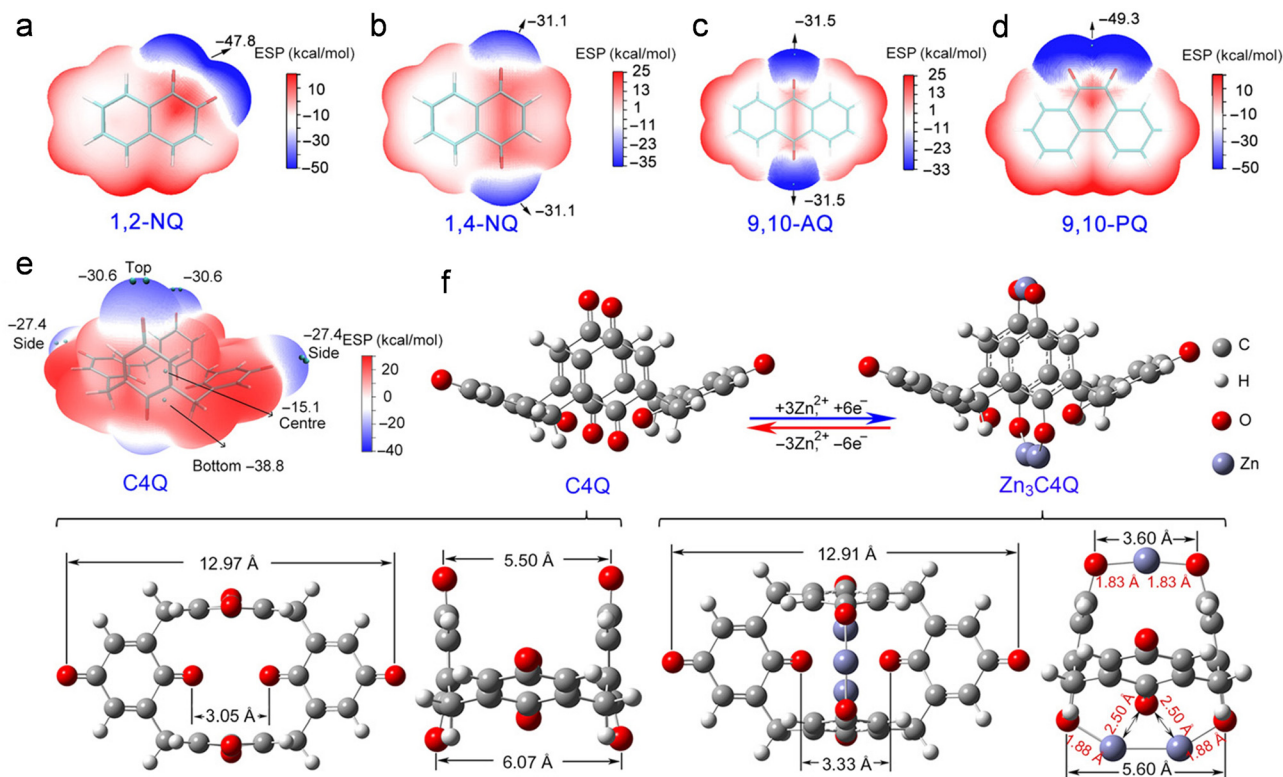
Fig. 10 Inferring the active site and structural evolution of quinone cathodes. (a)–(e) The ESP-mapped van der Waals surface of diverse organic molecules. (f) Optimized molecular structure of C4Q before and after Zn^{2+} absorption. Reproduced with permission from ref. 147. Copyright 2018 American Association for the Advancement of Science.

This journal is © The Royal Society of Chemistry 2024

Chem. Soc. Rev., 2024, **53**, 4877–4925 | 4887

ESP than the bilateral carbonyl groups, which indicates that the carbonyl groups on the molecule and below the molecule are more conducive to the adsorption of Zn^{2+}.

In contrast to their inorganic counterparts, organic cathode materials often exhibit intrinsically low crystallinity, posing challenges for accurate characterization through conventional methods such as XRD and TEM. Nevertheless, these organic cathode materials boast an abundance of oxygen- or nitrogen-containing functional groups. Consequently, the discernment of the reaction mechanism in Zn–organic batteries during redox processes is achievable through Raman spectroscopy, ultraviolet-visible spectroscopy, and attenuated total reflection Fourier transform infrared spectroscopy. For instance, Chen and colleagues employed various *in situ* spectroscopic techniques to investigate the energy storage mechanism of C4Q organic molecules during charging and discharging. As the discharge progresses, the two carbonyl groups positioned atop the C4Q molecule coordinate with a single Zn^{2+} ion, accepting two electrons. Simultaneously, the four carbonyl groups located at the base of the C4Q molecule coordinate with the remaining two Zn^{2+} ions. During the subsequent charging phase, C4Q undergoes oxidation, resulting in the release of the stored electron and zinc ion during the reverse discharging process (Fig. 10f). The coordination evolution between C4Q and Zn^{2+} throughout the charge and discharge phases can be succinctly expressed by the following equation:

$$C4Q + 3Zn^{2+} \leftrightarrow Zn_3C4Q \tag{7}$$
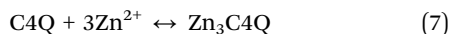
2.4. Catalysis-type mechanisms

The catalysis-type mechanism denotes the operational process in Zn-based batteries, wherein a catalyst is essential for facilitating the completion of the redox reaction at the cathode. This mechanism is observed in various Zn-based battery configurations, encompassing Zn–air batteries and Zn–CO$_2$ batteries. Extensive research has been undertaken to elucidate the mechanism of the oxygen reduction reaction (ORR) during discharging and the oxygen evolution reaction (OER) during charging in Zn–air batteries. To augment the overall performance of Zn–air batteries, numerous advanced catalysts, including high-performance bifunctional electrocatalysts, have been devised based on both OER and ORR mechanisms. In contrast to the swift progress observed in Zn–air batteries, the development of Zn–CO$_2$ batteries, an emerging category of Zn-based batteries, is at the beginning of its exploration phase. The catalytic conversion of carbon dioxide in Zn–CO$_2$ batteries is notably intricate compared to that of oxygen, rendering the mechanism more complex. Beyond the incorporation of the catalytic conversion mechanisms of oxygen and carbon dioxide into Zn-based batteries, various other catalytic conversion mechanisms have been introduced. Examples include the catalytic conversion of acetylene (Zn–acetylene battery) and the catalytic conversion of nitrate (Zn–nitrate battery). This section focuses predominantly on elucidating the mechanisms of Zn–air batteries and Zn–CO$_2$ batteries.

2.4.1. Zn–air chemistry. With a history spanning 150 years, the inaugural Zn–air battery emerged in 1868 as a primary battery employing an NH$_4$Cl aqueous solution as its electrolyte.[94] Although Zn–air batteries are an old and mature battery technology, these types of batteries have recently regained significant attention owing to their inherent advantages. Zn–air batteries present distinct advantages in energy density and safety compared to other battery types. Consequently, they emerge as a compelling alternative to Li-ion batteries for next-generation flexible/wearable electronic devices and automotive electrification applications.[148–154] A conventional Zn–air battery comprises essential components, including an air cathode, separator, Zn anode, and alkaline electrolyte. Its basic structure and working principle are shown in Fig. 11.[155] In the discharging phase of Zn–air batteries, an oxidation reaction occurs on the zinc electrode, producing Zn^{2+} ions. Subsequently, these ions undergo a reaction with OH$^-$ ions, resulting in the formation of acid anions ($Zn(OH)_4^{2-}$). As the discharge process advances, the electrolyte experiences a state of supersaturation in $Zn(OH)_4^{2-}$, leading to the decomposition of this compound into insoluble zinc oxide.[156,157]

During the discharging and charging process of the Zn–air batteries, O$_2$ in the atmosphere penetrates into the gas diffusion layer with a porous structure of the air cathode, as depicted in the schematic diagram. Subsequently, the ORR occurs on the catalyst layer of the cathode. Concurrently, hydroxide ions, produced as a byproduct at the air cathode, gradually migrate towards the zinc anode, culminating in the completion of the Zn–air battery discharge reaction. The charging process of Zn–air batteries is a reversible counterpart of the discharge phase. The overarching electrochemical reaction mechanism for Zn–air batteries is succinctly expressed by the following equation:

$$\text{Anode: } Zn + 4OH^- \leftrightarrow Zn(OH)_4^{2-} + 2e^- \tag{8}$$

$$Zn(OH)_4^{2-} \leftrightarrow H_2O + ZnO + 2OH^- \tag{9}$$

$$\text{Cathode: } 2H_2O + O_2 + 4e^- \leftrightarrow 4OH^- \tag{10}$$

$$\text{Overall reaction: } 2Zn + O_2 \rightarrow 2ZnO \tag{11}$$
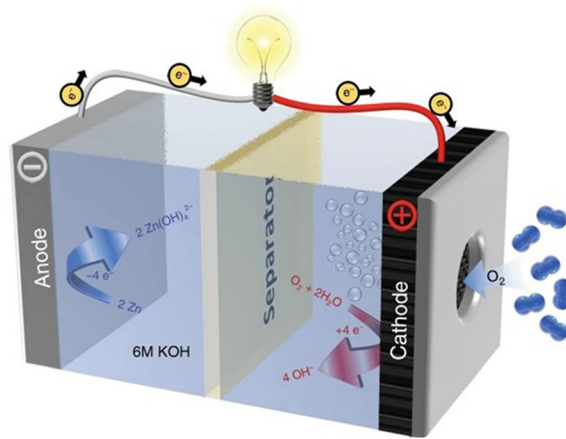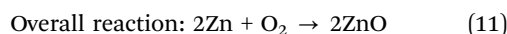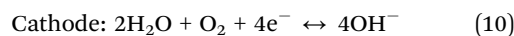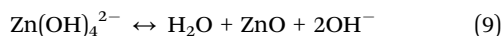
Fig. 11 Illustration depicting the fundamental structure and reaction mechanism of Zn–air batteries. Reproduced with permission from ref. 155. Copyright 2020 Springer Science & Business Media.

4888 | *Chem. Soc. Rev.*, 2024, **53**, 4877–4925

This journal is © The Royal Society of Chemistry 2024

2.4.2. Zn–CO₂ chemistry. Currently, electricity generation and chemical production stand as pivotal industries in contemporary society. However, most of these activities use highly polluting, non-renewable fossil fuels as energy supply sources, which results in the emission of large amounts of CO_2.[158–163] In response to these challenges, several efficacious electrochemical techniques for CO_2 conversion and recycling have been devised, among which metal–CO_2 batteries feature prominently. The appeal of metal–CO_2 batteries lies in their dual functionality of supplying energy while concurrently harnessing CO_2, garnering increasing attention.[164–166] This electrochemical system for CO_2 fixation and recycling facilitates concurrent real-time power input and the conversion of waste CO_2 into valuable chemicals. Metal–CO_2 batteries, akin in principle to metal–air batteries, exhibit promising application prospects in the storage of surplus electricity. Early researchers found in the study of Li–O_2 batteries that adding a certain amount of CO_2 to O_2 can effectively improve battery performance,[167] which made people realize the possibility of constructing Li–CO_2 batteries. Ongoing research advancements have enabled Li–CO_2 batteries to attain elevated operating voltage and enhanced energy density.[168–170] Nevertheless, the utilization of organic electrolytes significantly constrains the advancement of Li–CO_2 batteries.[171,172] In the context of Li–CO_2 batteries, the high cost associated with organic electrolytes on the one hand elevates the overall battery cost, while on the other hand, the utilization of nonaqueous electrolytes imposes constraints on the range of discharge products. In contrast, aqueous Zn–CO_2 batteries are gaining prominence owing to their clear advantages in terms of cost and diversity of discharge products.[173,174] The general configuration of Zn–CO_2 batteries is similar to that of Zn-based redox flow batteries, also consisting of two chambers separated by an ion exchange membrane (Fig. 12), where the cathode is in a compartment containing a neutral aqueous electrolyte and the zinc electrode is in a compartment containing an alkaline aqueous electrolyte. At the same time, the use of ion exchange membranes can effectively achieve CO_2 conversion/recycling. In addition, unlike the CO_2 reduction pathway in organic electrolytes that only involves electron transfer, Zn–CO_2 batteries based on aqueous electrolytes can achieve tunable CO_2 reduction because the entire reduction pathway involves not only the transfer of electrons but also the

participation of protons.[175] Depending on the reduction products, the redox mechanism of the Zn–CO_2 battery is succinctly conveyed through the following equation:
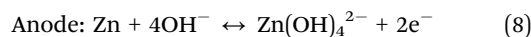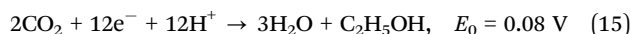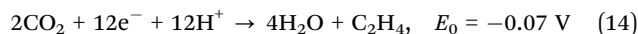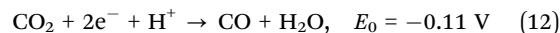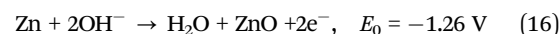
Cathode:

$$CO_2 + 2e^- + H^+ \rightarrow CO + H_2O, \quad E_0 = -0.11 \text{ V} \quad (12)$$

$$CO_2 + 2e^- + 2H^+ \rightarrow HCOOH, \quad E_0 = -0.20 \text{ V} \quad (13)$$

$$2CO_2 + 12e^- + 12H^+ \rightarrow 4H_2O + C_2H_4, \quad E_0 = -0.07 \text{ V} \quad (14)$$

$$2CO_2 + 12e^- + 12H^+ \rightarrow 3H_2O + C_2H_5OH, \quad E_0 = 0.08 \text{ V} \quad (15)$$

Anode:

$$Zn + 2OH^- \rightarrow H_2O + ZnO + 2e^-, \quad E_0 = -1.26 \text{ V} \quad (16)$$

Based on the standard electrode potential, the spontaneous discharge of aqueous Zn–CO_2 batteries is thermodynamically viable. However, the efficiency of these batteries is hindered by the low electrocatalytic efficiency in CO_2 conversion, attributed to the chemical inertness of CO_2 molecules and the competition for hydrogen evolution reaction (HER) in aqueous electrolytes. In recent years, researchers have innovatively developed efficient CO_2 conversion electrocatalysts, encompassing heteroatom-doped carbon, single-atom electrocatalysts, and metal catalysts. Aqueous Zn–CO_2 batteries employing these electrocatalysts have demonstrated successful reduction of CO_2 to CO, HCOOH, C_2H_5OH, and CH_4.[176,177] However, in these Zn–CO_2 battery systems, the charging process is still based on the water oxidation process (OER).[174,178] In addition, Wang and his colleagues accomplished a reversible conversion of CO_2 to formic acid (HCOOH) in an aqueous Zn–CO_2 battery, employing bifunctional Pd as a cathode catalyst.[179] As the discharge process proceeds, CO_2 is converted into HCOOH on the Pd catalyst. For the charging reaction, the reversible process of converting HCOOH into CO_2 will occur at the Pd cathode ($CO_2 + 2e^- + 2H^+ \leftrightarrow HCOOH$).
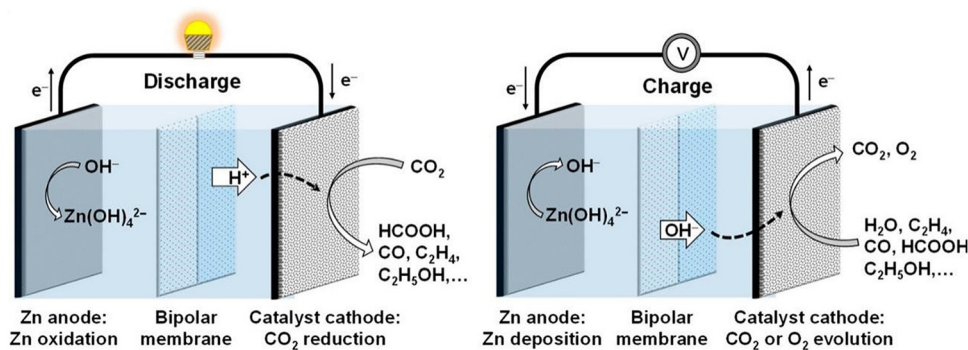

Fig. 12 Illustration depicting the discharge and charging processes of an aqueous Zn–CO_2 battery. Reproduced with permission from ref. 166. Copyright 2022 John Wiley & Sons.

This journal is © The Royal Society of Chemistry 2024

Chem. Soc. Rev., 2024, **53**, 4877–4925 | 4889

3. Design strategies for high-performance Zn-ion batteries

The Zn-ion battery is the earliest studied and most representative type of battery in Zn-based batteries. Capitalizing on attributes such as high safety, ample reserves, low price, and substantial energy density, the rechargeable Zn-ion battery has garnered considerable attention as an efficient energy storage solution. Nevertheless, when compared to conventional Li-based rechargeable batteries, the performance of Zn-ion batteries falls short of the target due to constraints like a narrow electrochemical stable potential window, limited discharge capacity, intricate side reactions, and low operating voltage. Addressing these challenges and striving for an ideal Zn-ion battery characterized by heightened reversibility and energy density, diverse strategies have been employed to optimize the electrochemistry, cathode materials, the Zn anode, and the electrolyte. The ensuing sections will delve into these design strategies, with a particular focus on enhancing electrochemical performance concerning capacity, working voltage, energy density, and cycle life.

3.1. Design strategies for high-capacity Zn-ion batteries

3.1.1. Exploiting cathode materials with high theoretical capacity.
The theoretical capacity of cathode materials is governed by the collective impact of the electron transfer number and the mass of the active material. This criterion guides the pursuit of cathode materials characterized by elevated theoretical capacities, as illustrated in Fig. 13a and b. At present, typical insertion-type materials, exemplified by Mn-based oxides or V-based oxides, demonstrate the theoretical capacity within the range of 300–590 mA h g^{-1} (Fig. 13c).[53,132,180–190] It is crucial to underscore that the mentioned values are exclusively contingent on active materials. Therefore, the imperative challenge is to diminish the content of the inactive component of the electrode while maintaining the stability of the overall structure.

Regrettably, these efforts frequently entail the active chemical element undergoing a reduction in its valence state during redox processes. Consequently, a crucial design strategy for high-capacity cathodes lies in realizing the goal of enhancing the electron transfer number through the augmentation of active centers for redox reactions.[191] Particularly, employing the initial charge of the battery for *in situ* activation stands out as a promising strategy for augmenting the electron transfer number. For example, researchers convert low-valent V-based compounds into high-valent V-based oxides (such as V_2O_{5-x}), thus giving the cathode a higher capacity (more than 590 mA h g^{-1}).[192–195] It is noteworthy that these materials with high capacity obtained through *in situ* conversion in the discharge process necessitate combination with carbon to preserve the stability of their overall structure.

In comparison to inorganic compounds, the coordination-type organic compounds have lower theoretical capacity due to the substantial proportion of inert carbon forming the skeleton (Fig. 13c).[90,196–198] Fortunately, since the carbon skeleton in coordination organic compounds has flexible and adjustable characteristics, it is very possible to introduce active coordination groups on the carbon skeleton in coordination-type organic compounds. In addition to being easy to introduce active groups, coordination-type organic compounds also have the advantage of low mass, so they are regarded as ideal candidates for electrode materials possessing high theoretical capacities.[90] As an illustration, enhancement of activity and augmentation of active coordination sites can be achieved by introducing redox-active quinone groups into 1,4,5,8,9,12-hexaazatriphenylene-based covalent organic frameworks (HAQ-COFs), leading to an increased capacity of 344 mA h g^{-1}.[199] Furthermore, the hierarchical arrangement of poly(*para*-aminophenol, pAP) and poly(1,5-naphthalene-diamine, 1,5-NAPD) on nanoporous carbon is able to enhance the full activation of active coordination centers (C=N/C=O) for Zn^{2+}.[200] Conversely, while certain coordination organic compounds, exemplified by benzoquinone (BQ) small molecules,
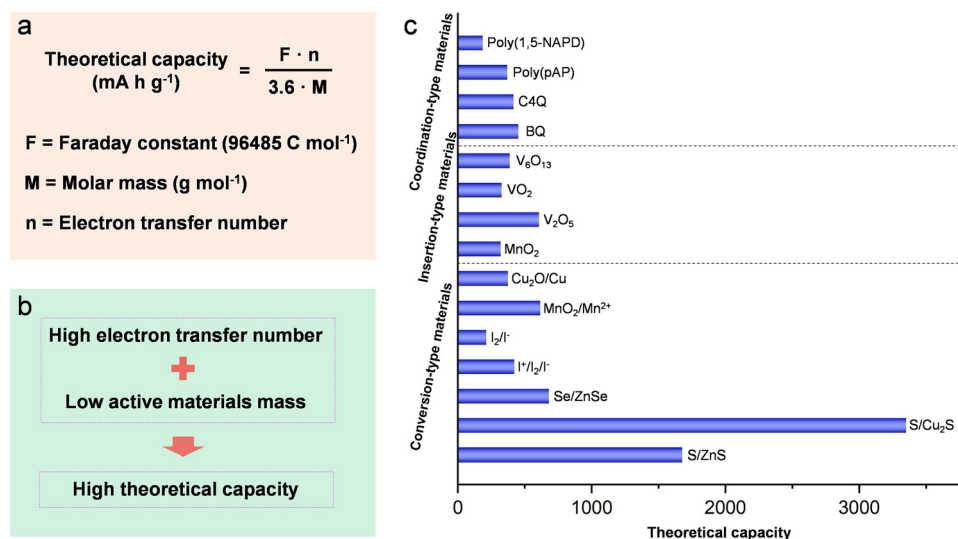

Fig. 13 Theoretical capacity. (a) Theoretical capacity calculation of electrode materials. (b) Factors affecting high theoretical capacity. (c) Comparing the theoretical capacities of various cathode materials.

4890 | Chem. Soc. Rev., 2024, 53, 4877–4925

This journal is © The Royal Society of Chemistry 2024

demonstrate high theoretical capacities, the cathode incorporating these organic small molecules is deficient in adequate covalent structure, thereby compromising battery stability. Therefore, while pursuing enhanced capacity in coordination-type organic compounds, it becomes imperative to prioritize the stability of the underlying structure. The target is to attain a harmonious equilibrium between electrochemical performance (capacity and cycling stability) and structure (active groups and carbon skeleton).

Unlike cathode materials of insertion or coordination types, conversion-type cathode materials hold a distinguished status in the realm of high-theoretical-capacity categories. A notable illustration of this is the prevalent utilization of sulfur as the electrode material in Zn-ion batteries, due to its engagement in diverse redox reaction pairs and ultrahigh theoretical capacity,[201–204] including S/Cu$_2$S (approximately 3350 mA h g^{-1}) and S/ZnS (approximately 1675 mA h g^{-1}) (Fig. 13c). Nevertheless, inherent challenges within Zn//S batteries, such as irreversible by-products, sluggish kinetics, and specific pH specifications, constrain both the practical electrode potential and the capacity of aqueous Zn//S batteries. To handle these issues, many methods have been proposed. The incorporation of the electrolyte additive I$_2$ has demonstrated effectiveness, as I$_2$ acts as a medium for Zn^{2+} while concurrently reducing reaction barriers. This property proves advantageous for achieving high energy efficiency and low-voltage hysteresis in Zn–S batteries.[203]

Moreover, the utilization of an infinite solid solution between sulfur (S) and selenium (Se), denoted as S–Se, serves to optimize the band structure, electronic structure as well as activation energy of S. Consequently, this leads to a significant improvement in both reactivity and conductivity.[205] Beyond S, the proposal to utilize Se as an electrode material for Zn-ion batteries holds promise, offering a notable capacity of 611 mA h g^{-1}.[206] Despite the intrinsic advantages of elemental S and Se concerning the electron transfer number and mass, a persistent challenge lies in their low output voltage range (0.455–1.01 V). A feasible solution involves pairing them with high-voltage redox reactions, exemplified by the S/Cu$_2$S system, which operates at a working voltage of 1.15 V.

3.1.2. Optimizing the actual capacity. The reduced actual capacity of cathode materials in Zn-ion batteries can be attributed to deleterious factors such as low intrinsic conductivity, inadequate selectivity of Zn^{2+} charge carriers, and the obstruction of active sites (Fig. 14). These factors impede the kinetics of the redox reaction at the cathode, thereby influencing the actual capacity of the battery. Consequently, optimizing the practical capacity of cathode materials is imperative, prompting the proposal of various strategies. These include manipulating the crystal structure and integrating it with additives with highly conductive properties.

In Zn-ion batteries based on the traditional insertion-type mechanism, a noteworthy challenge arises from the intense
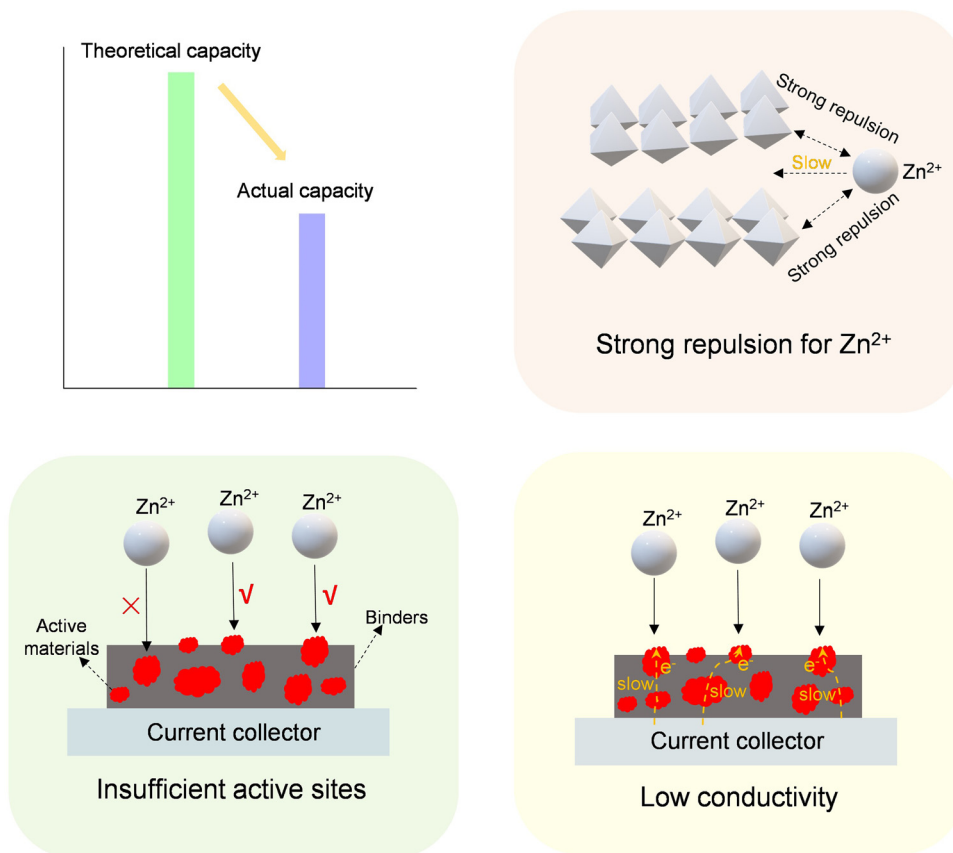

Fig. 14 Schematic diagram of the adverse effects of various factors (strong repulsive effect, insufficient active sites, and low conductivity) on the theoretical capacity of cathode materials.

This journal is © The Royal Society of Chemistry 2024

Chem. Soc. Rev., 2024, **53**, 4877–4925 | **4891**

electrostatic repulsion between the Zn^{2+} ion and the host materials. This phenomenon results in suboptimal utilization of the active material and diminished battery capacity.[207] To address this challenge, an effective approach involves the preliminary insertion of certain ions[182,208–211] or molecules[107,212–214] into layered cathode materials. This process serves to mitigate electrostatic interactions and widen the spacing between layers, consequently enhancing the storage capacity of Zn-ion batteries (425–550 mA h g^{-1}). It is noteworthy, however, that the introduction of inactive ingredients during insertion may lead to a reduction in valency and ratio of active ingredients within the cathode material. Additionally, semiconductor oxides face a challenge in their limited electron transfer capabilities, undermining the actual capacity. Broadly speaking, the enhancement of electrical conductivity can be attained by tuning the band gap of materials through heteroatom doping. As an illustration, the co-doping scheme involving the introduction of La and Ca into MnO_2, yielding Ca/La co-doped MnO_2, has demonstrated reduced charge transfer resistance (29.8 vs. 198.1 Ω) and increased capacity (297 vs. 199 mA h g^{-1}) in comparison to pure MnO_2.[215] In addition, defect engineering stands out as an additional effective strategy for enhancing actual capacity. The introduction of defects proves effective in diminishing electrostatic repulsion and elevating carrier concentration.[106,190,216–220] On the other hand, it is inevitable to accurately control and characterize these defects, while it can often be a complex and challenging endeavor.

Carbonaceous materials and lightweight carbon-based materials, like graphene, MXene, carbon nanotubes, and carbon fiber, are extensively employed as supports for active materials. Their utilization is driven by their substantial active surface area and high conductivity, facilitating enhanced contact between the cathode material and ions in the electrolyte and improving charge transfer rates.[221–225] As a consequence, there is a notable augmentation in the capacity of the cathode.[226] Beyond the intrinsic attributes of the active material that influence actual capacity, extrinsic factors also contribute to determining the practical capacity of the electrode materials. Frequently, binders obstruct a segment of the effective active area of the cathode material, impeding direct contact between active materials and charge carriers.[227–231] Carbon substrates featuring surface functional groups obviate the necessity for binders, facilitating adhesive-free immobilization of the cathode material and maximizing the exposure area of active materials. A case in point is the substantial enhancement in the actual capacity of the $Co-Mn_3O_4$ material, achieved by combining it with a carbon nanosheet array – from 220 mA h g^{-1} to 362 mA h g^{-1}.[232] Likewise, the incorporation of N-doped carbon cloth effectively secures benzoquinone, preventing its dissolution and thereby stabilizing its capacity.[233]

3.1.3. New energy storage mechanisms. For Zn-ion batteries, the redox mechanism corresponding to the cathode can be mainly divided into three types: insertion-type mechanisms, coordination-type mechanisms and conversion-type mechanisms. Broadly speaking, the charge carriers for both insertion-type and coordination-type mechanisms are Zn^{2+} and H^+. However, the high charge density and low diffusion rate of Zn^{2+} ions limit their fast and efficient storage in cathode

materials. Thus, searching for charge carriers with attributes of rapid diffusion, low corrosiveness, and small size is very important for high-capacity Zn-ion batteries. In recent studies, researchers have introduced a novel co-insertion mechanism in $Zn–MnO_2$ batteries. This mechanism involves the simultaneous co-insertion of H^+ and NH_4^+ ions into the cathode material (Fig. 15a and b).[234] In this mechanism, stable hydrogen bonds are formed between Mn–O groups and intercalated NH_4^+ ions, which can stabilize the $Mn^{3+}O_6$ octahedra. Additionally, the co-insertion of H^+ leads to an increase in the electron density of the O element in the cathode materials. Owing to the synergistic effect arising from the joint introduction of NH_4^+ and H^+, the battery showcased notable discharging capacity and energy density, registering at 365 mA h g^{-1} and 486 W h kg^{-1}, respectively. Furthermore, for Zn-ion batteries using Mn-based materials as the cathode, some research results show that their actual capacity (300–400 mA h g^{-1}) surpasses their theoretical capacity.[125] This outcome can be attributed to the conversion of Mn^{2+} ions in the electrolyte, resulting in the generation of MnO_2 that gets deposited on the electrode. Consequently, the observed capacity surpasses the theoretical capacity. Notably, the predominant contributor to this excess capacity is the deposition of MnO_2 resulting from the oxidation of Mn^{2+} in the electrolyte. However, achieving this phenomenon necessitates operation at a relatively low current density, a parameter closely linked to the acid/alkaline changes in the electrolyte and the associated electro-chemical polarization.

Compared with the insertion-type mechanism and the coordination-type mechanism, the conversion-type mechanism has some unique advantages such as high selectivity towards charge carriers and strong practical versatility. This suggests the potential for employing various redox reaction systems in Zn-ion batteries. When designing high-capacity energy storage mechanisms, it is essential to consider electron transfer numbers and the mass of active materials. Consequently, it is viable to pursue continuous transformation reactions involving large numbers of transferred electrons and exploit them for high-capacity energy storage mechanisms. For example, a unique continuous conversion reaction mechanism centered on continuous $I^+/I_2/I^-$ conversion reaction, which involves a four-electron transfer process, has been finely tailored.[135,235] This innovation has elevated Zn–I batteries to a remarkable capacity level of 594 mA h g^{-1}.[236] Furthermore, because the conversion reaction mechanism has the advantage of versatility, a variety of cathode materials with conversion-active functional groups can adapt to the conversion-type mechanism, thereby realizing high-capacity Zn-ion batteries. Recently, the conversion mechanisms based on Cu–CuI have been explored, and other types of Cu-based materials (Cu_2O, Cu_3N, Cu_2S, and so on) have shown high electrochemical capacity with their unique structures through this conversion-type mechanism (Fig. 15c and d).[237] Although the chemical process based on the conversion-type mechanism appears to be a relatively simple process, in addition to reaction stability, carrier compatibility with the electrolyte, anode, and additional electrolyte mass must also be considered.
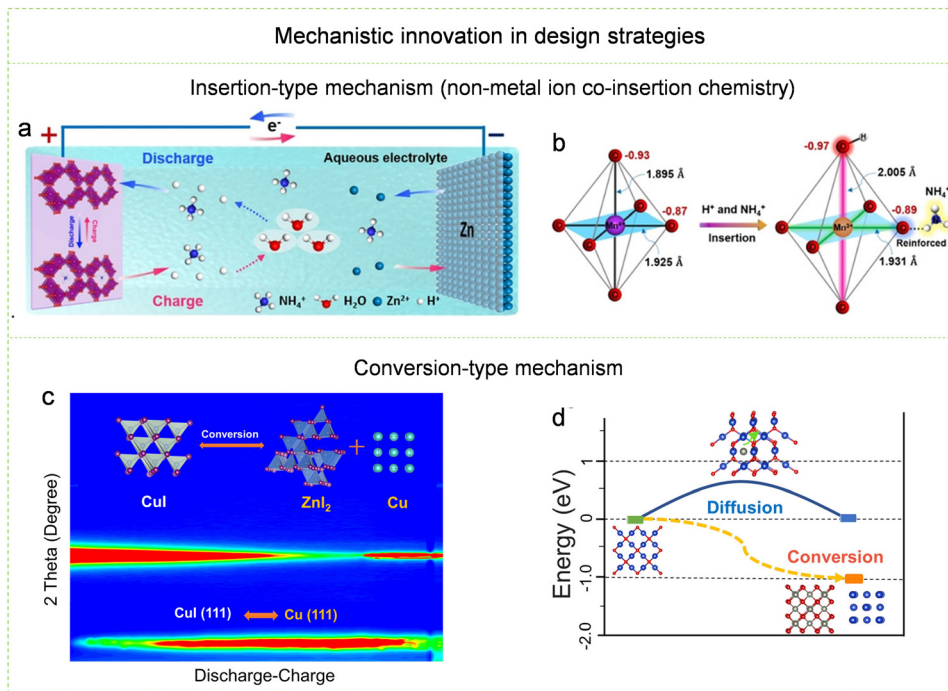
4892 | Chem. Soc. Rev., 2024, **53**, 4877–4925

This journal is © The Royal Society of Chemistry 2024

Fig. 15 Mechanism innovation in design strategies. (a) Illustration portraying the H^+/NH_4^+ co-insertion mechanism. (b) Alterations in local geometry and charge induced by the co-insertion of H^+ and NH_4^+ into MnO_2. Reproduced with permission from ref. 234. Copyright 2021 John Wiley & Sons. (c) Schematic diagram of direct conversion reaction. (d) Energy changes based on the two processes of the Zn^{2+} migration mechanism and the direct conversion mechanism. Reproduced with permission from ref. 237. Copyright 2021 John Wiley & Sons.

The paramount objective in realizing high-energy-density Zn-ion batteries is the design of batteries with elevated capacity. Through the introduction and advancement of diverse design strategies, a considerable number of Zn-ion batteries have made substantial strides in enhancing their capacity,[238] and the capacity of some Zn-ion batteries can even reach 2000 mA h g^{-1}. Achieving high-capacity performance alone is insufficient due to the inherent drawback of low working voltages (0.4–1.3 V). This limitation stems from the high ratio of the Gibbs free energy change (ΔG) to the number of electron transfers in the cathodic redox reaction (Fig. 16a).

3.2. Design strategies for high-voltage Zn-ion batteries

3.2.1. Exploiting cathode materials with high working voltage. In contrast to Zn-ion batteries with high capacity, the progress of high-voltage Zn-ion batteries hinges on two crucial components: attaining a high electrode voltage and utilizing electrolytes with a broad electrochemical stability potential window. However, these two aspects often impose constraints on each other.[57,239] Though diverse electrode materials with elevated discharging potentials, like Prussian blue material (PBA), have been investigated, it is common for these cathode materials to incorporate certain amounts of inactive components.[240] Fundamentally, while this hybrid molecular structure significantly diminishes the capacity of the cathode material, it proves indispensable for ensuring the stability of high-voltage redox reactions and maintaining the overall structure. In order to overcome the limitation of low capacity of PBA due to its single redox active center, multiple high-voltage redox components can be introduced into PBA

simultaneously, such as the $CoFe(CN)_6$ cathode material that simultaneously possesses a high-voltage Fe^{2+}/Fe^{3+} redox reaction center and a high-voltage Co^{2+}/Co^{3+} redox reaction center. The incorporation of Co species facilitates a high operating voltage of 1.75 V, while also endowing this cathode material with a commendable capacity of 173 mA h g^{-1}.[66] Nevertheless, modifying cathode materials with their own high capacities to achieve high voltages has proven challenging, given the requirement for high-voltage redox active groups to bind to specific anions (e.g. $Fe(CN)_6^{3-}$, PO_4^{3-}, PO_4F^{4-}).

3.2.2. Electrolyte optimization strategy. For traditional Zn-based batteries (such as alkaline $Zn–MnO_2$, $Zn–NiOOH$, and $Zn–Ag_2O$), alkaline aqueous solution is usually used as the electrolyte. Studies have indicated that substituting the alkaline aqueous electrolyte with a milder alternative can significantly enhance the operating voltage of Zn-ion batteries. In comparison to alkaline electrolytes, the Co^{3+}-rich Co_3O_4 material demonstrates an elevated operating voltage (1.8 vs. 1.5 V) and an enhanced capacity of 200 mA h g^{-1} in non-alkaline electrolytes.[241] In comparison to organic electrolytes, the electrochemical stability potential window of aqueous electrolytes is governed by both the cathodic OER and the anodic HER (Fig. 16b).[242] However, owing to the inherently low theoretical decomposition potential of water (1.23 V vs. SHE), the practical output voltage of conventional aqueous Zn-ion batteries seldom surpasses 2.0 V. Consequently, a major challenge in realizing high-voltage Zn-ion batteries is the limited electrochemical stability potential window. An effective strategy for expanding the electrochemical stability potential window revolves around
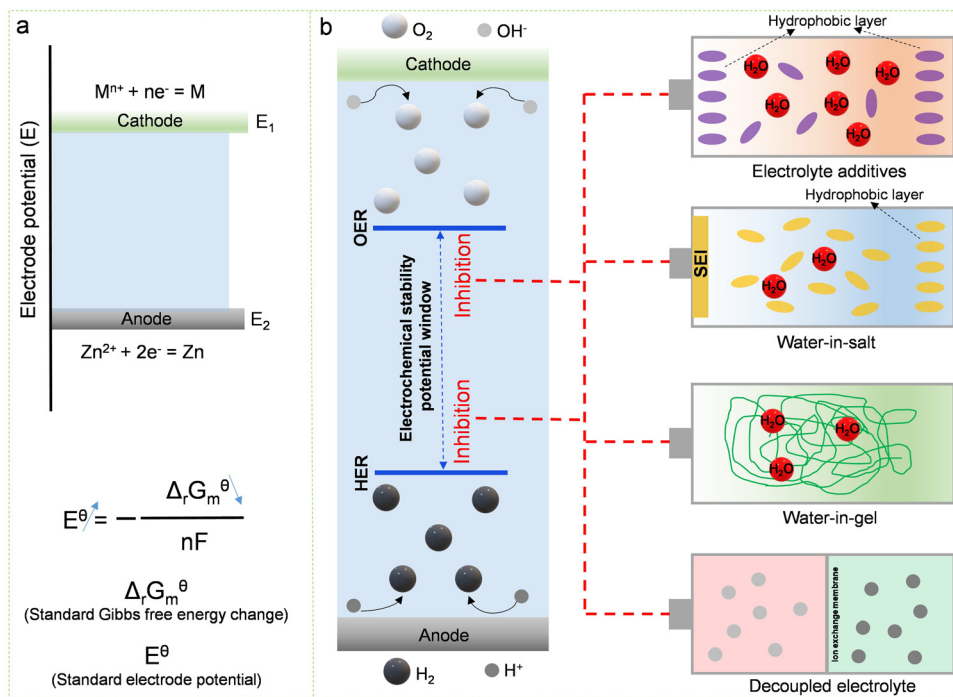
This journal is © The Royal Society of Chemistry 2024

Chem. Soc. Rev., 2024, **53**, 4877–4925 | **4893**

Fig. 16 Design strategies for high-voltage Zn-ion batteries. (a) Design principles for high potential reactions. (b) Various strategies for expanding the electrochemical stability potential window.

reducing the interaction between the electrodes and water molecules. For instance, researchers utilized high concentration (21 M) lithium bis(trifluoromethane)sulfonimide (LiTFSI) and sodium dodecyl sulfate (SDS) with a high electrochemical stability voltage window (>2.5 V) as electrolytes to achieve high operating voltage. This water-in-salt strategy serves to induce the generation of an ultra-thin hydrophobic layer on the cathode surface, effectively impeding the infiltration of H_2O (Fig. 16b).[243] However, while LiTFSI can generate a fluoride-based solid–electrolyte interphase (SEI) on the zinc electrode surface, excessive concentration can simultaneously result in reduced ionic conductivity. Addressing this challenge, the incorporation of low-concentration SDS proves beneficial. Yet, the hydrophobic layer produced by the water-in-salt strategy also hampers the diffusion of charge carriers on the electrode surface. To resolve this dilemma, the utilization of a sodium alginate hydrogel electrolyte has been reported as an effective solution. The polar groups within this type of hydrogel capture H_2O molecules, restricting their movement through hydrogen bonds. This action weakens the contact between H_2O and active materials, thereby significantly expanding the electrochemically stable potential window of the battery beyond 2.7 V.[116] Moreover, the carboxylate groups within the gel create specialized pathways for ion transfer, ensuring a sufficiently high level of ionic conductivity. Additionally, employing ion-exchange membranes to separate the electrolytes of the cathode and anode proves to be an effective strategy for expanding the electrochemical stability potential window beyond 3.0 V. This decoupling allows the anode to achieve a high concentration of OH^- to inhibit HER, while the cathode attains a high concentration of H^+ to suppress OER (Fig. 16b). Only when the electrochemical stability voltage window

of the electrolyte is sufficiently large can various high-voltage reactions be achieved in Zn-ion batteries. As an illustration, the $VOPO_4$ cathode material can engage in additional O^{2-}/O^- high-voltage redox reactions solely in the electrolyte in the form of water-in-salt.[244] Similarly, the insertion of Na^+ and the extraction of $ZnCl_4^{2-}$ at high potential also depend on the gel electrolyte and SDS. It is important to highlight that certain high-voltage reactions, particularly those involving H^+, necessitate alignment with specific electrolytes. This requirement further underscores the need for ion exchange membranes to decouple the battery. While the utilization of high-concentration electrolytes (water-in-salt) and ion-exchange membranes substantially elevates battery voltage, it is crucial not to underestimate the associated costs and environmental implications.

Currently, while high-capacity Zn-ion batteries find extensive application, only a restricted subset of high-voltage Zn-ion batteries have attained a relatively high energy density, ranging from 200 to 440 W h kg^{-1}. This is attributed to their narrow electrochemical stability potential window and inherently low theoretical capacity. It is evident that numerous challenges persist in achieving groundbreaking advancements in both high-capacity and high-voltage Zn-ion batteries due to their intrinsic limitations. Therefore, dedicated efforts are required to explore strategies that enable the simultaneous achievement of high-voltage and high-capacity Zn-ion batteries.

3.3. Design strategies for high-energy-density Zn-ion batteries

3.3.1. High-energy-density cathode materials. Certainly, the energy density of a battery is contingent upon both its capacity and voltage. Consequently, the pursuit of cathode

4894 | Chem. Soc. Rev., 2024, **53**, 4877–4925

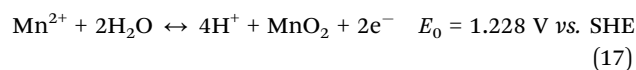This journal is © The Royal Society of Chemistry 2024

materials with elevated energy density mandates the identification of substances characterized by both high voltage and high capacity. Although some materials (such as α-MnO$_2$, MnV$_2$O$_6$, Co$_{0.247}$V$_2$O$_5 \cdot$0.944H$_2$O) have been reported to have relatively high capacities and voltages in recent years,[67,245] these electrode materials based on the insertion-type mechanism are still not considered as promising candidates for high-energy-density Zn-ion batteries. Their capacity is constrained by the inherent structure of the cathode material. For these cathode materials operating through the insertion mechanism, theoretical capacity is limited by the high mass of their active materials and low electron transfer numbers. Moreover, the actual capacity is further diminished due to restricted redox active sites, low charge transfer capabilities, and slow reaction kinetics within the cathode material's structure. Although the anode of a Zn-ion battery can offer an ideal negative electrode potential (-0.763 V), the cathode's slow redox reactions result in a low positive electrode potential. Consequently, the overall Zn-ion battery exhibits a low operating voltage. In light of these challenges, exploring and optimizing new storage mechanisms characterized by multiple electron transfers, low active material mass, and high electrode potential are deemed effective strategies for achieving high-energy-density Zn-ion batteries.
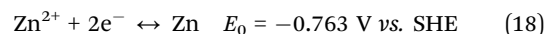
3.3.2. Optimizing the conversion reaction mechanism. Compared with cathode materials based on the insertion-type mechanism and the coordination-type mechanism, the cathode materials based on the conversion-type mechanism have greater advantages and adjustability in terms of the electron transfer number, active material mass, and electrode potential. For Zn//MnO$_2$ batteries, the cathode performs the redox process based on the insertion-type mechanism under normal alkaline conditions. The inherent structural limitations of insertion-type cathode materials pose significant challenges in realizing high-energy-density Zn//MnO$_2$ batteries. To address this issue, in 2019, Chao *et al.* proposed an innovative approach for a Zn//MnO$_2$ battery.[246] This novel design is grounded in the MnO$_2$/Mn^{2+} conversion

mechanism and utilizes a high-concentration acid (pH < 1) as the electrolyte, aiming to achieve a Zn//MnO$_2$ battery with high energy density. The newly proposed conversion mechanism based on MnO$_2$/Mn^{2+} is depicted in eqn (17)–(19). Leveraging the high theoretical capacity (616 mA h g^{-1}) and theoretical electrode potential (1.991 V *vs.* Zn^{2+}/Zn), this battery attains an exceptionally high practical capacity (570 mA h g^{-1}), a substantial output voltage of 1.95 V, and an unprecedented energy density of 1100 W h kg^{-1} (Fig. 17a). This strategy of optimizing the conversion-type mechanism opens up new ways to increase energy density.

Cathode:

$$Mn^{2+} + 2H_2O \leftrightarrow 4H^+ + MnO_2 + 2e^- \quad E_0 = 1.228 \text{ V } vs. \text{ SHE} \tag{17}$$

Anode:

$$Zn^{2+} + 2e^- \leftrightarrow Zn \quad E_0 = -0.763 \text{ V } vs. \text{ SHE} \tag{18}$$

Overall:

$$Zn^{2+} + 2H_2O + Mn^{2+} \leftrightarrow Zn + MnO_2 + 4H^+ \quad E = 1.991 \text{ V } vs. \text{ Zn/Zn}^{2+} \tag{19}$$
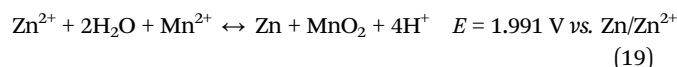
While the MnO$_2$ dissolution/deposition process within the MnO$_2$/Mn^{2+} conversion mechanism opens up new possibilities for high-energy-density Zn-ion batteries, it introduces the complexity of a liquid–solid phase reaction. To navigate this complexity, effective design strategies for the liquid–solid phase interface become crucial.[247] Examining the MnO$_2$ dissolution/deposition process during charge and discharge reveals two elementary reactions: MnO$_2$ to Mn^{3+} and Mn^{3+} to Mn^{2+}. Consequently, the diffusion and aggregation of Mn^{2+}, Mn^{3+}, and H$^+$ at the liquid–solid interface significantly impact the discharging voltage and platform of the Zn//MnO$_2$ battery. It is noteworthy that during discharge, the ion insertion mechanism may prevail over the conversion mechanism. The reversible
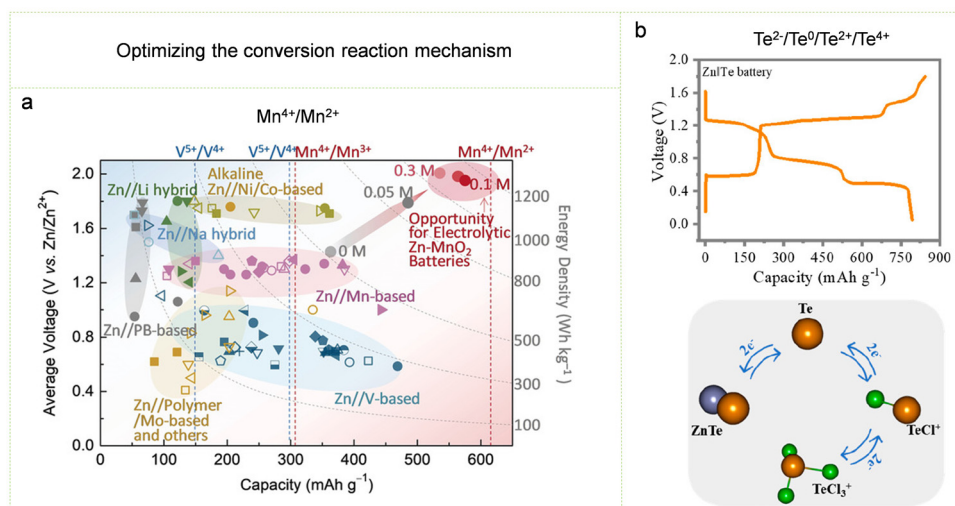
Fig. 17 Optimizing the conversion reaction mechanism. (a) Performance comparison of various Zn-based batteries. Reproduced with permission from ref. 246. Copyright 2019 John Wiley & Sons. (b) Charging and discharging curves of Zn//Te batteries and schematic diagram of their six-electron reversible transfer chemistry. Reproduced with permission from ref. 264. Copyright 2023 American Chemical Society.

This journal is © The Royal Society of Chemistry 2024

Chem. Soc. Rev., 2024, **53**, 4877–4925 | **4895**

MnO$_2$ deposition/dissolution capability is intricately tied to the specific surface area of the current collector and the number of redox active sites. To optimize performance, precautions should be taken to avert the excessive generation of a MnO$_2$ layer on the cathode surface. This is essential, as an overly thick MnO$_2$ layer can compromise cathode conductivity, leading to diminished reaction reversibility and sluggish reaction kinetics. At the same time, the use of strong acidic electrolytes will also cause the side reaction of HER on the zinc anode.[248] For each of the factors mentioned above, it will adversely affect the output voltage, coulombic efficiency, and energy efficiency of Zn–MnO$_2$ batteries. To circumvent the challenges associated with MnO$_2$ dissolution/deposition in Zn–MnO$_2$ batteries following the conversion mechanism, researchers typically adopt a specific battery configuration. However, this approach inevitably leads to increased volume and mass of the battery. Subsequent to the pivotal findings in this domain, numerous researchers have proposed innovative strategies. These include designing decoupled electrolytes and incorporating liquid flow devices, all aligned with the conversion mechanism, to address the aforementioned issues. These strategic designs have successfully elevated the output voltage of Zn//MnO$_2$ batteries beyond 2.0 V, achieving an extraordinary energy density ranging from 600 to 1700 W h kg^{-1}.[249,250]

While optimizing the conversion mechanism in a strong acidic electrolyte can improve the energy density of Zn–MnO$_2$ batteries, it comes with a trade-off. The strong acidic electrolyte has the drawback of corroding the electrode and inducing the side reaction of HER on the zinc anode. This underscores the importance of balancing electrolyte conditions to ensure both performance enhancement and prevention of undesired side reactions. In this regard, optimizing the conversion mechanism in a mild, less corrosive electrolyte can both achieve high energy density and increase battery durability. Conversely, employing a low-acidity electrolyte introduces its own set of challenges. The reduced acidity can also lead to low Coulombic efficiency in the battery due to the competing side reaction between OER and MnO$_2$ deposition during charging. In order to inhibit the occurrence of OER, the Mn^{2+} concentration in the electrolyte should be adjusted to a range that is conducive to the reversible MnO$_2$/Mn^{2+} reaction.[251] Following this, the researchers implemented a cathode composed of a Mn^{2+}-rich multivalent manganese oxide layer supported on carbon cloth. The presence of oxygen vacancies in this cathode material serves to diminish local oxygen mobility and restrain the onset of OER. Simultaneously, the abundance of Mn^{2+} enhances the dynamics of electron transfer.[252] In addition, the nature of anions in the electrolytes contributes to influencing the electrochemical behavior of the Zn//MnO$_2$ battery utilizing the conversion mechanism. In a mild electrolyte containing CH$_3$COO$^-$, the coordination of CH$_3$COO$^-$ facilitates the direct conversion of Mn^{2+} into MnO$_2$ during the charging process, bypassing the intermediate state of Mn^{3+}. This also greatly improves the reversibility of the battery.[253,254] However, the use of CH$_3$COO$^-$ will reduce the output voltage of the battery, so an appropriate CH$_3$COO$^-$ concentration needs to be used. In addition, adding redox mediators such as KI to the electrolyte

can promote the dissolution of residual MnO$_2$ in the electrolyte,[255] thereby promoting the output performance of Zn-based batteries. Hence, the use of redox mediators also provides a new direction for optimizing the conversion mechanism.

Additionally, beyond the mentioned MnO$_2$ cathodes relying on the conversion mechanism, diverse conversion cathodes have emerged and been investigated for Zn-ion batteries in recent years, encompassing halogens (Cl$_2$, Br$_2$, and I$_2$) and chalcogens (S, Se, and Te).[205,206,256–260] Te, one of the chalcogen elements, is used as an example to further illustrate the optimization strategy of the conversion mechanism. Given Te's plentiful valence state transitions spanning from -2 to $+4$ and its substantial intrinsic conductivity of 2×10^{-2} S m^{-1}, a Zn-ion battery employing Te as the cathode boasts an exceedingly high theoretical capacity of 1692 mA h g^{-1} (under six electron transfers) and the prospect of a high electrode potential.[261] Yet, the present Zn–Te battery, with Te as the cathode material, only demonstrates a modest output voltage of 0.59 V.[262] This low output voltage is caused by the fact that the conversion reaction of Te is limited to the redox of Te^{2-}/Te^0 rather than the expected positive valence state transition from Te^0 to Te^{n+}, which also limits the progression of the Zn–Te battery toward high output voltage and high energy density.[239,263] Recently, Zhi and his colleagues successfully activated the required reversible Te^{2-}/Te^0/Te^{2+}/Te^{4+} redox behavior and the transfer of up to six electrons by using high-concentration Cl-containing electrolytes (Fig. 17b).[264] This Zn–Te battery has three flat discharge platforms (at 1.24, 0.77 and 0.51 V respectively), and its total capacity can reach 802.7 mA h g^{-1}. In addition, a modified ionic liquid was used as the electrolyte, which improved the stability of Te^{2+}/Te^{4+} and enhanced the cycle stability, thereby achieving an impressive energy density of 542 W h kg$_{Te}^{-1}$.

3.3.3. Innovation of battery configurations. The conversion mechanism of cathode materials can be effectively optimized in strong acidic electrolytes, thereby achieving high energy density in Zn-ion batteries. However, strong acidic electrolytes will greatly corrode the zinc anode and promote the occurrence of the side reaction of HER. Therefore, a decoupling strategy is implemented to segregate the strongly acidic environment on the cathode side from the strongly alkaline electrolyte on the zinc anode side. This not only ensures high energy density while maintaining battery stability but also effectively suppresses side reactions such as HER and OER, along with mitigating excessive zinc anode dissolution. The strategy significantly broadens the electrochemical stability potential window of the battery, reaching 3.4 V. Additionally, it introduces a low anode electrode potential (Zn/Zn(OH)$_4^{2-}$, -1.199 V $vs.$ SHE) (Fig. 18a). In addition, the output performance of such decoupled cells will also be affected by the ion exchange membrane used.[265] For instance, a bipolar membrane comprising a proton exchange membrane (PEM) and an anion exchange membrane (AEM) serves the dual purpose of slowing down pH changes in the catholyte and anolyte. Simultaneously, it ensures that the catalyst Ni^{2+} remains exclusive to the cathode.[69] Additionally, while the bipolar membrane effectively reduces the distance between the cathode and the anode, its high cost and limited ion storage space render
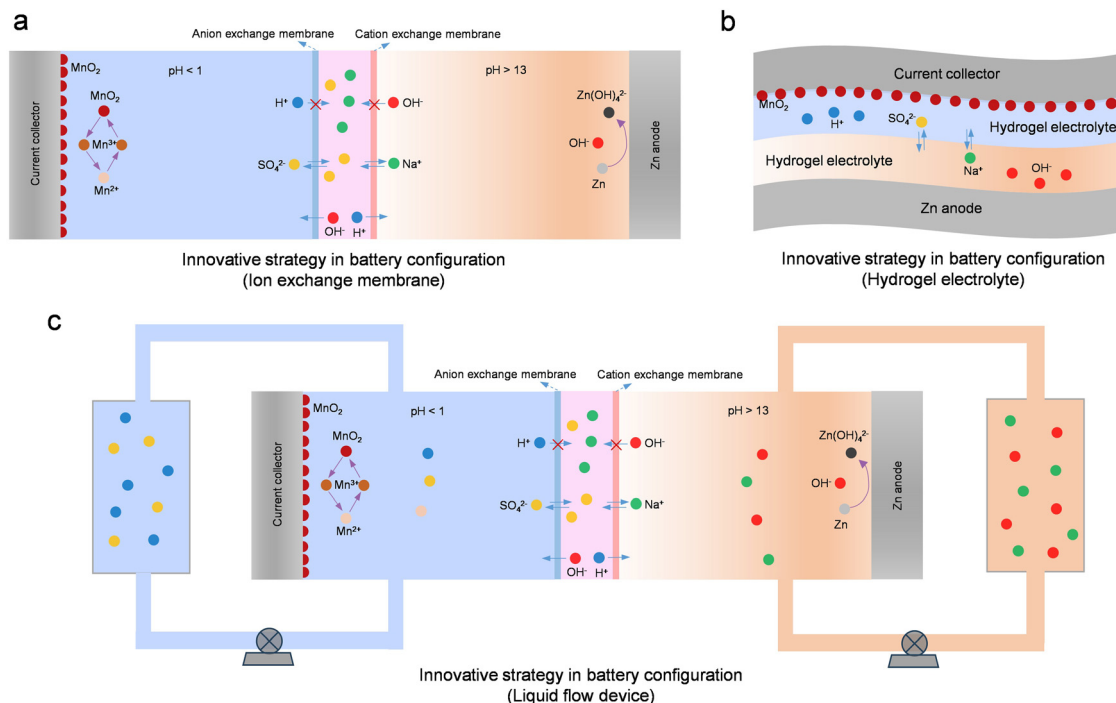
4896 | Chem. Soc. Rev., 2024, 53, 4877–4925

This journal is © The Royal Society of Chemistry 2024

Fig. 18 Innovative strategies in battery configuration. (a) Decoupled battery based on the ion exchange membrane. (b) Hydrogel-based decoupled battery. (c) Decoupled batteries using liquid flow devices.

the Zn//MnO$_2$ battery, configured with two membranes and three chambers, unsuitable for consumer electronics applications. But because the middle neutral chamber of this battery can hold enough ions for transport, this battery can provide a high discharge capacity of up to 3000–6000 mA h. Therefore, Zn-ion batteries with this configuration are regarded as the most promising solution for large-scale energy storage, specifically for storing electricity generated by wind and photovoltaic power systems.[24,68,266]

While ion exchange membranes effectively decouple the electrolyte in Zn-ion batteries, their high cost significantly limits their widespread application. The use of low-cost hydrogels instead of ion exchange membranes offers a promising approach to decoupling electrolytes (Fig. 18b). Because the water content in the hydrogel is relatively low, the ion mobility inside it is relatively low. Therefore, the zinc anode and cathode can be effectively separated even without the use of the ion exchange membrane.[267] At the same time, because hydrogel materials have the advantages of mechanical flexibility and good electrochemical stability, Zn-ion batteries using hydrogels as the electrolyte have a great practical application value, such as being used as flexible and wearable batteries.[267,268] Moreover, employing a decoupled hydrogel electrolyte can effectively augment the operating voltage and energy density of battery devices. For instance, in a Zn//MnO$_2$ battery utilizing hydrogels as the electrolyte, its operating voltage can reach 2.4 V, and the energy density can reach an impressive 1700 W h kg^{-1}.[249] Yet, when utilizing a hydrogel electrolyte, addressing challenges like compromised battery cycle stability and diminished voltage efficiency arising from the crossover of cathode and anode ions is imperative.

While ion exchange membranes and hydrogel electrolytes can effectively decouple battery devices, ion crossover between the anode and the cathode poses a persistent challenge. Throughout the battery's charging and discharging processes, water in the electrolyte decomposes into OH$^-$ and H$^+$. Driven by the electric field, H$^+$ passes through the cation exchange membrane, neutralizing the alkaline electrolyte, while OH$^-$ moves through the anion exchange membrane, neutralizing the strongly acidic electrolyte. Therefore, strategies are needed to further address the ion crossover problem. In this regard, integrating the respective advantages of flow batteries and decoupled batteries provides a very promising strategy to avoid ion crossover (Fig. 18c). In recent years, various high-energy-density Zn-ion batteries based on this integration strategy have been proposed, such as Zn//Br$_2$, Zn//MnO$_2$, Zn//V, Zn//Fe, Zn//Ce, and others.[269–277] The introduction of liquid flow devices provides new possibilities for realizing high-energy-density Zn-ion batteries.

3.4. Design strategies for long-cycle-life Zn-ion batteries

3.4.1. Modification of the zinc anode. The cycle life of Zn-ion batteries is predominantly influenced by the performance of the zinc anode. In the context of zinc anodes, three critical challenges affecting cycle stability – namely, dendrite formation, HER, and passivation – arise during the redox cycles of Zn-ion batteries, consequently diminishing the overall cycle longevity of these batteries (Fig. 19a).[70,73,278–283] Generally speaking, zinc dendrites exhibit a needle-like morphology, and their needle-like tips can provide charge centers for subsequent dendrite growth and gather positive and negative ions
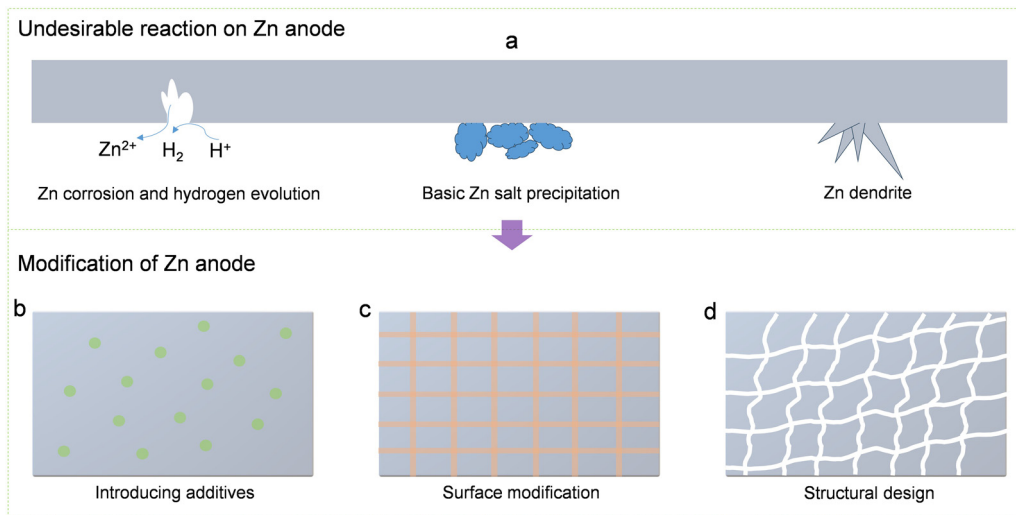
This journal is © The Royal Society of Chemistry 2024

Chem. Soc. Rev., 2024, **53**, 4877–4925 | **4897**

Fig. 19 Modification of the zinc anode. (a) Summary of undesirable reactions on Zn anodes. (b) Illustration depicting the introduction of additives on the Zn anode. (c) Schematic diagram of surface modification of the Zn anode. (d) Schematic diagram illustrating the structural design applied to the Zn anode.

with higher ion concentrations to form more and more zinc dendrites. When harmful dendrites grow to a certain extent, zinc dendrites may pierce the separator, leading to serious consequences such as battery short circuit. Throughout the charging process of the Zn-ion battery, the water in the electrolyte undergoes a HER reaction on the Zn anode, driven by the reduction potential. This HER reaction significantly diminishes the coulombic efficiency of the Zn-ion battery, and the substantial production of hydrogen inevitably elevates the internal pressure within the battery. Concurrently, the HER side reactions generate a substantial number of OH^- ions near the zinc anode, resulting in the generation of irreversible by-products like $Zn(OH)_2$, ZnO, and $Zn_4(OH)_6SO_4 \cdot nH_2O$ on the electrode surface.[71,72,284] Irreversible by-products cover the surface of the zinc electrodes, preventing subsequent reactions from occurring and passivating the zinc anode. To enhance the overall cycle life of the Zn-ion battery, it is imperative to address the challenges associated with the zinc anode. One effective strategy involves the introduction of specific additives into zinc anodes, a straightforward yet impactful approach for enhancing anode reversibility (Fig. 19b). The incorporation of these additives mitigates issues related to zinc dendrite growth, suppresses HER side reactions, and moderates surface passivation. For instance, the introduction of metallic mercury as an additive into a zinc anode proves effective in inhibiting HER side reactions and self-corrosion, leveraging mercury's inert nature towards hydrogen evolution. Although the introduction of mercury can effectively suppress the side reaction of HER, due to its high toxicity and environmental problems, the use of mercury in many battery products has been banned. As an alternative to the potentially harmful mercury, various elements like Sn, Bi, Ni, In, and N are introduced as additives into zinc anodes. This strategic inclusion serves to inhibit the side reaction (HER) and enhance the reversibility of the Zn electrode.[80,285–288] Moreover, incorporating certain metal oxides like Bi_2O_3, BaO, $Ca(OH)_2$, $In(OH)_3$, and

$[Zn_4Al(OH)_{10}]_2(CO_3) \cdot nH_2O$, among others, as additives to the zinc anode has demonstrated effectiveness in suppressing the HER and improving the performance of Zn anodes.[95] The above-mentioned metal/nonmetal elements or metal oxides have a higher hydrogen overpotential than zinc, so the introduction of these substances can effectively suppress the HER side reaction. For instance, by incorporating Bi_2O_3 as an additive to the zinc anode, Brousse et al. employed in situ XRD technology to demonstrate the attainment of uniform Zn^{2+} deposition. This was attributed to the reduction of Bi_2O_3 to metallic bismuth prior to Zn^{2+} deposition, establishing a nanoscale conductive network that optimized current distribution.[289] Incorporating carbon materials, like activated carbon or carbon black, into zinc anodes as additives is recognized as an effective strategy to prevent passivation and enhance the reversibility of zinc anodes. For example, Li and colleagues demonstrated that the introduction of activated carbon as additive into zinc anodes can significantly inhibit the production of irreversible by-product $Zn_4SO_4(OH)_6 \cdot nH_2O$, thereby improving the reversibility of the zinc anode.[290] At the same time, researchers also found that these activated carbons with rich pore structures can also accommodate the deposition of irreversible by-products and Zn dendrites to a certain extent, thereby helping to improve the cycle life of Zn-ion batteries.

Surface modification of electrodes emerges as a very effective strategy for enhancing the cycling stability of the Zn anode (Fig. 19c). This approach enhances the accessibility of the zinc anode bulk and surface, mitigates the occurrence of side reactions, and augments the reversibility of the zinc anode.[71,291–306] In recent years, researchers have formulated diverse protective layers, encompassing organic materials, metals, and metal compounds, to improve the longevity of the Zn-ion battery by modifying zinc anodes. Notably, Kang and co-workers used a $CaCO_3$ coating with porous structure as a protective layer for the zinc anode to achieve uniform zinc stripping/plating.[307] This

4898 | Chem. Soc. Rev., 2024, **53**, 4877–4925

This journal is © The Royal Society of Chemistry 2024

approach proves effective in suppressing zinc dendrite growth, preventing short circuits, and ultimately enhancing the cycle stability of Zn-ion batteries. The zinc anode coated with a porous nano-CaCO$_3$ layer was then assembled into a Zn–MnO$_2$ battery. This coated zinc anode exhibited remarkable performance in capacity retention, delivering 177 mA h g^{-1} even after 1000 cycles at a current of 1 A g^{-1}. In stark contrast, a battery assembled with a pure Zn anode under identical conditions provided a lower capacity of 124 mA h g^{-1}. In addition, Mai *et al.* used atomic layer deposition technology (ALD) to successfully coat an ultra-thin TiO$_2$ layer on the zinc anode.[308] The amorphous TiO$_2$ coating with high conductivity can serve as a protective layer for the zinc anodes to suppress irreversible by-products and side reactions (HER), thus promoting the cycle stability of the Zn-ion battery. The zinc electrode with a TiO$_2$ coating was incorporated into a Zn–MnO$_2$ battery, exhibiting exceptional cycle stability. It retained 85% of its capacity even after undergoing 1000 cycles at a current density of 3 mA cm^{-2}.

The design of the structure of zinc anodes plays a crucial role in achieving reversibility as it directly influences the generation of zinc dendrites, the overall structural changes of the electrodes, and the internal resistance levels (Fig. 19d).[309,310] For instance, introducing a porous structure to achieve zinc anodes with high specific surface area is beneficial to improving the contact between the Zn electrode and the electrolyte, thereby reducing ion transmission distances and significantly improving zinc utilization. Moreover, a zinc anode with high surface area minimizes the deposition overpotential of Zn^{2+}, effectively restraining the generation of Zn dendrites and the generation of the by-product. Various configurations of zinc anodes with substantial specific surface areas, including sheets, fibers, ribbons, spheres, and foams, have been documented.[311] Taking a cue from this, Rolison and colleagues crafted a three-dimensional, sponge-like zinc anode characterized by a highly porous structure, aiming to enhance the utilization of zinc anodes.[312] The three-dimensional porous structure, featuring a high specific surface area, facilitates a more uniform distribution of charge during battery charging and discharging. This design proves effective in inhibiting the growth of zinc dendrites. In addition, this three-dimensional porous structure can limit the deposition of Zn^{2+} inside the pore channels, which further reduces the generation of zinc dendrites during charge and discharge. Leveraging its distinctive three-dimensional framework, the sponge-like zinc anode exhibits a dendrite-free performance even under high-rate cycling conditions, reaching up to 188 mA h g^{-1}. Building upon this foundation, Rolison and collaborators subsequently refined this innovative three-dimensional porous sponge-like zinc anode, culminating in the development of a nickel-3D zinc rechargeable battery with high safety and high energy density.[313] In battery performance tests, the Ni-3D Zn battery was able to provide high specific energy competitive with commercial lithium-ion batteries. In addition, this Ni-3D Zn battery can achieve ultra-long cycle life and therefore has a great practical value.

3.4.2. Electrolyte optimization strategy. Because battery stability is closely related to the electrolyte, finding a suitable electrolyte system is crucial to achieving long-cycle-life Zn-ion batteries.[284,314–338] The cycling stability of Zn-ion batteries is significantly affected by the type and concentration of the zinc salt in the electrolytes. Presently, a myriad of zinc salts, like ZnSO$_4$, Zn(CH$_3$COO)$_2$, ZnCl$_2$, ZnF$_2$, Zn(ClO$_4$)$_2$, Zn(NO$_3$)$_2$, and Zn(CF$_3$SO$_3$)$_2$, have been explored and developed for use in Zn-ion batteries.[339] Among these reported zinc salts, the wide application of ZnCl$_2$ and ZnF$_2$ is limited due to their low solubility. For Zn(NO$_3$)$_2$, because nitrate ions are strong oxidants that can cause electrode corrosion, Zn(NO$_3$)$_2$ is rarely used.[340] In addition, Zn(CH$_3$COO)$_2$ cannot provide better battery performance and Zn(ClO$_4$)$_2$ has a high zinc dissolution/deposition overpotential, which also limits the further application of these two types of zinc salts. Therefore, the most commonly employed zinc salt at present is ZnSO$_4$, because it has the advantages of cheap price and high solubility in water, and can provide the possibility of realizing high battery stability. However, ZnSO$_4$ solution as the electrolyte of Zn-ion batteries will produce Zn$_4$(OH)$_6$SO$_4$·nH$_2$O, which will lead to the loss of battery capacity.[341] Recent research indicates that Zn(CF$_3$SO$_3$)$_2$ serves as a promising electrolyte for Zn-ion batteries. In a study by Chen *et al.*, electrochemical tests under identical conditions revealed that the CV curves conducted in a 1 M Zn(CF$_3$SO$_3$)$_2$ solution displayed a reduced peak spacing corresponding to zinc deposition/dissolution and a higher peak current density compared to those tested in a 1 M ZnSO$_4$ electrolyte.[31] These findings suggest that employing the Zn(CF$_3$SO$_3$)$_2$ electrolyte is advantageous for improving battery reversibility. This phenomenon can be attributed to the voluminous nature of CF$_3$SO$_3^-$, which limits the presence of H$_2$O around zinc ions and diminishes the solvation effect. Consequently, this promotes charge transport and transfer. Therefore, enhancing zinc salt concentration proves effective in bolstering the cycle stability of Zn-ion batteries by curbing water splitting activity and related irreversible side reactions. However, it is crucial to strike a balance, as excessively high electrolyte concentrations lead to heightened solution viscosity, resulting in reduced ionic conductivity. Moreover, the cost of high-concentration zinc salts, although beneficial, remains a factor that needs consideration for widespread adoption. In a recent development, Xu and colleagues devised a high-concentration electrolyte comprising 20 mol L^{-1} LiTFSI and 1 mol L^{-1} Zn(TFSI)$_2$.[280] This electrolyte can achieve dendrite growth-free cycling with nearly 100% coulombic efficiency during the redox process. Its application in a Zn–LiMn$_2$O$_4$ battery demonstrates an exceptional energy density of 180 W h kg^{-1}, with capacity retention exceeding 80% after over 4000 cycles. The synergy between experimental findings and theoretical simulations indicates that elevated TFSI$^-$ concentrations foster the creation of a tight ion pair (Zn-TFSI)$^+$ between Zn^{2+} and TFSI$^-$. Concurrently, it inhibits the formation of (Zn-(H$_2$O)$_6$)$^{2+}$, thereby enhancing the cycling stability of Zn-ion batteries.

Moreover, the introduction of additives into the electrolyte is another avenue to enhance the cycle stability of Zn-ion batteries. For instance, the inclusion of MnSO$_4$ in the ZnSO$_4$ electrolyte serves as an effective measure to prevent the cathode from dissolving in the Zn–MnO$_2$ battery.[125] Furthermore, incorporating additives proves instrumental in addressing issues

This journal is © The Royal Society of Chemistry 2024

Chem. Soc. Rev., 2024, **53**, 4877–4925 | **4899**

related to Zn anodes that impact battery cycle stability, including the generation of Zn dendrites, the occurrence of HER, and the formation of by-products.[286,342–346] Various types of additives (such as dimethyl sulfoxide,[347] polyacrylamide,[348] arginine,[349] polyethylene oxide,[350] urea,[351] lignin sulfate,[352] *etc.*) have been reported to be feasible for improving the cycle stability of the battery. For example, Hu and colleagues added nontoxic xylitol as an additive to the traditional $ZnSO_4$ electrolyte to achieve dendrite-free stripping/plating of zinc metal anodes.[344] According to experimental tests and theoretical simulations, the introduction of a small amount of xylitol (100 mM) effectively regulates the interaction between Zn^{2+} ions, H_2O molecules, and SO_4^{2-} ions through the rearrangement of hydrogen bonds. Concurrently, xylitol molecules exhibit a preference for adsorption on the zinc surface, creating a shielding buffer layer that delays sedimentation and hinders the planar diffusion of Zn^{2+} ions. For batteries containing xylitol molecules, their cycle stability is significantly better than the cycle stability of batteries that do not use additives. How to stabilize the pH environment between the electrode and the electrolytes while suppressing dendrite growth and side reactions is also a key point in achieving the high cycle stability of Zn-ion batteries. In a recent study, Parkin and collaborators introduced a multifunctional additive, ammonium dihydrogen phosphate, which not only suppressed the generation of Zn dendrites and side reactions but also maintained a stable pH environment (Fig. 20).[353] Electrochemical investigations, coupled with theoretical calculations, reveal that NH_4^+ in the additive exhibits a preference for adsorption on the zinc electrode surface, creating a "shielding effect" that diminishes contact between the zinc electrode surface and H_2O. Additionally, the interaction between $(H_2PO_4)^-$ and NH_4^+ contributes to pH stabilization at the electrode–electrolyte interface. This multifunctional additive facilitates highly reversible zinc plating/stripping behavior in Zn//Zn and Zn//Cu cells.

3.4.3. Cathode modification. For some organic small molecule compounds with redox active centers, although their solubility in aqueous electrolytes is low, their reduction products are usually easily dissolved in the electrolyte after battery discharge. The solubility of these organic small molecules, along with their corresponding reduction products, in the electrolyte significantly influences the cycle life of the Zn–organic battery. Therefore, using appropriate methods to avoid the solubility problems of small organic molecules and their corresponding reduction products is an effective strategy to improve battery cycle stability. In this regard, linking or grafting small organic molecules onto the polymer backbone provides a promising way to avoid the dissolution of organic molecules. Because polymers have high molecular weight, their solubility in aqueous electrolytes is generally very low. At the same time, this grafting method does not affect the redox active centers of small organic molecules. In other words, the use of polymer molecules as carriers not only reduces the solubility of small organic molecules but also maintains their own redox activity. As an illustration, a Zn-ion battery incorporating poly(1,5-naphthalenediamine) as the polymer electrode material demonstrates remarkable endurance, retaining 91% of its initial capacity even after 10 000 cycles at a substantial current density of 10 A g^{-1}.[354] In addition to using chain polymers as carriers, small organic molecules with redox active centers can also be grafted onto covalent organic framework materials (COFs). Utilizing COFs as carriers endows small organic molecules with the advantageous attributes of high specific surface area and exceptional stability inherent to COFs. This enhancement facilitates the swift transport of ions during charge and discharge processes, contributing to an extended cycle life.[355–360] As an illustration, Kurungot and colleagues employed a hydroquinone-linked β-ketoenamine COF as zinc ion anchors in Zn–organic batteries.[361] Owing to the high porosity and stable
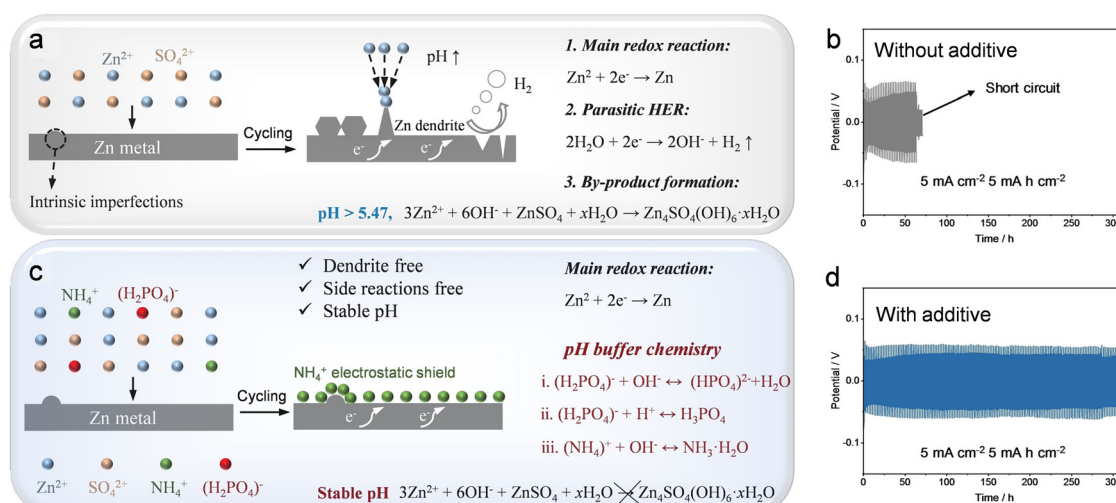
Fig. 20 Optimization of electrolytes using additives. (a) Schematic diagram of the zinc deposition process in a 1 M $ZnSO_4$ electrolyte. (b) Cycle performance of Zn//Zn symmetrical batteries in 1 M $ZnSO_4$ electrolytes. (c) Schematic diagram of the zinc deposition process in 1 M $ZnSO_4$ and additive electrolyte. (d) Cycle performance of Zn//Zn symmetrical batteries in 1 M $ZnSO_4$ and additive electrolyte. Reproduced with permission from ref. 353. Copyright 2023 John Wiley & Sons.

4900 | *Chem. Soc. Rev.*, 2024, **53**, 4877–4925

This journal is © The Royal Society of Chemistry 2024

structure of the COF, the battery maintains an impressive 95% of its initial capacity after enduring 1000 cycles at a substantial current density of 3750 mA g^{-1}.

4. Design strategies for high-performance Zn–air batteries

Zn–air batteries have garnered widespread research interest due to their remarkable theoretical energy density (1086 W h kg^{-1}), intrinsic safety associated with aqueous electrolytes and stable zinc anode, cost-effectiveness of abundant Zn ore (20 times less than Li), and the straightforward preparation, storage, and environmentally friendly nature of Zn.[47,98,362–374] Significantly, Zn–air batteries offer the potential for synergy with other energy storage systems, providing complementary advantages. In terms of commercial viability, Zn–air batteries are widely regarded as holding substantial promise, garnering extensive attention over the past decade. Despite the escalating reports on Zn–air batteries, challenges persist, including the sluggish kinetics and instability of the air electrode, limited Coulombic efficiency of the anode, and the generation of dendrites. These issues contribute to limited discharge capacity, low energy density, and shortened cycle life. To address these challenges and achieve Zn–air batteries with high performance, diverse design strategies have been proposed and developed. The subsequent sections will delve into various approaches aimed at enhancing the capacity, output voltage, energy density, and cycle life of Zn–air batteries.

4.1. Design strategies for high-capacity Zn–air batteries

4.1.1. Optimizing the actual capacity. The decline in actual capacity observed in Zn–air batteries should be attributed to factors such as sluggish kinetics of oxygen electrocatalysis (both ORR and OER), restricted contact area between the electrocatalyst and oxygen, and inadequate cathode conductivity.[94,375] Hence, enhancing the kinetics of O electrocatalysis at the electrocatalyst's surface/interface and improving the mass transfer efficiency and conductivity of the cathode electrode (as depicted in Fig. 21a) are crucial for optimizing the practical capacity of Zn–air batteries. Various strategies, including atomic-level modulation engineering and structural design, have been proposed to address these challenges.

High-performance oxygen electrocatalysts with bifunctional properties (ORR/OER) play a pivotal role in facilitating the practical application of Zn–air batteries.[376] The oxygen electrocatalytic reaction typically takes place at the three-phase interface involving gas (O$_2$), solid (catalyst), and liquid (electrolyte). The intrinsic activity of this reaction is intricately linked to the electronic structure on the surface of the solid electrocatalyst. Consequently, optimizing the adsorption/desorption behavior of the reaction intermediate, reducing the energy barrier of the reaction, and expediting OER and ORR kinetics necessitate precise tuning of the electronic structure. This underscores the significance of atomic-level modulation engineering.[377–385] Currently, numerous reports have surfaced regarding the application of atomic-level engineering strategies to improve the OER and ORR kinetics in electrocatalysts.[151,386–404] This approach aims to augment the capacity of Zn–air batteries. Various atomic-level engineering strategies, such as heteroatom doping, defect engineering, and hybrid structure construction, are considered as effective methods to promote oxygen electrocatalysis (Fig. 21b). Heteroatom doping involves the incorporation of heteroatom elements characterized by distinct
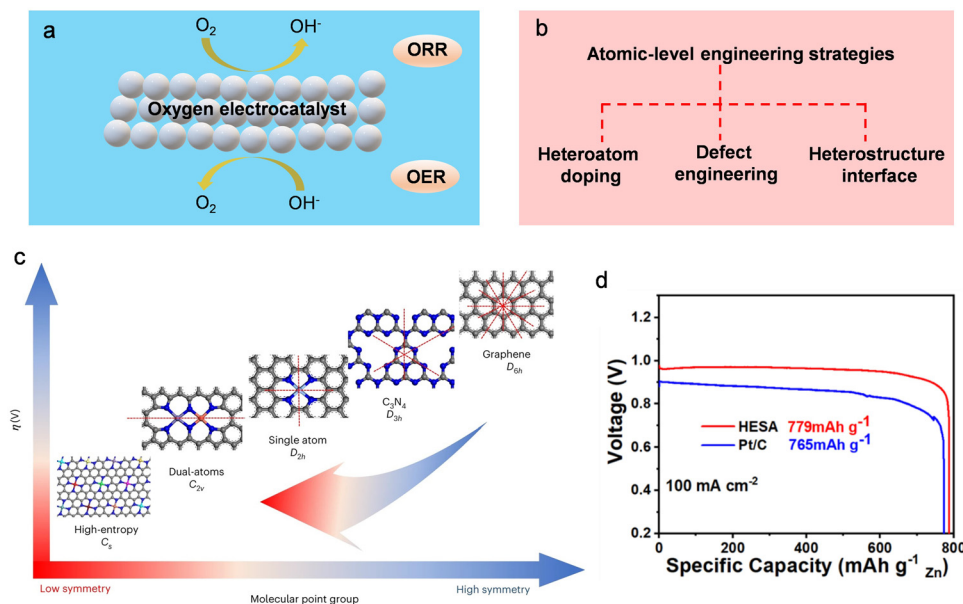
Fig. 21 Tuning the local electronic structure and surface/interface properties of oxygen electrocatalysts through atomic-scale modulation engineering. (a) The schematic delineates the operational principles governing the oxygen electrocatalyst at the three-phase interface. (b) Schematic diagram of the content of atomic-scale modulation engineering. (c) Relationship between symmetry of atomic modulation and electrocatalytic performance. (d) The specific capacity normalized with the consumed zinc for HESA and Pt/C (20%) at 100 mA cm^{-2}. Reproduced with permission from ref. 411. Copyright 2023 Springer Science & Business Media.

This journal is © The Royal Society of Chemistry 2024

Chem. Soc. Rev., 2024, **53**, 4877–4925 | **4901**

electronegativity and atomic size in the crystalline structure of the foundational electrocatalyst. This process serves to finely tune the catalyst's inherent electronic configuration, consequently influencing its catalytic performance.[405–410] As an illustration, high-entropy single-atom-doped carbon catalysts exhibit exceptional catalytic performance in both OER and ORR, surpassing the capabilities of Pt/C and RuO$_2$ catalysts.[411] Their utilization in Zn–air batteries yields significantly increased specific capacity compared to a benchmark RuO$_2$ and Pt/C electrocatalyst (779 mA h g$_{Zn}^{-1}$ versus 765 mA h g$_{Zn}^{-1}$, respectively) (refer to Fig. 21c and d). Concurrently, defect engineering stands as a widely acknowledged method for adjusting the electronic structure of host materials.[219,372,412–417] Surface defects play a pivotal role in the modulation of electron density in proximity to the Fermi level, facilitating enhanced orbital hybridization. This effect yields a surplus of unsaturated coordination sites and dangling bonds. Moreover, at the heterostructure interface, there is room for efficient adsorption of electron-donating and electron-withdrawing groups, consequently promoting rapid electrocatalytic rates characterized by high reaction kinetics.[418] Crucially, the fabrication of heterostructures stands as a rational strategy for attaining bifunctional properties in catalysts.[419]

Strategies involving atomic-scale engineering for oxygen electrocatalysts exhibit notable enhancements in OER/ORR catalytic performance,[420,421] mitigating the concentration polarization issue in Zn–air batteries. Nonetheless, the exclusive reliance on atomic engineering to modify the surface/interface of electrocatalysts falls short of fully optimizing the actual capacity of Zn–air batteries. This discrepancy arises from the variance between the operational conditions of the rotating disk electrode (RDE) and the authentic working environment of air electrodes in Zn–air batteries. In RDE tests, the swift rotation of the RDE minimizes mass transfer resistance, thereby alleviating concentration polarization and maximizing the intrinsic catalytic activity of the bifunctional electrocatalyst. In contrast, the static conditions prevalent in the air electrodes of Zn–air batteries highlight reactant diffusion resistance as a pivotal factor influencing mass transfer efficiency.[422] Despite the development of advanced OER/ORR electrocatalysts, enhancing the practical capacity of Zn–air batteries for real-world applications remains imperative. Therefore, in tandem with the atomic-scale design of oxygen electrocatalysts, a concurrent focus on optimizing the electrode structure is essential to enhance mass transfer efficiency,[423] ultimately realizing the goal of augmenting the actual capacity of the battery. Typically, air cathodes are fabricated through drop-coating or spray-coating processes, establishing a constrained two-dimensional interface between the gas diffusion layer and the electrocatalyst layer. However, the inadequacy in leveraging the active site and maintaining stable interfacial contacts renders the air cathode prone to inactive reactivity, leading to diminished battery capacity. To address this issue, Yu et al. advocated the use of asymmetric air electrodes, allowing the catalytic process to also take place inside the gas diffusion layer.[424] The asymmetric configuration of the air cathode facilitates gas diffusion and electrolyte permeation within this 3D conductive framework. This interconnected 3D framework structure markedly amplifies the active site density and expedites mass transfer. Consequently, the Zn–air battery featuring an asymmetric air cathode demonstrates an elevated capacity (800 mA h g$_{Zn}^{-1}$) compared to its symmetric cathode counterpart (749 mA h g$_{Zn}^{-1}$).

4.1.2. Innovation of battery configurations. A pivotal challenge inherent in conventional two-electrode Zn–air batteries stems from the bifunctional oxygen electrocatalyst in the air electrode. This catalyst serves dual functions, namely, facilitating the OER and the ORR. Despite the temporal distinction in the occurrence of OER and ORR during battery charge and discharge cycles, both reactions take place at the same electrode as well as entail contrasting requirements.[425–438] In kinetic terms, the efficiency of OER catalysts hinges on a superhydrophilic environment, fostering the catalytic reaction at the interface. This environment facilitates the expeditious release of O2 bubbles on the catalyst surface.[439–443] Conversely, ORR catalysts necessitate the maintenance of a relatively hydrophobic environment coupled with an efficient gas diffusion path. This configuration supports the occurrence of the OER at the gas–liquid–solid interface, preventing the submersion of active sites by water.[444–446] From a thermodynamic point of view, OER and ORR, which are mutually reversible reactions, both have high overpotentials. Hence, under highly oxidative conditions during the OER process, bifunctional catalysts are prone to oxidation, leading to a subsequent reduction in their ORR activity.[447] Simultaneously, the adsorption of reaction intermediates during the OER and ORR on the catalyst surface diminishes the available active sites. This reduction in active sites contributes to the sluggish nature of both OER and ORR reactions.[448] Presently, substantial research efforts are dedicated to crafting highly efficient bifunctional catalysts tailored for Zn–air batteries.[449] Nonetheless, the conflicting demands of the ORR and OER in cathodes remain unresolved, resulting in the majority of reported Zn–air batteries exhibiting discharge capacity below 5 mA h cm^{-2}.[450] To tackle the aforementioned challenges, researchers subsequently introduced a three-electrode configuration to augment the capacity of Zn–air batteries. This configuration incorporates two distinct air electrodes dedicated to the OER and ORR, respectively. Positioned between these electrodes is the zinc electrode. In the charging process, the OER electrode is linked to the zinc anode, while during discharge, the ORR electrode connects to the Zn anode. Dai and colleagues effectively engineered rechargeable Zn–air batteries, exploring both two-electrode and three-electrode configurations.[149] NiFe layered double hydroxide/carbon tube composites and CoO/carbon nanotube (CNT) hybrids were used as OER and ORR catalysts, respectively. Battery performance test results show that Zn–air batteries with three-electrode configurations have higher capacity than two-electrode Zn–air batteries.

An additional significant challenge encountered in two-electrode Zn–air batteries arises from the zinc anode. The formation of zinc dendrites and the occurrence of HER on the Zn electrode surface during the charging process contribute to diminished Coulombic efficiency and short circuits.[309,451]

4902 | Chem. Soc. Rev., 2024, **53**, 4877–4925

This journal is © The Royal Society of Chemistry 2024

Moreover, elevated discharge depths of the metallic zinc plate per cycle can induce uneven charging/discharging, resulting in shape alterations and irreversible damage of the Zn electrode throughout repeated cycles.[452] Recent research efforts predominantly center on developing protective layers for zinc anodes, aiming to impede dendrite growth and mitigate hydrogen evolution.[453,454] Nevertheless, these studies conducted each cycle at a low depth of discharge to extend cycling stability, a practice that fails to meet the capacity demands essential for the anode in practical Zn–air batteries.[455] Therefore, only after solving the problems of anode and cathode simultaneously, Zn–air batteries can have high discharge capacity, and then it is possible to meet the requirements of actual commercialization. To address the challenges inherent in traditional two-electrode Zn–air batteries, a three-electrode Zn–air battery was devised. This configuration includes a hydrophilic charging cathode, a hydrophobic discharge cathode, and a Zn-free anode (Fig. 22).[456] This innovative three-electrode Zn–air battery capitalizes on the decoupling of the cathode, facilitating rapid OER and ORR kinetics. The separation of cathodes allows the OER and ORR processes to unfold on distinct cathodes, preventing the oxidation of the ORR electrocatalyst. Simultaneously, a Zn-free anode, comprising tin-plated copper foam, is employed. This anode induces growth along the (002)Zn plane, effectively curbing hydrogen evolution and mitigating zinc corrosion. Consequently, the novel three-electrode Zn–air battery demonstrates an impressive high capacity of 800 mA h cm^{-2} per cycle and a minimal voltage gap between charge and discharge platforms, measuring at 0.66 V.

4.2. Design strategies for high-voltage Zn–air batteries

4.2.1. Decoupling the electrolyte. In the context of Zn–air batteries, the primary factor contributing to low output voltage is the electrolyte employed in the battery system. Typically, an aqueous solution of 6–7 M potassium hydroxide is utilized as the electrolyte for Zn–air batteries under standard conditions. This choice is made to optimize ionic conductivity and enhance both the OER and ORR kinetics.[386] In this alkaline environment, as per the Nernst equation, the theoretical voltage of the Zn–air battery is limited to 1.65 V,[457] and its usual actual operating potential is only about 1 V.[458] Compared with the operating voltage of aqueous Li–air batteries (about 3.5 V), the actual operating voltage of Zn–air batteries is only one-third.[459] In contrast, the ORR reaction in acidic electrolytes can provide a higher redox potential, resulting in a higher overall output voltage of the Zn–air battery.[460] Furthermore, in acidic electrolytes, the issue of carbonate clogging, stemming from the reaction of CO$_2$ in the air with alkaline electrolytes, can be alleviated. Nevertheless, the use of acidic electrolytes poses challenges, as metallic zinc is prone to corrosion and undergoes a vigorous hydrogen evolution reaction. Achieving a high output voltage in Zn–air batteries within acidic electrolytes necessitates meticulous optimization of the electrolyte and the implementation of adequate protection measures for the zinc anode. In this
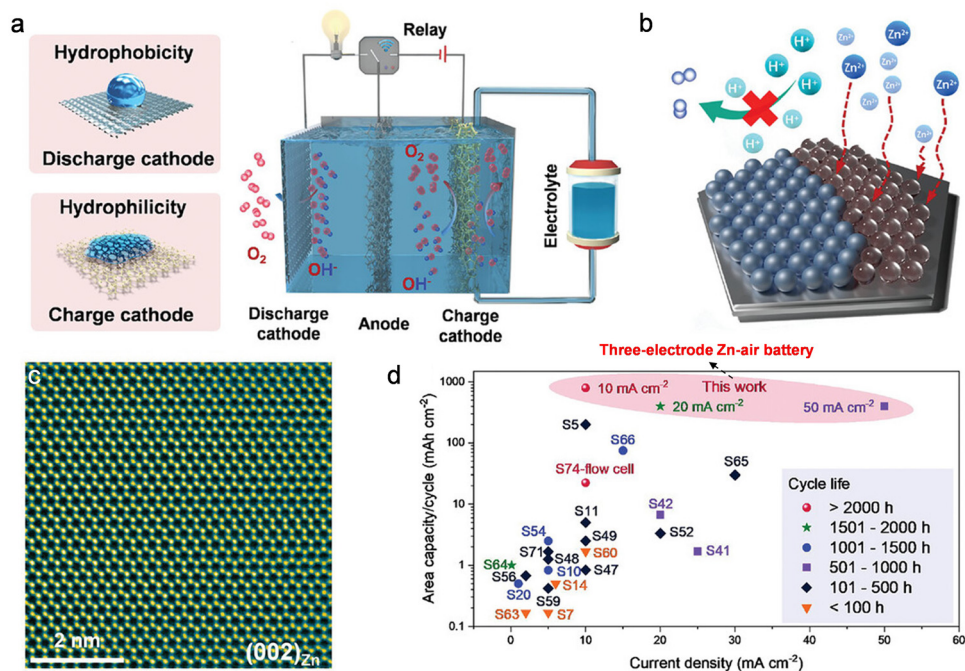
Fig. 22 Working principle and performance of three-electrode Zn–air batteries. (a) Illustration delineating the operational principle of a three-electrode Zn–air battery. Its overall structure includes three parts: a hydrophilic charging cathode, a hydrophobic discharge cathode, and a Zn-free anode. During charging, the anode is linked to the hydrophilic charging cathode, while in discharge the anode is connected to the hydrophobic discharging cathode. (b) Anode design that inhibits hydrogen evolution and produces dendrite-free (002)Zn growth. (c) High-resolution electron microscope image of (002)Zn. (d) Comparison of capacity and stability between three-electrode Zn–air battery and other Zn–air battery systems. Reproduced with permission from ref. 456. Copyright 2023 John Wiley & Sons.

context, the decoupling of electrolytes emerges as an effective strategy for realizing acidic Zn–air batteries and, consequently, attaining elevated output voltages. For example, Manthiram and colleagues reported acidic Zn–air batteries with a decoupled air cathode,[461] which is expected to eliminate the low output voltage problem of traditional Zn–air batteries (Fig. 23a–c). The decoupled Zn–air battery comprises a zinc electrode, an alkaline electrolyte on the anode side, a NASICON-type Li-ion solid electrolyte (LTAP), an acidic electrolyte on the cathode side, and a distinct air cathode featuring a Pt/C electrocatalyst dispersed on the gas diffusion layer for ORR and an IrO_2 thin film grown on the Ti mesh for OER. Within this system, the LTAP serves the primary function of separating the acidic cathode electrolyte and the alkaline anode electrolyte, concurrently establishing ion channels. While LTAP does not directly conduct Zn^{2+} ions, it acts as an ion "messenger" for Li^+, ensuring charge balance on both sides of the cathode and anode. Furthermore, the segregation of the ORR catalyst used in the discharge reaction and the OER catalyst employed in the charging reaction circumvents the oxidation of the ORR catalyst during high-voltage charging, effectively mitigating dissolution and oxidation issues associated with the ORR catalyst. On the other hand, the isolated OER catalyst does not contain carbon and binders, thus ensuring that the OER catalyst has good mechanical integrity in high-pressure oxidation environments.[462] It turns out that the implementation of the decoupling strategy can also effectively avoid the problem of carbonate produced by the reaction of alkaline electrolytes with CO_2 in the air. Significantly, this approach empowers this Zn–air battery to achieve a high voltage

of nearly 2.0 V. Nevertheless, it is pertinent to acknowledge that while utilizing solid electrolytes or other isolation membranes to decouple the electrolyte in the Zn–air battery effectively enhances the battery's output voltage, the associated costs of these solid electrolytes and membranes are typically higher.

4.2.2. Light-assisted strategy. Enhancing the output performance of Zn–air batteries through external light holds potential for sustainable utilization of renewable energy. Consequently, the utilization of light energy with the help of Zn–air batteries has garnered significant attention and interest. However, successfully integrating light energy and Zn–air batteries remains an exceptionally challenging endeavor.[463] To realize the combination of light energy and Zn–air batteries, rational selection of oxygen electrocatalysts with light-absorbing ability is essential. Confining $Ni_{12}P_5$ nanoparticles in N-doped carbon nanotubes promotes strong coupling of the two materials, and the entire hybrid material exhibits a relatively sensitive response to light irradiation.[464] Following the incorporation of the photoresponsive oxygen catalyst into a Zn–air battery, the overall battery exhibited enhanced output performance in the presence of light. In the context of light conditions, semiconductor materials with specific energy levels undergo excitation of electrons and holes, thereby facilitating reduction and oxidation reactions. For instance, photoanodes such as $BiVO_4$ or α-Fe_2O_3, when subjected to light, effectively enhance OER kinetics, resulting in a substantial reduction in the charging voltage of the Zn–air battery.[465] Notably, the Fe_2O_3 photoanode demonstrated a charging voltage of 1.43 V under illumination, significantly below the theoretical charging voltage of 1.65 V.
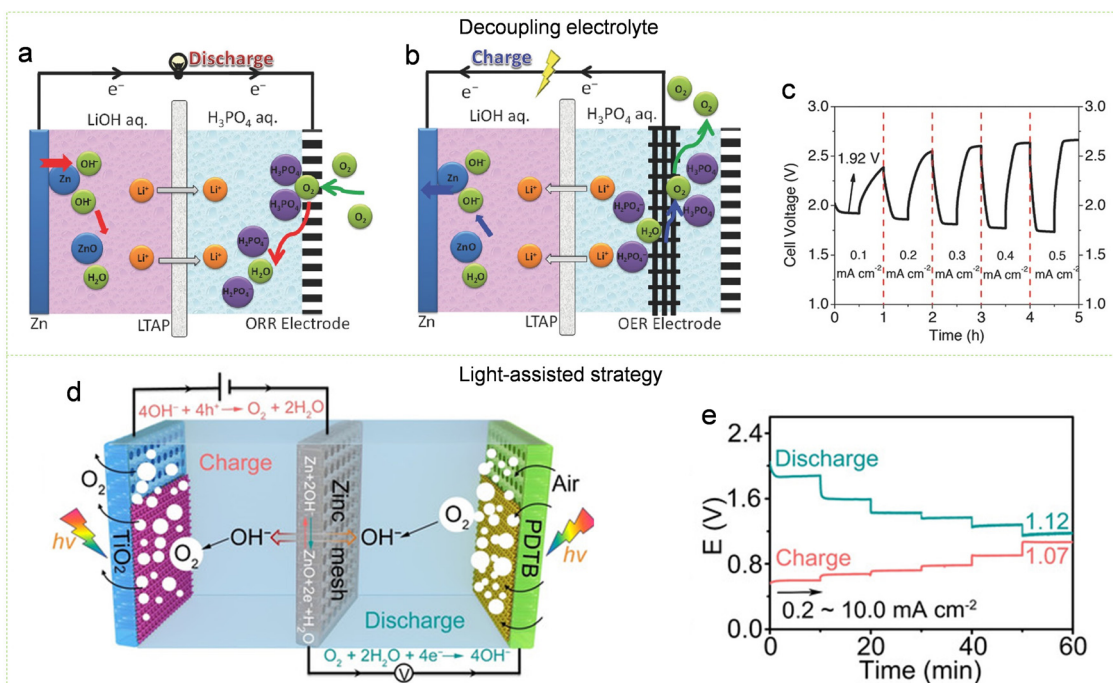
Fig. 23 Design strategies for high-voltage Zn–air batteries. (a) Schematic diagram of how a decoupled Zn–air battery works during discharge. (b) Illustration depicting the charging process of a decoupled Zn–air battery. (c) Rate performance of decoupled Zn–air batteries. Reproduced with permission from ref. 461. Copyright 2016 John Wiley & Sons. (d) Illustration delineating the operational principle of a light-involved Zn–air battery. (e) Discharging/charging curves at different current densities. Reproduced with permission from ref. 466. Copyright 2020 John Wiley & Sons.

4904 | Chem. Soc. Rev., 2024, **53**, 4877–4925

This journal is © The Royal Society of Chemistry 2024

The solar-assisted strategy effectively mitigates the high charging voltage issue in Zn–air batteries. Furthermore, leveraging additional light energy, Chen and colleagues achieved unprecedented full use of light energy throughout the discharging/charging process of a Zn–air battery (Fig. 23d and e).[466] A light-involved Zn–air battery was engineered, employing TiO_2 and poly(1,4-di(2-thienyl))benzene (PDTB) grown on carbon paper as independent cathodes. During discharge, the PDTB cathode is illuminated, exciting photoelectrons to the conduction band of PDTB, thereby facilitating the ORR process as well as elevating Zn–air battery's output voltage. Conversely, during charging, the holes in the valence band of the illuminated TiO_2 electrode are deactivated by the applied voltage and then participate in the OER process. With the aid of light, the light-involved Zn–air battery provided a remarkably low charging voltage of 0.59 V and a record-high discharge voltage of 1.90 V. Despite the effective enhancement of Zn–air battery output voltage through light-assisted strategies, research on light-involved Zn–air batteries remains limited, primarily due to the scarcity of photosensitive O_2 catalysts. Furthermore, a comprehensive understanding of the mechanisms governing Zn–air batteries involving light is currently underexplored. Nevertheless, the convergence of photochemistry, electrocatalysis, and batteries

in the utilization of light energy in Zn–air batteries represents a significant interdisciplinary research avenue.

4.3. Design strategies for high-energy-density Zn–air batteries

4.3.1. Integration strategy. In recent years, rechargeable Zn–air batteries have once again garnered significant research attention, leading to notable advancements in their development. Characterized by an exceptionally high theoretical energy density of 1086 W h kg^{-1}, these batteries also exhibit outstanding safety features. Because energy density is related to capacity and operating voltage, achieving high energy density requires increasing both capacity and operating voltage. For Zn–air batteries (Fig. 24a), they can usually achieve a high discharge capacity, but the working voltage is difficult to be further improved because their theoretical potential is only 1.65 V. Conversely, certain traditional Zn–M batteries (where M denotes a metal or metal oxide/hydroxide) may present enhanced operating voltage despite possessing a low capacity. Notably, examples like Zn–Mn, Zn–Ni, and Zn–Ag batteries exhibit this characteristic owing to their redox pairs featuring high potential. The synthesis of electrode materials that amalgamate the cathode reactions in both Zn–air and Zn–M batteries has led to the development of a hybrid Zn battery,
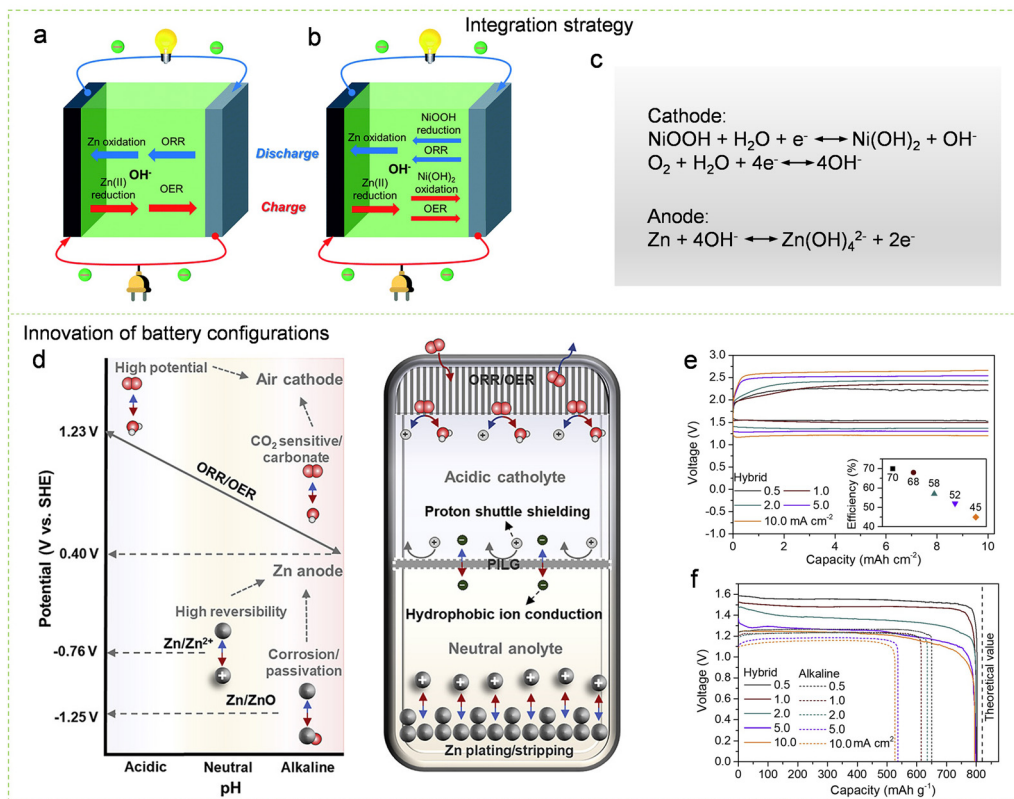
Fig. 24 Design strategies for high-energy-density Zn–air batteries. (a) A visual representation illustrating the operational principles of conventional Zn–air batteries. (b) A visual depiction outlining the operational principles of hybrid Zn–Ni/air batteries. (c) Working mechanism of hybrid Zn–Ni/air batteries. Reproduced with permission from ref. 467. Copyright 2019 Royal Society of Chemistry. (d) Schematic diagram of the design principles and working principle of decoupled Zn–air batteries. (e) Discharge and charging curves of decoupled Zn–air batteries at different current densities. (f) Comparing the discharge capacity curves of the zinc anode in decoupled Zn–air batteries and traditional Zn–air batteries at different currents. Reproduced with permission from ref. 481. Copyright 2022 Elsevier Inc.

This journal is © The Royal Society of Chemistry 2024

Chem. Soc. Rev., 2024, **53**, 4877–4925 | **4905**

characterized by a high-energy density. This innovative battery design enables the concurrent attainment of elevated capacity and operating voltage.[467–474] Fig. 24b illustrates the operational concept of the integrated Zn–air battery. Resembling the fundamental configuration of a Zn–air battery, this integrated system comprises a Zn anode, an electrolyte, and a cathode featuring active materials. Using the hybrid Zn–air/Ni configuration as an illustration, where $Ni(OH)_2$ serves as cathode's active ingredient, the cathode undergoes the faradaic redox reaction characteristic of Zn–Ni batteries, alongside the electrocatalytic oxygen reduction/oxidation reactions typical in Zn–air batteries (see Fig. 24c). During the discharge process of the integrated Zn–air battery, the initial step involves the reduction of transition metal hydroxide (NiOOH) on the cathode electrode, succeeded by the ORR. The charging process involves the sequential occurrence of $Ni(OH)_2$ oxidation and the OER. Concurrently, at the anode, Zn oxidation and Zn^{2+} ion reduction reactions occur during the redox process. The faradaic redox reaction in Zn–Ni batteries contributes to reversible pseudocapacitive current within a confined potential range. Consequently, integrated Zn–air batteries exhibit higher discharge voltages compared to their Zn–air counterparts. Simultaneously, the electrocatalytic ORR in integrated Zn–air batteries facilitates a heightened discharge capacity by leveraging ambient air oxygen. By amalgamating the merits of Zn–Ni batteries and Zn–air batteries, the integrated Zn–air batteries achieve concomitant elevation in voltage and capacity, resulting in superior energy density compared to traditional single Zn-based batteries. This integration approach holds significant appeal for various practical applications demanding high energy density, notably in electric vehicles. The augmentation of voltage is particularly advantageous for facilitating swift acceleration in electric vehicles, while enhanced energy density contributes to prolonged driving endurance. It is worth noting that while cathodic redox reactions in integrated Zn–air batteries adhere to similar principles, involving changes in the valence state of metal elements, the specific reactions differ across various metal elements. In an integrated Zn–air battery incorporating nickel (Ni), the cathode undergoes redox reactions resulting in NiOOH as the final product during the charging process. Specifically, the cathode experiences redox reactions between NiO and NiOOH or $Ni(OH)_2$ and NiOOH. Conversely, for Zn–air batteries containing cobalt (Co) or silver (Ag) elements, the ultimate products are high-valence oxides (namely, CoO_2 and AgO) formed in the redox reactions. In summary, this integration strategy effectively enhances the energy density of the Zn–air battery by amalgamating the strengths of the Zn–M battery, characterized by high discharge voltage, and the Zn–air battery, recognized for its high capacity.

4.3.2. Innovation of battery configurations. Energy density is determined by both capacity and operating voltage. Zn–air batteries typically operate with an output voltage of approximately 1 V, emphasizing the necessity of attaining elevated output voltage for achieving high energy density. The constrained practical output voltage of Zn–air batteries predominantly stems from the low redox potential associated with the oxygen reduction reaction in alkaline electrolytes. Researchers have

collectively directed their endeavors towards improving the overall performance of Zn–air batteries, with a particular emphasis on crafting catalysts for air cathodes that are both highly active and stable. Additionally, strategies such as electrode structure design and the incorporation of electrolyte additives aim to prevent the corrosion of the Zn anode.[96,475–477] While progress has been made through these strategies, fundamental challenges stemming from alkaline electrolytes persist. Recent investigations indicate that near-neutral aqueous electrolytes present a viable solution, enabling the preservation of highly reversible zinc stripping/plating behavior. This adaptation allows neutral Zn-ion batteries to manifest improved output performance.[478,479] Nevertheless, the unsatisfactory performance of neutral Zn–air batteries should be attributed to sluggish kinetics of the OER and ORR processes in neutral electrolytes. This drawback becomes particularly pronounced when considering the low battery voltages, typically around ∼1.00 V.[480] Theoretically, air electrodes demonstrate a more positive voltage of approximately 1.23 V *vs.* SHE in strongly acidic electrolytes. Zn–air batteries operating in acidic electrolytes also circumvent the issue of CO_2 poisoning. However, while the utilization of acidic electrolytes enhances the air cathode voltage, it concurrently accelerates the corrosion of the zinc anode. In this regard, decoupling electrolytes is regarded as a very promising approach to solving the above problems. By decoupling the electrolyte, a high discharge voltage can be achieved while maintaining the stability of the zinc anode. For example, Zhang and collaborators documented a hybrid Zn–air battery characterized by prolonged life and elevated operating voltage (Fig. 24d–f).[481] This hybrid Zn–air battery uses a double hydrophobic membrane with proton shuttle shielding function to decouple the electrolyte, so that the zinc anode is in the neutral electrolyte and the air cathode is in the acidic electrolyte. Hybrid Zn–air batteries operate by achieving stable electrochemical stripping and plating of Zn with neutral anolytes, coupled with high-potential oxygen redox reaction in acidic catholytes. This integration of a double-hydrophobic membrane with a proton-shuttling shielding function selectively facilitates the transport of hydrophobic bis(trifluoromethanesulfonyl)imide anions, effectively preventing the undesired cross-transport of protons. Consequently, the hybrid Zn–air battery demonstrates an exceptionally high output voltage of 1.50 V in ambient air and provides a notable energy density of 1243.6 W h kg^{-1} based on the Zn anode.

Despite the effective decoupling of the alkaline electrolyte in Zn–air batteries achieved through the use of an ion exchange membrane, the substantial cost associated with this membrane has significantly constrained its large-scale application. At this point, low-cost hydrogel electrolytes are viewed as a promising alternative.[482] Hydrogel electrolytes, owing to their comparatively low water content, impede ion migration and prevent the crossover of ions in decoupled hydrogel electrolytes. This characteristic effectively mitigates the mixing of anode and cathode electrolytes without the need for additional membranes. In addition, using hydrogel electrolytes to replace alkaline water electrolytes can form flexible and stretchable Zn–air batteries, which have broad practical application

4906 | *Chem. Soc. Rev.*, 2024, **53**, 4877–4925

This journal is © The Royal Society of Chemistry 2024

prospects in wearable devices, robots, *etc.* These types of zinc–air batteries that use hydrogels as the electrolyte are called quasi-solid-state Zn–air batteries. These quasi-solid-state Zn–air batteries mainly have two configurations: sandwich type and cable type.[156,157,483] In sandwich-type quasi-solid-state Zn–air batteries, hydrogel electrolytes are positioned between the air electrode and the zinc electrode. This configuration ensures stable performance output even when subjected to various bending or twisting conditions. Conversely, cable-type quasi-solid-state Zn–air batteries embrace a coil design, positioning the zinc electrode at the center and completely surrounded by the hydrogel electrolyte. The air electrode, featuring the catalyst layer, is encased around the outer periphery. Presently, quasi-solid-state Zn–air batteries demonstrate remarkable resilience to intricate mechanical forces and deformations. Additionally, their output performance can be customized by interconnecting battery packs in either series or parallel configurations. Despite substantial enhancements in the output performance of quasi-solid-state Zn–air batteries in recent years, the semi-open form of the air electrode poses a challenge, potentially resulting in the depletion of H_2O within the hydrogel electrolyte. The advent of all-solid-state electrolytes emerges as an appealing solution to address these issues. All-solid-state systems can deliver high energy density to the power supply in the form of bipolar stacked electrodes and provide higher volumetric energy density by reducing dead space. As an illustration, Lee and colleagues showcased a practical Zn–air pouch battery featuring a cathode composed of (101) faceted copper phosphorus sulfide [CPS(101)], coupled with an antifreeze chitosan biocellulose serving as the superionic conductor electrolyte.[484] The employed CPS(101) demonstrates exceptional activity and stability, surpassing 30 000 cycles for reversible ORR and OER. Its performance outshines the performance of Pt/C and RuO_2 catalysts. Simultaneously, the hydroxide superionic conductor, comprising polymerized chitosan biocellulose, exhibits noteworthy electrical conductivity (86.7 mS cm^{-1} at 25 °C) along with robust mechanical and chemical stability. The resulting commercially viable all-solid-state Zn–air batteries, at 1 A h scale, achieve an ultrahigh battery-level energy density of 460 W h kg$_{cell}^{-1}$ and 1389 W h l^{-1}.

4.4. Design strategies for long-cycle-life Zn–air batteries

4.4.1. Modification of the zinc anode. Presently, the anodes employed in commercial Zn–air batteries consist of a slurry derived from zinc powder. While this anode facilitates ample contact between electrolytes and zinc anodes, its reversibility is notably compromised by the generation of dendrites and the occurrence of the concurrent side reaction. Consequently, substantial endeavors have been devoted to enhancing the reversibility of zinc anodes. Building upon insights from lithium anode research in lithium metal batteries, diverse strategies have been documented to address issues related to zinc dendrites and side reactions. A commendable zinc anode, in essence, should exhibit the following attributes: (1) elevated electrical conductivity, (2) minimal HER activity, (3) outstanding electrochemical stability, and (4) a substantial affinity for zinc coupled with heightened reversibility.[485] To obtain highly

reversible zinc anodes, diverse strategies have been used to improve the electrochemical reversibility of these anodes. In this section, we will mainly introduce the two strategies of structural design of zinc anodes and modification of the zinc anode interface with additives or coatings.

By structurally designing the electrode, the zinc anode with a continuous pore network architecture can be developed, thereby enhancing the stable phase change between ZnO and Zn throughout the charge and discharge cycles. Simultaneously, the three-dimensional framework structure, characterized by its high specific surface area, elevated electronic conductivity, and fully exposed zinc affinity sites, proves advantageous for the even deposition of zinc and mitigates the risk of uncontrolled zinc dendrite proliferation.[486,487] Moreover, the utilization of zinc foam featuring a three-dimensional pore structure proves effective in mitigating passivation issues, thereby enhancing the accessibility of zinc to 90%. Compared with the traditional zinc powder, the introduction of continuous nanoporous structures into zinc electrodes has been proven to be able to effectively stabilize the electrochemical transformation between metallic Zn and ZnO, thereby exhibiting excellent battery cycle stability. For example, Chen's team synthesized a Zn electrode with a bicontinuous nanoporous structure.[488] This nanoporous zinc can stabilize the phase transition of zinc during charge and discharge while retaining a continuous network of conductive pores. Conversely, in the initial charge and discharge cycles, the zinc powder lacking a nanoporous structure exhibited a notable alteration in surface morphology. Subsequently, the nanoporous zinc anode was assembled into a Zn–air coin cell, and the electrochemical performance test results showed that the Zn–air battery with a nanoporous anode achieved enhanced charge–discharge behavior and high energy efficiency after 80 cycles.

Modifications at the anode interface, including the incorporation of additives and coatings, represent another effective strategy for enhancing the reversibility of zinc anodes.[489–491] The introduction of small amounts of additives into the zinc anode brings about a substantial enhancement in its electrochemical reversibility, resulting in the enhanced long-term cycling performance of the Zn–air battery. Specifically, incorporating carbon-based materials with expansive specific surface areas into zinc anodes offers ample zinc-philic sites for Zn nucleation. This approach helps prevent the formation of Zn dendrites, ensuring the uniform deposition of Zn^{2+} on the electrode. For example, Yang *et al.* introduced graphene into a zinc anode and prepared a Zn/graphene composite electrode.[492] This Zn/graphene composite anode can effectively prevent Zn corrosion in harsh electrolytes. Simultaneously, Zn–air batteries employing Zn/graphene composites as anodes exhibit lower overpotential and more consistent electrochemical behavior compared to Zn–air batteries utilizing pure zinc anodes over extended charge and discharge cycles. This outcome underscores the positive impact of introducing graphene additives in mitigating the self-corrosion and dendrite generation of Zn anodes. In addition, Qian and colleagues improved the reversibility of zinc during charge and discharge by coating a chemical buffer layer on the zinc metal anode.[493] Its chemical buffer layer

This journal is © The Royal Society of Chemistry 2024

Chem. Soc. Rev., 2024, **53**, 4877–4925 | 4907

is constructed by uniformly dispersing ZnO nanorods in the graphene skeleton. For the buffer layer, the adsorption affinity of graphene to zinc ions and the role of ZnO nanorods as uniformly deposited crystal nuclei cooperate with each other to achieve the purpose of reducing passivation and dissolution at the zinc anode interface, thus achieving the reversible precipitation–dissolution behavior of zinc. The integration of a zinc anode with a buffer layer into a Zn–air battery resulted in robust stability over 100 cycles, characterized by minimal voltage fluctuations. As the deposition time of Zn^{2+} increases, the zinc anode featuring a buffer layer maintains a relatively flat electrode surface, in stark contrast to the evident dendrite formation observed on the surface of the zinc electrode lacking a buffer layer. Consequently, the Zn anode with a buffer layer demonstrated an impressive long-term cycling performance, lasting for 450 hours in an alkaline Zn–air battery. Overall, this chemical buffering strategy provides new ideas and strategies for developing Zn–air batteries with long cycle life.

4.4.2. Electrolyte optimization strategy. In aqueous Zn–air batteries, the solvation structure of Zn^{2+} can be adjusted by changing the types of solvents and salts in the electrolyte. Additionally, the use of additives aids in the generation of a stable electrode/electrolyte interface.[319] Notably, the dissolution/deposition behavior of zinc electrodes is closely linked to the solvation structure of Zn ions. For instance, the addition of LiOH to the KOH electrolyte has proven effective in substantially extending the cycle life of Zn–air batteries.[494] The introduction of Li^+ into the electrolyte extends cycle life primarily by virtue of Li^+'s pivotal role in the dissociation of intermediate zincate species during the charging process, consequently mitigating the charging overpotential. Moreover, the design of water-in-salt electrolytes is regarded as an effective strategy for electrolyte modification. This approach aims to optimize the solvation structure of Zn^{2+}, thereby enhancing the reversibility of Zn. Water-in-salt electrolytes mean that the volume and mass of H_2O in the system are much smaller than that of the dissolved salt.[280] In water-in-salt electrolyte systems, the conventional solvation sheath is not established due to an insufficient number of H_2O molecules. In these systems, all available H_2O molecules actively participate in the ion solvation shell. Therefore, water-in-salt electrolytes that do not contain free water molecules can effectively suppress various side reactions caused by water during charging and discharging. However, achieving high-concentration electrolytes still faces huge challenges. Current highly concentrated electrolytes are expensive to prepare, and state-of-the-art formulations either lack zinc ions or rely on halogen salts. These factors have greatly limited the large-scale application of the water-in-salt strategy. Recently, Lu *et al.* prepared a highly concentrated aqueous electrolyte from zinc acetate, which has poor water solubility but is cheap and environmentally friendly, by introducing hydrotropic agents (such as potassium acetate, urea, acetamide).[495] This strategy provides a reference for the subsequent design of high-concentration aqueous electrolytes.

Recently, the exploration of high-concentration Zn salts, such as $ZnCl_2$, $Zn(ClO_4)_2$, $Zn(CF_3SO_3)_2$, $Zn(Ac)_2$, $Zn(OTF)_2$, $Zn(TFSI)_2$,

and $ZnSO_4$, as non-alkaline electrolytes is emerging as a promising avenue to enhance the cycling stability of Zn–air batteries.[496–501] Zn–air batteries utilizing highly concentrated non-alkaline electrolytes demonstrate superior reversibility compared to conventional alkaline Zn–air batteries, primarily attributed to the reduction of by-reactions. For example, Wang and his colleagues achieved an efficient and stable operation of Zn–air batteries using a high-concentration $Zn(OTF)_2$ aqueous solution as the electrolyte.[502] In particular, owing to the use of the high-concentration aqueous electrolyte, the traditional four-electron process in alkaline Zn–air batteries is transformed into a novel two-electron $Zn-O_2/ZnO_2$ electrochemical process. Under the influence of the electric field, hydrophobic OTF anions tend to establish a Zn^{2+}-rich/H_2O-poor inner Helmholtz layer (IHL) on the surface of the air electrode (Fig. 25a). The Zn^{2+}-rich/H_2O-poor environment, on the one hand, diminishes the opportunities for H_2O molecules to participate in electrode reactions. On the other hand, this environment also provides better contact with Zn^{2+} for the intermediate species generated by the redox reaction of the oxygen cathode. Theoretical calculations and kinetic simulation results indicate that the formation of superoxide species takes place from the weak interaction between OTF anions and Zn^{2+} in the high concentration electrolyte ($Zn(OTF)_2$). This interaction promotes the subsequent highly reversible ZnO_2 chemical reaction. Consequently, a two-electron oxygen reduction mechanism is realized in the high-concentration aqueous electrolyte instead of the four-electron oxygen reduction mechanism in alkaline electrolytes. Consequently, this non-alkaline Zn–air battery with the $Zn(OTF)_2$ electrolyte achieved stable operation for 1600 hours at a current density of 0.1 mA cm^{-2} and 160 hours at a current density of 1 mA cm^{-2} in ambient air (Fig. 25b). Moreover, Wang and colleagues engineered a H_2O-proof and Zn^{2+}-conducting SEI layer by elevating the content of the $Zn(OTF)_2$ electrolyte and incorporating trimethylethyl ammonium trifluoromethanesulfonate ($Me_3EtNOTF$) as an additive (Fig. 25c).[503] The development of this SEI layer notably enhances the electrochemical output performance of the Zn-based battery. The assembled Zn–air battery demonstrates a high energy density of 325 W h kg^{-1} and maintains robust cycling stability over 300 cycles.

4.4.3. Innovation of battery configurations. Apart from the issues of Zn dendrite generation, hydrogen production, and Zn corrosion at the Zn electrode, which impact the stability of the traditional two-electrode Zn–air battery, the conflicting demands of OER and ORR also contribute to the long-term cycling stability of the Zn–air battery. The primary reason for the influence of the ORR/OER reactions on the cycling performance of the traditional two-electrode Zn–air battery is the occurrence of the OER/ORR on the same air cathode in the discharge/charge processes.[504] In general, the open circuit voltage of Zn–air batteries in the discharge process typically hovers around 1.2 V. However, owing to the substantial overpotential associated with the OER process, the charging voltage of Zn–air batteries must be elevated to approximately 2.0 V or even higher.[97] The strong oxidizing environment during high voltage charging can cause oxidation and deactivation of the ORR catalyst. Furthermore, the gas

4908 | *Chem. Soc. Rev.*, 2024, **53**, 4877–4925

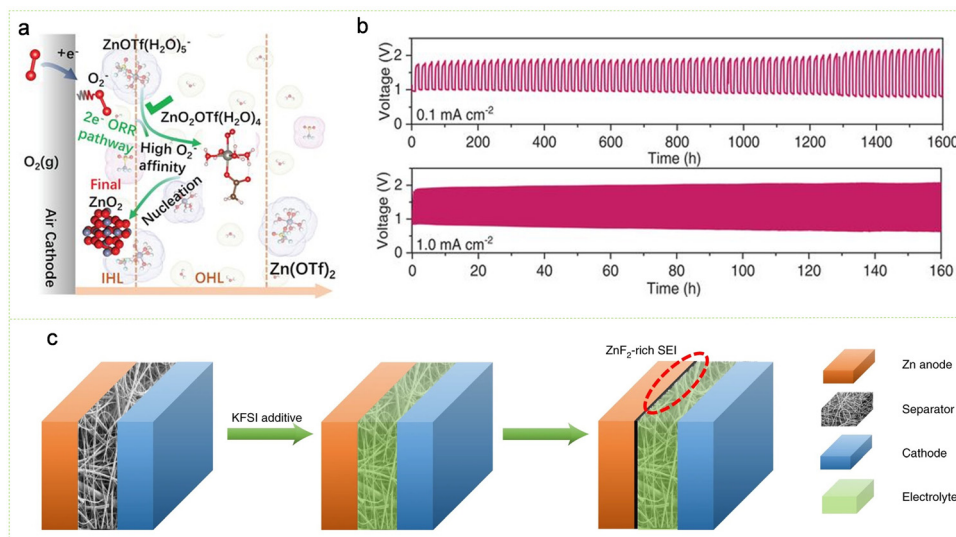This journal is © The Royal Society of Chemistry 2024

Fig. 25 Electrolyte optimization strategy. (a) Illustration outlining the reaction process of the double capacitor layer on the cathode surface in a $Zn(OTf)_2$ electrolyte. (b) Long-term cycling stability of Zn–air batteries at different current densities. Reproduced with permission from ref. 502. Copyright 2021 American Association for the Advancement of Science. (c) Schematic illustration of *in situ* generation of the ZnF_2-rich SEI layer. Reproduced with permission from ref. 503. Copyright 2021 Springer Science & Business Media.

produced during the OER in the charging process can adversely affect and compromise the electrode structure. This may result in mechanical damage to the electrode, catalyst loss, and ultimately render the battery inoperable. In addressing this issue, constructing three-electrode Zn–air batteries by segregating the OER and ORR offers an effective strategy.[150] The three-electrode configuration involves two distinct air cathodes dedicated to the OER and ORR, respectively. The zinc anode is positioned between OER electrodes and ORR electrodes. During charging, the OER electrode is connected to the zinc anode, while during discharging, the ORR electrode is connected to the zinc anode. This strategic setup proves effective in enhancing the cycling life of the Zn–air battery.

Substituting traditional alkaline aqueous electrolytes with hydrogel electrolytes proves to be an effective strategy in improving the long cycle life of Zn–air batteries.[505,506] Unfortunately, to date, the development of high-performance hydrogel electrolytes has severely lagged behind the development of bifunctional catalysts.[507] Conventional polyvinyl alcohol (PVA)-based hydrogel electrolytes encounter challenges such as low ionic conductivity, limited stretchability, and inadequate water retention capacity.[508] In order to obtain hydrogel electrolytes with better performance, researchers began to try to modify PVA. For example, combining PVA with additives with high hydrophilicity and/or alkali resistance (such as guar hydroxypropyltrimonium chloride,[509] quaternary ammonium[510]) can greatly improve the ionic conductivity and stability of PVA. In addition, if other polymers with excellent water retention capabilities, such as polyacrylic acid (PAA)[511] and polyacrylamide (PAM),[512] are combined with PVA, it can also improve the water retention capacity of PVA. As an illustration, Zhong and colleagues synthesized alkaline gel polymer electrolytes *via* multiple cross-linking reactions involving polyacrylic acid (PAA), polyvinyl alcohol (PVA),

graphene oxide, alkali, and potassium iodide (KI) (Fig. 26a).[513] The developed hydrogel electrolyte surpasses conventional PVA gel electrolytes in terms of mechanical strength, ionic conductivity, and H_2O retention capacity. Moreover, the incorporation of iodide ions alters the conventional oxygen evolution pathway on the air electrode, resulting in a thermodynamically more favorable route. With this optimized alkaline gel electrolyte, the flexible Zn–air battery achieves an extremely low charging potential of 1.69 V and maintains long-term cycling stability for 200 hours (Fig. 26b and c). Considering that the stability of a battery is determined by multiple factors, subsequent research should also invest more efforts in electrolyte design and battery configuration while developing high-performance electrocatalysts.

5. Design strategies for Zn–CO₂ batteries and other Zn-based batteries

Since the industrial revolution, the levels of CO_2 in the atmosphere have continued to rise, far exceeding the upper limit recommended by environmentalists (350 ppm).[176] At the same time, CO_2, as the main greenhouse gas and acidic gas, is closely related to the environment and ecology. High concentrations of CO_2 in the atmosphere will change the global climate and increase the acidity of the ocean, thereby causing damage to the marine ecosystem. But from another perspective, if there are suitable environmentally friendly technologies that can realize the conversion and utilization of CO_2, CO_2 will be the most abundant and cheapest C1 raw material in nature. It is noteworthy that Takechi *et al.* have recently ascertained that the incorporation of CO_2 positively influences the energy density of Li-air batteries,[514] since the presence of CO_2 contributes to the rapid consumption of superoxide anion radicals and slows
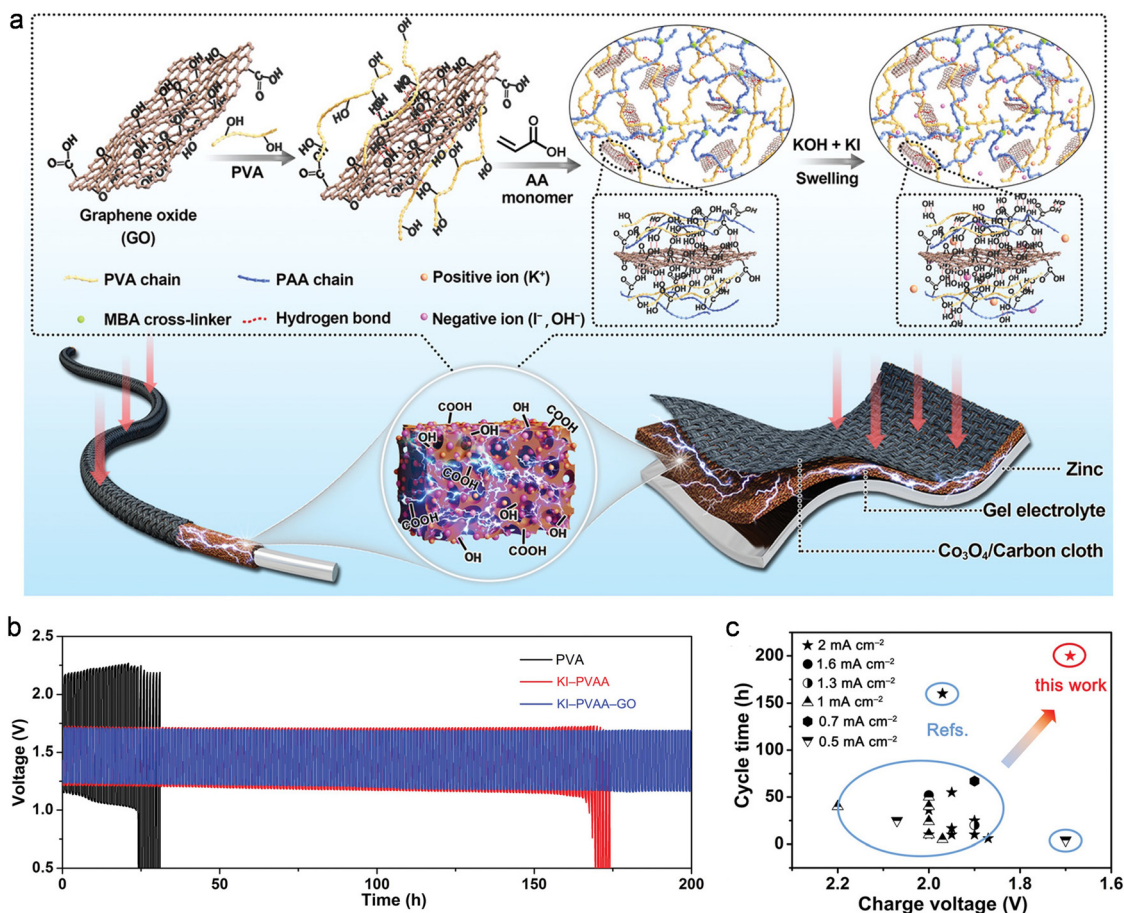
Fig. 26 Hydrogel electrolytes for long-cycle-life Zn–air batteries. (a) Diagram outlining the process of hydrogel electrolyte preparation and the corresponding configuration of the Zn–air battery. (b) Galvanostatic discharge and charge curves at 2 mA cm^{-2}. (c) Examining the disparities in cycle life and charging potential between sandwich-type KI-PVAA-GO-based Zn–air batteries and certain previously documented flexible Zn–air batteries. Reproduced with permission from ref. 513. Copyright 2020 John Wiley & Sons.

down the filling of Li_2CO_3 in the cathode. This research result shows that it is possible to design metal–CO_2 batteries and use them as a platform to convert CO_2.[164] In metal–CO_2 batteries, the typical operational mechanism involves the oxidation of the metal at the anode. Subsequently, the generated electrons are conveyed through an external circuit to the cathode, where they participate in the reduction of CO_2. Compared with commonly used CO_2 conversion and utilization technologies, metal–CO_2 battery technology is unique in that it combines CO_2 conversion with energy generation, rather than pure energy input.

Amidst the array of presently documented metal–CO_2 batteries, Zn–CO_2 batteries stand out as a promising environmentally efficient option due to their avoidance of organic electrolytes. As an emerging Zn-based battery, there are currently few reports on Zn–CO_2 batteries. Because of the chemical inertness of CO_2 molecules, current design strategies for Zn–CO_2 batteries mainly focus on the design of efficient electrocatalysts.[515–517] As an illustration, Hou and colleagues devised a gas diffusion strategy to craft nitrogen-doped porous carbon polyhedra featuring minute quantities of isolated iron atoms.[178] The optimized electrocatalyst, featuring Fe–N_3 sites, demonstrates outstanding performance in CO_2 reduction, achieving a CO faradaic efficiency of 96% at −0.5

V, coupled with remarkable stability. Its CO_2-to-CO conversion efficiency surpasses that of nearly all previously documented non-noble metal single-atom electrocatalysts relying on nitrogen-doped carbon. This exceptional performance can be ascribed to the enhanced intrinsic activity and the heightened exposure of active sites. The augmented exposure of catalytic sites results primarily from size adjustments designed to amplify the electrochemical surface area. Simultaneously, the heightened intrinsic activity stems predominantly from nitrogen species doping, inducing alterations in the electronic structure. Subsequently, the synthesized material was integrated into a Zn–CO_2 battery as a cathode catalyst, yielding robust battery performance characterized by a notable power density of 526 mW cm^{-2} and an open circuit voltage of 0.727 V. Additionally, Wang *et al.* introduced and successfully implemented a reversible Zn–CO_2 battery, capitalizing on the reversible conversion between carbon dioxide and liquid HCOOH facilitated by a bifunctional Pd cathode (Fig. 27).[179] Leveraging their abundant edge and pore structure, the three-dimensional porous Pd nanosheets, upon preparation, manifest a highly electrochemically active surface. This characteristic facilitates selective CO_2 reduction during discharging and HCOOH oxidation at low overpotential. When Pd nanosheets are assembled
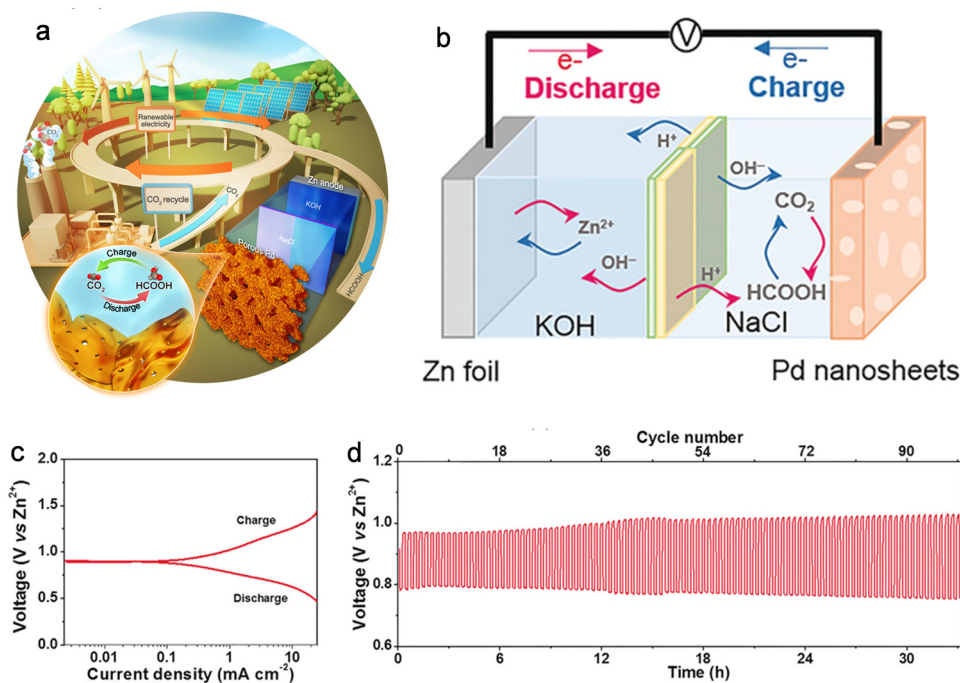
4910 | *Chem. Soc. Rev.*, 2024, **53**, 4877–4925

This journal is © The Royal Society of Chemistry 2024

Fig. 27 Zn–CO_2 batteries. (a) Illustration outlining the prospective application of the Zn–CO_2 battery in future energy storage. (b) Visual representation elucidating the operational principles of a reversible aqueous Zn–CO_2 battery. (c) Charge and discharge polarization curve. (d) Charge and discharge cycle curve under 0.56 mA cm^{-2} constant current. Reproduced with permission from ref. 179. Copyright 2018 John Wiley & Sons.

into Zn–CO_2 batteries as cathode catalysts, the charging voltage is only 1 V, the cycle durability can exceed 100 cycles, and the energy efficiency can be as high as 81.2%.

Apart from the emerging Zn–CO_2 batteries,[518] recent years have witnessed the proposal and development of various other Zn-based batteries, such as the Zn–acetylene battery, Zn–nitrate battery, and several hybrid battery configurations. For these emerging Zn-based batteries, current design strategies mainly focus on the design of cathode electrocatalysts and innovation of battery configurations.[519,520] Illustratively, Zhang et al. employed copper dendrites, known for their superior catalytic performance in acetylene semi-hydrogenation, as the cathode catalyst to establish a novel Zn–C_2H_2 battery. This innovative design integrates zinc oxidation at the anode with alkyne semi-hydrogenation at the cathode.[521] This new type of battery can simultaneously achieve selective alkyne reduction and power generation. The engineered Zn–C_2H_2 battery demonstrates significant open circuit potential and elevated energy density throughout its charge and discharge cycles. Moreover, in the stable discharge phase, the Zn–C_2H_2 battery achieves exceptional faradaic efficiency and ethylene productivity, yielding polymer-grade ethylene raw materials. Consequently, the advancement of functional Zn–C_2H_2 batteries not only introduces innovative concepts and applications for next-generation batteries but also presents a promising avenue for energy-efficient and cost-effective alkyne removal technology in olefin purification. Furthermore, some high-performance hybrid batteries have also been proposed and developed through the design of electrolytes. As an illustration, Xia and collaborators devised Zn–air/iodide hybrid batteries, employing an innovative

dual-network structured hydrogel as the electrolyte.[522] The dual-network structure in the electrolyte imparts enhanced mechanical strength and heightened ionic conductivity to the material. Notably, the incorporation of iodine species brings about more favorable cathode kinetics in the iodide/iodate redox process compared to oxygen electrocatalysis. Simultaneously, iodine species influence the solvation structure of Zn^{2+}, contributing to improved interface stability. Consequently, the assembled hybrid battery demonstrates an outstanding long cycle stability of 110 hours and a commendable energy efficiency of 80%. While these emerging Zn-based batteries are in the nascent stages of research, further endeavors are imperative to explore diverse strategies aimed at achieving optimal battery performance.

6. Conclusions and outlook

Exploring the energy storage mechanisms of batteries and enhancing the performance of diverse battery types remain a prevalent theme in the realm of energy storage. The pursuit of these aims is intricately tied to both human life and societal advancement. Zn-based batteries, recognized for their low cost, environmental sustainability, inherent safety, and substantial theoretical energy density, emerge as an ideal candidate for the next generation of secure battery technologies. This review first systematically summarizes various energy storage mechanisms existing in Zn-based batteries, including insertion-type, conversion-type, coordination-type, and catalysis-type mechanisms. Furthermore, the design strategies aiming at enhancing their electrochemical performance in terms of output voltage,
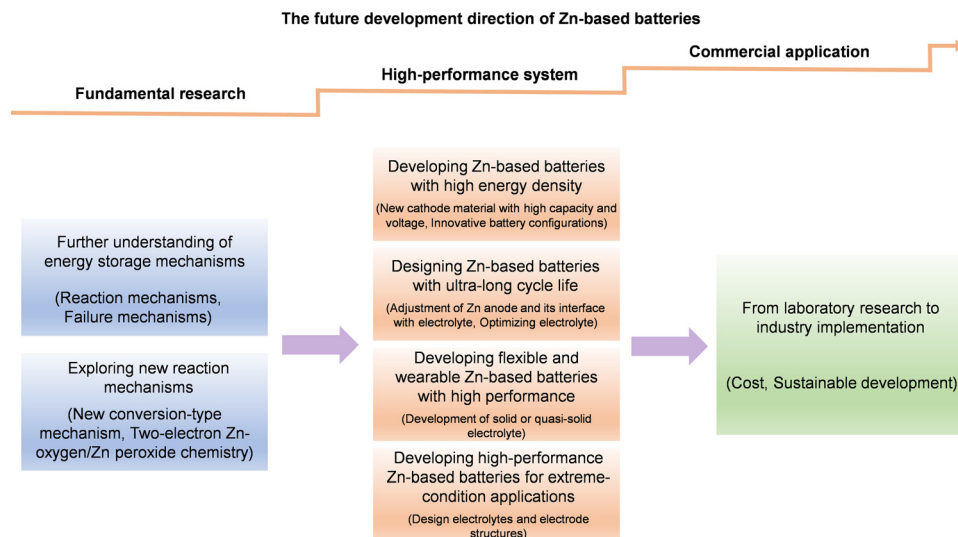
This journal is © The Royal Society of Chemistry 2024

Chem. Soc. Rev., 2024, **53**, 4877–4925 | **4911**

Fig. 28 Direction for future development of Zn–based batteries.

specific capacity, energy density, and cycle life are introduced. In addition to these achievements discussed in this review (Table 1), there are still many issues that need to be solved in order to render high-performance Zn-based batteries. Because of the complexity of battery processes and devices, more efforts need to be invested to deeply understand the reaction mechanism of Zn-based batteries. Concurrently, it is necessary to realize that the excellent performance of Zn-based batteries stems from the collective enhancement of each constituent rather than isolated improvements in individual components. The following points represent unsolved and important areas in Zn-based batteries that require further research and exploration (Fig. 28):

(1) Further understanding of energy storage mechanisms

While the insertion-type, conversion-type, coordination-type, and catalysis-type mechanisms collectively encompass the spectrum of redox reactions occurring at the cathode in Zn-based batteries, it is noteworthy that high-performance variants often exhibit a concurrent presence of multiple reaction mechanisms, rather than being exclusively governed by a singular type of redox reaction. Simultaneously, the intricate nature of the constituents within Zn-based batteries contributes to heightened challenges in comprehending the underlying reaction mechanisms. To glean insights into the factors influencing the performance of Zn-based batteries and to facilitate the design of high-performance variants, it is imperative to dedicate increased efforts towards the exploration and comprehension of the associated reaction mechanisms. In this regard, the utilization of diverse advanced characterization techniques and theoretical calculations opens avenues for enhanced comprehension of reaction mechanisms.

Despite recent advances in the performance of Zn-based batteries, the mechanisms leading to electrode material deactivation and battery failure processes remain elusive, posing a constraint on further evolution of Zn-based battery technology.

The seamless functionality of Zn-based batteries is intricately linked to the stability of the zinc anode/electrolyte/cathode interface. Consequently, substantial efforts are warranted to elucidate the intricacies of the charge and discharge processes occurring at this interface. Specifically, the employment of diverse *in situ* characterization techniques, such as *in situ* XRD, *in situ* Raman, *in situ* XAFS, and *in situ* TEM, is crucial to monitor dynamic alterations at the electrolyte/electrode interface. Such effort facilitates a comprehensive understanding of the battery failure process. Furthermore, a profound comprehension of Zn-based battery failures serves as a valuable reference for the design of high-performance Zn-based batteries.

(2) Exploring new reaction mechanisms to achieve high performance

Zn-ion batteries inherently benefit from the natural capacity advantage offered by sulfur in conversion-type materials. However, the proposed sulfur redox reactions thus far exhibit limited valence changes, resulting in a constrained electrode potential. To enhance energy density, a promising approach involves devising a novel conversion reaction mechanism that facilitates a broader valence change range for sulfur in redox processes. Achieving an expanded valence change range for sulfur in redox reactions necessitates the minimization of side reactions, such as the HER and OER. Consequently, the implementation of a high-concentration electrolyte, specifically a water-in-salt configuration, emerges as an effective strategy to circumvent side reactions. This approach successfully eliminates undesired reactions, thereby widening the valence change range for sulfur in the redox process.

In the realm of alkaline Zn–air batteries, the well-established $4e^-/O_2$ chemistry is a cornerstone. Nevertheless, the incorporation of functional additives possesses the potential to induce alterations in the Zn^{2+} solvation sheath structure, hydrogen bonding configuration, or the reaction pathway within the alkaline electrolyte. By incorporating high-concentration additives,

4912 | *Chem. Soc. Rev.*, 2024, **53**, 4877–4925

This journal is © The Royal Society of Chemistry 2024

the conventional four-electron process undergoes a transformation into a two-electron Zn–oxygen/Zn peroxide chemistry, exemplifying a notable alteration in reaction dynamics. These changes, in turn, yield unexpected performance enhancements, effectively overcoming inherent bottlenecks. Concurrently, the adoption of a non-alkaline electrolyte not only circumvents the constraints associated with an alkaline electrolyte but also ensures excellent reversibility. The commendable performance observed in non-alkaline Zn–air batteries signifies a promising avenue for the design of sustainable batteries capable of prolonged and stable operation. The anticipation for innovative electrolytes and novel reaction mechanisms is high, yet their development poses a significant challenge.

(3) Developing Zn-based batteries with high energy density

High energy density in Zn-based batteries necessitates the concurrent optimization of both capacity and voltage, as energy density is inherently determined by the product of these two factors. Cathode materials, including Prussian blue materials, polyanionic compounds, and Co-based oxides, demonstrate distinctive high-voltage features, yet their theoretical capacity remains unsatisfactory. Consequently, a critical focus lies in enhancing the actual capacity of cathode materials with high voltage characteristics. Various strategies, including introduction of multispecies redox reactions and adjustment of ion concentrations in the cathode material, can be employed to reduce the proportion of inactive components and increase the electron transfer number. This, in turn, enhances the intrinsic capacity of redox-active materials. Conversely, addressing the intrinsic low electrode potential of high-capacity cathode materials remains a persistent challenge. While maintaining stable operation of the Zn anode, the introduction of various charge carriers, such as Al^{3+}, Li^+, Na^+, etc., offers the potential to establish a higher output voltage platform. It is essential, however, to ensure the compatibility of introduced charge carriers with the structure of the cathode material.

Beyond the investigation of cathode materials exhibiting simultaneous high capacity and voltage, exploring innovative battery configurations stands out as a highly promising avenue for achieving elevated energy density in zinc-based batteries. Currently, the predominant method for decoupling electrolytes involves the utilization of ion exchange membranes. This design approach facilitates a substantial increase in the potential difference between anode and cathode, expanding the stable electrochemical window of the electrolyte and, consequently, realizing high-energy-density Zn-based batteries. However, it is imperative to acknowledge the associated cost escalation, primarily due to the expense of ion exchange membranes commonly employed for decoupling. Future investigations should prioritize the development of more economical ion exchange membranes. Additionally, exploring the feasibility of cost-effective gel electrolytes as substitutes for ion exchange membranes holds promise as a crucial avenue for further research. Furthermore, the integration of flow devices presents an additional avenue for enhancing the energy density of Zn-based batteries.

(4) Designing Zn-based batteries with ultra-long cycle life

The growing demand for practical applications underscores the increasing need for Zn-based batteries characterized by ultra-long cycle life. Given the intimate connection between reversibility at the zinc anode and the long-term cycling stability of Zn-based batteries, an effective strategy to prolong cycle life involves the careful adjustment of the zinc anode and its interface with the electrolyte. Through the modification and structural design of the zinc anode, it is possible to mitigate the formation of zinc dendrites, prevent the occurrence of the side reaction (HER), and restrict the production of irreversible by-products. Moreover, the introduction of additives into the electrolyte facilitates the effective modulation of the interface between the zinc anode and the electrolyte, thereby enabling the reversible dissolution and deposition of zinc.

The electrolyte also plays a crucial role in influencing the cycle stability of Zn-based batteries. Currently, the decoupling of electrolytes stands out as a highly effective approach to enhance the cycle stability of Zn-based batteries. This method involves isolating the cathode and anode in distinct electrolyte environments, effectively mitigating the occurrence of side reactions and preserving the stability of the electrode structure. The two predominant methods for decoupling electrolytes are through the use of ion exchange membranes and hydrogel electrolytes. In the case of ion exchange membranes, the high cost necessitates further research and development focused on achieving more cost-effective alternatives. Regarding gel electrolytes, considerations should extend to the water retention effect and compatibility with both positive and negative electrodes.

(5) Developing flexible and wearable Zn-based batteries with high performance

The pursuit of flexible, wearable, and multifunctional Zn-based batteries with innovative features, including self-protection, self-healing, stretchability, photoelectric detection, shape memory, and thermal response, represents a highly promising direction. This endeavor is poised to potentially shape the next generation of electronic products. A primary challenge is manifested in the development of solid or quasi-solid electrolytes that concurrently exhibit robust mechanical strength, high ionic conductivity, and multifunctionality. Addressing this challenge requires not only the optimization of device structures but also the incorporation of smart designs. These considerations aim to improve compatibility between the multifunctional electrolyte and the intelligent material, as well as other parts within battery devices. The overarching goal is to realize multifunctional devices without compromising electrochemical performance significantly.

(6) Developing high-performance Zn-based batteries for extreme-condition applications

While Zn-based batteries have found extensive applications in the consumable electronics market, their performance experiences significant degradation under extreme conditions,

including polar expeditions, ocean exploration, and high-altitude drone operations. As such, the imperative lies in the development of Zn-based batteries characterized by heightened performance in challenging environmental conditions, encompassing low and high temperatures, elevated pressure, humidity, and radiation exposure. Extreme conditions frequently influence the electrochemical behavior of specific components within battery devices. For instance, low temperature may result in diminished ion transport rates, while elevated temperatures can induce undesirable side reactions. Therefore, in subsequent research, it is important to design corresponding electrolytes and electrode structures for specific extreme conditions.

(7) From laboratory research to industry implementation

Zn-based batteries hold considerable promise for sustainable advancements in future energy and environmental initiatives. Despite extensive research and development efforts in laboratory settings, the transition from theoretical concepts to practical implementation poses substantial challenges. It is crucial to acknowledge that testing conditions in the laboratory substantially differ from those encountered in practical applications. Therefore, careful consideration of performance variations arising from disparate testing conditions becomes imperative. Notably, the path forward requires a holistic approach, emphasizing the synergistic effects among battery components to enhance overall Zn-based battery performance, rather than isolated improvements in individual elements. Furthermore, the broad adoption of Zn-based batteries calls for a thoughtful equilibrium between cost considerations and the pursuit of performance enhancement.

Overall, the prospect of employing a singular strategy as a panacea for addressing the myriad challenges inherent in Zn-based batteries appears improbable. Clearly, the key to realizing large-scale applications entails the judicious integration of diverse strategies. Nanotechnology, by introducing innovative avenues, holds promise in mitigating these multifaceted issues. Concurrently, the utilization of advanced characterization techniques contributes significantly by furnishing additional insights crucial for informed material design. Given the active research landscape surrounding Zn-based batteries, concerted endeavors in mechanism exploration, strategic design, and battery engineering are vital to render their viability feasible.

Conflicts of interest

There are no conflicts to declare.

Acknowledgements

References

1 S. Chu and A. Majumdar, *Nature*, 2012, **488**, 294–303.
2 S. Chu, Y. Cui and N. Liu, *Nat. Mater.*, 2017, **16**, 16–22.
3 M. Armand and J. M. Tarascon, *Nature*, 2008, **451**, 652–657.
4 D. Larcher and J. M. Tarascon, *Nat. Chem.*, 2015, 7, 19–29.
5 B. Dunn, H. Kamath and J. M. Tarascon, *Science*, 2011, **334**, 928–935.
6 L. Tang, X. G. Meng, D. H. Deng and X. H. Bao, *Adv. Mater.*, 2019, **31**, 1901996.
7 O. Schmidt, S. Melchior, A. Hawkes and I. Staffell, *Joule*, 2019, **3**, 81–100.
8 O. Schmidt, A. Hawkes, A. Gambhir and I. Staffell, *Nat. Energy*, 2017, **2**, 17110.
9 R. P. Fang, S. Y. Zhao, Z. H. Sun, W. Wang, H. M. Cheng and F. Li, *Adv. Mater.*, 2017, **29**, 1606823.
10 D. H. Liu, Z. Y. Bai, M. Li, A. P. Yu, D. Luo, W. W. Liu, L. Yang, J. Lu, K. Amine and Z. W. Chen, *Chem. Soc. Rev.*, 2020, **49**, 5407–5445.
11 J. X. Zheng, M. S. Kim, Z. Y. Tu, S. Choudhury, T. Tang and L. A. Archer, *Chem. Soc. Rev.*, 2020, **49**, 2701–2750.
12 M. Winter, B. Barnett and K. Xu, *Chem. Rev.*, 2018, **118**, 11433–11456.
13 D. C. Lin, Y. Y. Liu and Y. Cui, *Nat. Nanotechnol.*, 2017, **12**, 194–206.
14 Z. P. Cano, D. Banham, S. Y. Ye, A. Hintennach, J. Lu, M. Fowler and Z. W. Chen, *Nat. Energy*, 2018, **3**, 279–289.
15 Y. C. Ding, P. W. Cai and Z. H. Wen, *Chem. Soc. Rev.*, 2021, **50**, 1495–1511.
16 Y. Zhao, Y. Q. Kang, J. Wozny, J. Lu, H. Du, C. L. Li, T. Li, F. Y. Kang, N. Tavajohi and B. H. Li, *Nat. Rev. Mater.*, 2023, **8**, 623–634.
17 C. J. Xu, B. H. Li, H. D. Du and F. Y. Kang, *Angew. Chem., Int. Ed.*, 2012, **51**, 933–935.
18 L. E. Blanc, D. Kundu and L. F. Nazar, *Joule*, 2020, **4**, 771–799.
19 Y. L. Liang, H. Dong, D. Aurbach and Y. Yao, *Nat. Energy*, 2020, **5**, 646–656.
20 Z. X. Liu, Y. Huang, Y. Huang, Q. Yang, X. L. Li, Z. D. Huang and C. Y. Zhi, *Chem. Soc. Rev.*, 2020, **49**, 180–232.
21 B. Y. Tang, L. T. Shan, S. Q. Liang and J. Zhou, *Energy Environ. Sci.*, 2019, **12**, 3288–3304.
22 D. L. Chao, W. H. Zhou, F. X. Xie, C. Ye, H. Li, M. Jaroniec and S. Z. Qiao, *Sci. Adv.*, 2020, **6**, eaba4098.
23 Y. M. Sui and X. L. Ji, *Chem. Rev.*, 2021, **121**, 6654–6695.
24 Y. Y. Liu, X. Lu, F. L. Lai, T. X. Liu, P. R. Shearing, I. P. Parkin, G. J. He and D. J. L. Brett, *Joule*, 2021, **5**, 2845–2903.
25 W. C. Du, E. H. X. Ang, Y. Yang, Y. F. Zhang, M. H. Ye and C. C. Li, *Energy Environ. Sci.*, 2020, **13**, 3330–3360.
26 Z. Hou, Y. Gao, H. Tan and B. A. Zhang, *Nat. Commun.*, 2021, **12**, 3083.
27 L. J. Kong, M. Liu, H. Huang, Y. H. Xu and X. H. Bu, *Adv. Energy Mater.*, 2022, **12**, 2100172.
28 T. Xue and H. J. Fan, *J. Energy Chem.*, 2021, **54**, 194–201.
29 J. X. Zheng and L. A. Archer, *Sci. Adv.*, 2021, **7**, eabe0219.
30 X. M. Xu, F. Y. Xiong, J. S. Meng, X. P. Wang, C. J. Niu, Q. Y. An and L. Q. Mai, *Adv. Funct. Mater.*, 2020, **30**, 1904398.

4914 | *Chem. Soc. Rev.*, 2024, **53**, 4877–4925

This journal is © The Royal Society of Chemistry 2024

31 N. Zhang, F. Y. Cheng, Y. C. Liu, Q. Zhao, K. X. Lei, C. C. Chen, X. S. Liu and J. Chen, *J. Am. Chem. Soc.*, 2016, **138**, 12894–12901.

32 G. Z. Fang, J. Zhou, A. Q. Pan and S. Q. Liang, *ACS Energy Lett.*, 2018, **3**, 2480–2501.

33 N. Zhang, X. Y. Chen, M. Yu, Z. Q. Niu, F. Y. Cheng and J. Chen, *Chem. Soc. Rev.*, 2020, **49**, 4203–4219.

34 A. Konarov, N. Voronina, J. H. Jo, Z. Bakenov, Y. K. Sun and S. T. Myung, *ACS Energy Lett.*, 2018, **3**, 2620–2640.

35 N. Zhang, F. Y. Cheng, J. X. Liu, L. B. Wang, X. H. Long, X. S. Liu, F. J. Li and J. Chen, *Nat. Commun.*, 2017, **8**, 405.

36 Y. C. Shi, Y. Chen, L. Shi, K. Wang, B. Wang, L. Li, Y. M. Ma, Y. H. Li, Z. H. Sun, W. Ali and S. J. Ding, *Small*, 2020, **16**, 2000730.

37 M. Song, H. Tan, D. L. Chao and H. J. Fan, *Adv. Funct. Mater.*, 2018, **28**, 1802564.

38 H. Jia, Z. Q. Wang, B. Tawiah, Y. D. Wang, C. Y. Chan, B. Fei and F. Pan, *Nano Energy*, 2020, **70**, 104523.

39 P. Yu, Y. X. Zeng, H. Z. Zhang, M. H. Yu, Y. X. Tong and X. Lu, *Small*, 2019, **15**, 1804760.

40 F. Wan, Z. M. Hao, S. Wang, Y. X. Ni, J. C. Zhu, Z. W. Tie, S. S. Bi, Z. Q. Niu and J. Chen, *Adv. Mater.*, 2021, **33**, 2102701.

41 P. He, Y. L. Quan, X. Xu, M. Y. Yan, W. Yang, Q. Y. An, L. He and L. Q. Mai, *Small*, 2017, **13**, 1702551.

42 B. Li, X. T. Zhang, T. L. Wang, Z. X. He, B. A. Lu, S. Q. Liang and J. Zhou, *Nano-Micro Lett.*, 2022, **14**, 6.

43 X. L. Xu, Y. Chen, D. Zheng, P. C. Ruan, Y. H. Cai, X. J. Dai, X. X. Niu, C. J. Pei, W. H. Shi, W. X. Liu, F. F. Wu, Z. Y. Pan, H. Li and X. H. Cao, *Small*, 2021, **17**, 2101901.

44 C. Xia, J. Guo, Y. J. Lei, H. F. Liang, C. Zhao and H. N. Alshareef, *Adv. Mater.*, 2018, **30**, 1705580.

45 X. X. Jia, C. F. Liu, Z. G. Neale, J. H. Yang and G. Z. Cao, *Chem. Rev.*, 2020, **120**, 7795–7866.

46 V. Verma, S. Kumar, W. Manalastas and M. Srinivasan, *ACS Energy Lett.*, 2021, **6**, 1773–1785.

47 Y. P. Deng, R. L. Liang, G. P. Jiang, Y. Jiang, A. P. Yu and Z. W. Chen, *ACS Energy Lett.*, 2020, **5**, 1665–1675.

48 W. H. Yang, Y. Yang, H. J. Yang and H. S. Zhou, *ACS Energy Lett.*, 2022, **7**, 2515–2530.

49 R. F. Service, *Science*, 2021, **372**, 890–891.

50 A. R. Mainar, L. C. Colmenares, J. A. Blázquez and I. Urdampilleta, *Int. J. Energy Res.*, 2018, **42**, 903–918.

51 D. L. Chao and S. Z. Qiao, *Joule*, 2020, **4**, 1846–1851.

52 X. Wang, Z. C. Y. Zhang, B. J. Xi, W. H. Chen, Y. X. Jia, J. K. Feng and S. L. Xiong, *ACS Nano*, 2021, **15**, 9244–9272.

53 Y. L. Zhao, Y. H. Zhu and X. B. Zhang, *InfoMat*, 2020, **2**, 237–260.

54 Y. Fang, X. S. Xie, B. Y. Zhang, Y. Z. Chai, B. A. Lu, M. K. Liu, J. Zhou and S. Q. Liang, *Adv. Funct. Mater.*, 2022, **32**, 2109671.

55 J. Fu, R. L. Liang, G. H. Liu, A. P. Yu, Z. Y. Bai, L. Yang and Z. W. Chen, *Adv. Mater.*, 2019, **31**, 1805230.

56 J. H. Song, K. Xu, N. Liu, D. Reed and X. L. Li, *Mater. Today*, 2021, **45**, 191–212.

57 J. P. Yan, E. H. Ang, Y. Yang, Y. F. Zhang, M. H. Ye, W. C. Du and C. C. Li, *Adv. Funct. Mater.*, 2021, **31**, 2010213.

58 B. F. Cui, X. P. Han and W. B. Hu, *Small Struct.*, 2021, **2**, 2000128.

59 Y. X. Zeng, D. Y. Luan and X. W. Lou, *Chem*, 2023, **9**, 1118–1146.

60 Y. Lu, Y. Y. Lu, Z. Q. Niu and J. Chen, *Adv. Energy Mater.*, 2018, **8**, 1702469.

61 X. Wang, Y. G. Li, S. Wang, F. Zhou, P. Das, C. L. Sun, S. H. Zheng and Z. S. Wu, *Adv. Energy Mater.*, 2020, **10**, 2000081.

62 B. Yong, D. T. Ma, Y. Y. Wang, H. W. Mi, C. X. He and P. X. Zhang, *Adv. Energy Mater.*, 2020, **10**, 2002354.

63 Q. L. Li, Q. C. Zhang, C. L. Liu, Z. Y. Zhou, C. W. Li, B. He, P. Man, X. N. Wang and Y. G. Yao, *J. Mater. Chem. A*, 2019, **7**, 12997–13006.

64 Y. P. Xu, P. W. Cai, K. Chen, Y. C. Ding, L. Chen, W. F. Chen and Z. H. Wen, *Angew. Chem., Int. Ed.*, 2020, **59**, 23593–23597.

65 Y. H. Zhu, Y. F. Cui, Z. L. Xie, Z. B. Zhuang, G. Huang and X. B. Zhang, *Nat. Rev. Chem.*, 2022, **6**, 505–517.

66 L. T. Ma, S. M. Chen, C. B. Long, X. L. Li, Y. W. Zhao, Z. X. Liu, Z. D. Huang, B. B. Dong, J. A. Zapien and C. Y. Zhi, *Adv. Energy Mater.*, 2019, **9**, 1902446.

67 L. T. Ma, N. Li, C. B. Long, B. B. Dong, D. L. Fang, Z. X. Liu, Y. W. Zhao, X. L. Li, J. Fan, S. M. Chen, S. J. Zhang and C. Y. Zhi, *Adv. Funct. Mater.*, 2019, **29**, 1906142.

68 C. Zhong, B. Liu, J. Ding, X. R. Liu, Y. W. Zhong, Y. Li, C. B. Sun, X. P. Han, Y. D. Deng, N. Q. Zhao and W. B. Hu, *Nat. Energy*, 2020, **5**, 440–449.

69 D. L. Chao, C. Ye, F. X. Xie, W. H. Zhou, Q. H. Zhang, Q. F. Gu, K. Davey, L. Gu and S. Z. Qiao, *Adv. Mater.*, 2020, **32**, 2001894.

70 C. Han, W. J. Li, H. K. Liu, S. X. Dou and J. Z. Wang, *Nano Energy*, 2020, **74**, 104880.

71 Q. Zhang, J. Y. Luan, Y. G. Tang, X. B. Ji and H. Y. Wang, *Angew. Chem., Int. Ed.*, 2020, **59**, 13180–13191.

72 Z. H. Yi, G. Y. Chen, F. Hou, L. Q. Wang and J. Liang, *Adv. Energy Mater.*, 2021, **11**, 2003065.

73 L. Ma, M. A. Schroeder, O. Borodin, T. P. Pollard, M. S. Ding, C. S. Wang and K. Xu, *Nat. Energy*, 2020, **5**, 743–749.

74 X. Z. Yang, C. Li, Z. T. Sun, S. Yang, Z. X. Shi, R. Huang, B. Z. Liu, S. Li, Y. H. Wu, M. L. Wang, Y. W. Su, S. X. Dou and J. Y. Sun, *Adv. Mater.*, 2021, **33**, 2105951.

75 Z. Wang, J. H. Huang, Z. W. Guo, X. L. Dong, Y. Liu, Y. G. Wang and Y. Y. Xia, *Joule*, 2019, **3**, 1289–1300.

76 P. Xue, C. Guo, L. Li, H. P. Li, D. Luo, L. C. Tan and Z. W. Chen, *Adv. Mater.*, 2022, **34**, 2110047.

77 P. Sun, L. Ma, W. H. Zhou, M. J. Qiu, Z. L. Wang, D. L. Chao and W. J. Mai, *Angew. Chem., Int. Ed.*, 2021, **60**, 18247–18255.

78 F. W. Ming, Y. P. Zhu, G. Huang, A. H. Emwas, H. F. Liang, Y. Cui and H. N. Alshareef, *J. Am. Chem. Soc.*, 2022, **144**, 7160–7170.

79 H. Chen, C. L. Dai, F. Y. Xiao, Q. J. Yang, S. N. Cai, M. W. Xu, H. J. Fan and S. J. Bao, *Adv. Mater.*, 2022, **34**, 2109092.

80 F. X. Xie, H. Li, X. S. Wang, X. Zhi, D. L. Chao, K. Davey and S. Z. Qiao, *Adv. Energy Mater.*, 2021, **11**, 2003419.

81 F. Wang, W. Sun, Z. Shadike, E. Y. Hu, X. Ji, T. Gao, X. Q. Yang, K. Xu and C. S. Wang, *Angew. Chem., Int. Ed.*, 2018, **57**, 11978–11981.

This journal is © The Royal Society of Chemistry 2024

Chem. Soc. Rev., 2024, **53**, 4877–4925 | 4915

82 D. Kundu, S. H. Vajargah, L. W. Wan, B. Adams, D. Prendergast and L. F. Nazar, *Energy Environ. Sci.*, 2018, **11**, 881–892.

83 P. Li, Y. Q. Wang, Q. Xiong, Y. Hou, S. Yang, H. L. Cui, J. X. Zhu, X. L. Li, Y. B. Wang, R. Zhang, S. C. Zhang, X. Q. Wang, X. Jin, S. C. Bai and C. Y. Zhi, *Angew. Chem., Int. Ed.*, 2023, **62**, e202303292.

84 F. Wan and Z. Q. Niu, *Angew. Chem., Int. Ed.*, 2019, **58**, 16358–16367.

85 Q. Yang, Q. Li, Z. X. Liu, D. H. Wang, Y. Guo, X. L. Li, Y. C. Tang, H. F. Li, B. B. Dong and C. Y. Zhi, *Adv. Mater.*, 2020, **32**, 2001854.

86 M. Li, Z. L. Li, X. P. Wang, J. S. Meng, X. Liu, B. K. Wu, C. H. Han and L. Q. Mai, *Energy Environ. Sci.*, 2021, **14**, 3796–3839.

87 S. Guo, L. P. Qin, T. S. Zhang, M. Zhou, J. Zhou, G. Z. Fang and S. Q. Liang, *Energy Storage Mater.*, 2021, **34**, 545–562.

88 S. Liu, L. Kang, J. M. Kim, Y. T. Chun, J. Zhang and S. C. Jun, *Adv. Energy Mater.*, 2020, **10**, 2000477.

89 V. Mathew, B. Sambandam, S. Kim, S. Kim, S. Park, S. Lee, M. H. Alfaruqi, V. Soundharrajan, S. Islam, D. Y. Putro, J. Y. Hwang, Y. K. Sun and J. Kim, *ACS Energy Lett.*, 2020, **5**, 2376–2400.

90 Z. W. Tie and Z. Q. Niu, *Angew. Chem., Int. Ed.*, 2020, **59**, 21293–21303.

91 H. Zhang, X. Liu, H. H. Li, I. Hasa and S. Passerini, *Angew. Chem., Int. Ed.*, 2021, **60**, 598–616.

92 T. Xiong, Y. X. Zhang, W. S. V. Lee and J. M. Xue, *Adv. Energy Mater.*, 2020, **10**, 2001769.

93 H. Y. Liu, J. G. Wang, Z. Y. You, C. G. Wei, F. Y. Kang and B. Q. Wei, *Mater. Today*, 2021, **42**, 73–98.

94 Q. C. Wang, S. Kaushik, X. Xiao and Q. Xu, *Chem. Soc. Rev.*, 2023, **52**, 6139–6190.

95 J. Yi, P. C. Liang, X. Y. Liu, K. Wu, Y. Y. Liu, Y. G. Wang, Y. Y. Xia and J. J. Zhang, *Energy Environ. Sci.*, 2018, **11**, 3075–3095.

96 T. P. Zhou, N. Zhang, C. Z. Wu and Y. Xie, *Energy Environ. Sci.*, 2020, **13**, 1132–1153.

97 Y. G. Li and H. J. Dai, *Chem. Soc. Rev.*, 2014, **43**, 5257–5275.

98 P. Tan, B. Chen, H. R. Xu, H. C. Zhang, W. Z. Cai, M. Ni, M. L. Liu and Z. P. Shao, *Energy Environ. Sci.*, 2017, **10**, 2056–2080.

99 Z. Z. Yuan, Y. B. Yin, C. X. Xie, H. M. Zhang, Y. Yao and X. F. Li, *Adv. Mater.*, 2019, **31**, 1902025.

100 H. F. Li, L. T. Ma, C. P. Han, Z. F. Wang, Z. X. Liu, Z. J. Tang and C. Y. Zhi, *Nano Energy*, 2019, **62**, 550–587.

101 J. H. Huang, Z. Wang, M. Y. Hou, X. L. Dong, Y. Liu, Y. G. Wang and Y. Y. Xia, *Nat. Commun.*, 2018, **9**, 2906.

102 P. He, M. Y. Yan, G. B. Zhang, R. M. Sun, L. N. Chen, Q. Y. An and L. Q. Mai, *Adv. Energy Mater.*, 2017, **7**, 1601920.

103 M. H. Alfaruqi, V. Mathew, J. Gim, S. Kim, J. Song, J. P. Baboo, S. H. Choi and J. Kim, *Chem. Mater.*, 2015, **27**, 3609–3620.

104 Y. Y. Lu, T. Y. Zhu, W. van den Bergh, M. Stefik and K. Huang, *Angew. Chem., Int. Ed.*, 2020, **59**, 17004–17011.

105 S. Z. Deng, Z. S. Yuan, Z. W. Tie, C. D. Wang, L. Song and Z. Q. Niu, *Angew. Chem., Int. Ed.*, 2020, **59**, 22002–22006.

106 J. Cao, D. D. Zhang, Y. L. Yue, X. Wang, T. Pakornchote, T. Bovornratanaraks, X. Y. Zhang, Z. S. Wu and J. Q. Qin, *Nano Energy*, 2021, **84**, 105876.

107 S. C. Liu, H. Zhu, B. H. Zhang, G. Li, H. K. Zhu, Y. Ren, H. B. Geng, Y. Yang, Q. Liu and C. C. Li, *Adv. Mater.*, 2020, **32**, 2001113.

108 P. He, G. B. Zhang, X. B. Liao, M. Y. Yan, X. Xu, Q. Y. An, J. Liu and L. Q. Mai, *Adv. Energy Mater.*, 2018, **8**, 1702463.

109 Y. F. Yuan, R. Sharpe, K. He, C. H. Li, M. T. Saray, T. C. Liu, W. T. Yao, M. Cheng, H. L. Jin, S. Wang, K. Amine, R. Shahbazian-Yassar, M. S. Islam and J. Lu, *Nat. Sustain.*, 2022, **5**, 890–898.

110 S. M. Chen, Y. Ying, L. T. Ma, D. M. Zhu, H. T. Huang, L. Song and C. Y. Zhi, *Nat. Commun.*, 2023, **14**, 2925.

111 W. Sun, F. Wang, S. Y. Hou, C. Y. Yang, X. L. Fan, Z. H. Ma, T. Gao, F. D. Han, R. Z. Hu, M. Zhu and C. S. Wang, *J. Am. Chem. Soc.*, 2017, **139**, 9775–9778.

112 D. Kundu, B. D. Adams, V. Duffort, S. H. Vajargah and L. F. Nazar, *Nat. Energy*, 2016, **1**, 16119.

113 Z. G. Yao, Q. P. Wu, K. Y. Chen, J. J. Liu and C. L. Li, *Energy Environ. Sci.*, 2020, **13**, 3149–3163.

114 X. H. Zeng, J. N. Hao, Z. J. Wang, J. F. Mao and Z. P. Guo, *Energy Storage Mater.*, 2019, **20**, 410–437.

115 L. P. Wang, P. F. Wang, T. S. Wang, Y. X. Yin, Y. G. Guo and C. R. Wang, *J. Power Sources*, 2017, **355**, 18–22.

116 W. D. Pan, Y. F. Wang, X. L. Zhao, Y. Zhao, X. H. Liu, J. Xuan, H. Z. Wang and D. Y. C. Leung, *Adv. Funct. Mater.*, 2021, **31**, 2008783.

117 J. N. Hao, J. Long, B. Li, X. L. Li, S. L. Zhang, F. H. Yang, X. H. Zeng, Z. H. Yang, W. K. Pang and Z. P. Guo, *Adv. Funct. Mater.*, 2019, **29**, 1903605.

118 H. Z. Li, C. J. Firby and A. Y. Elezzabi, *Joule*, 2019, **3**, 2268–2278.

119 P. Hu, T. Zhu, X. P. Wang, X. F. Zhou, X. J. Wei, X. H. Yao, W. Luo, C. W. Shi, K. A. Owusu, L. Zhou and L. Q. Mai, *Nano Energy*, 2019, **58**, 492–498.

120 F. Wan, L. L. Zhang, X. Dai, X. Y. Wang, Z. Q. Niu and J. Chen, *Nat. Commun.*, 2018, **9**, 1656.

121 J. L. Liu, C. H. Xu, Z. Chen, S. B. Ni and Z. X. Shen, *Green Energy Environ.*, 2018, **3**, 20–41.

122 J. Yan, J. Wang, H. Liu, Z. Bakenov, D. Gosselink and P. Chen, *J. Power Sources*, 2012, **216**, 222–226.

123 K. W. Nam, W. S. Yoon, H. Shin, K. Y. Chung, S. Choi and X. Q. Yang, *J. Power Sources*, 2009, **192**, 652–659.

124 Y. F. Huang, J. Mou, W. B. Liu, X. L. Wang, L. B. Dong, F. Y. Kang and C. J. Xu, *Nano-Micro Lett.*, 2019, **11**, 49.

125 H. L. Pan, Y. Y. Shao, P. F. Yan, Y. W. Cheng, K. S. Han, Z. M. Nie, C. M. Wang, J. H. Yang, X. L. Li, P. Bhattacharya, K. T. Mueller and J. Liu, *Nat. Energy*, 2016, **1**, 16039.

126 T. Wang, H. C. Chen, F. Yu, X. S. Zhao and H. X. Wang, *Energy Storage Mater.*, 2019, **16**, 545–573.

127 Y. X. Zeng, Z. Z. Lai, Y. Han, H. Z. Zhang, S. L. Xie and X. H. Lu, *Adv. Mater.*, 2018, **30**, 1802396.

128 P. Hu, T. S. Wang, J. W. Zhao, C. J. Zhang, J. Ma, H. P. Du, X. G. Wang and G. L. Cui, *ACS Appl. Mater. Interfaces*, 2015, **7**, 26396–26399.

4916 | *Chem. Soc. Rev.*, 2024, **53**, 4877–4925

This journal is © The Royal Society of Chemistry 2024

129 L. Y. Zhang, R. Z. Feng, W. Wang and G. H. Yip, *Nat. Rev. Chem.*, 2022, **6**, 524–543.

130 C. K. Zhang, L. Y. Zhang, Y. Ding, X. L. Guo and G. H. Yu, *ACS Energy Lett.*, 2018, **3**, 2875–2883.

131 J. A. Luo, B. Hu, M. W. Hu, Y. Zhao and T. L. Liu, *ACS Energy Lett.*, 2019, **4**, 2220–2240.

132 L. T. Shan, Y. R. Wang, S. Q. Liang, B. Y. Tang, Y. Q. Yang, Z. Q. Wang, B. A. Lu and J. Zhou, *InfoMat*, 2021, **3**, 1028–1036.

133 B. P. Gindt, D. G. Abebe, Z. J. Tang, M. B. Lindsey, J. Chen, R. A. Elgammal, T. A. Zawodzinski and T. Fujiwara, *J. Mater. Chem. A*, 2016, **4**, 4288–4295.

134 L. Hu, L. Gao, M. T. Di, X. B. Jiang, X. M. Wu, X. M. Yan, X. F. Li and G. H. He, *Energy Storage Mater.*, 2021, **34**, 648–668.

135 D. Lin and Y. Li, *Adv. Mater.*, 2022, **34**, 2108856.

136 J. Zhang, G. P. Jiang, P. Xu, A. G. Kashkooli, M. Mousavi, A. P. Yu and Z. W. Chen, *Energy Environ. Sci.*, 2018, **11**, 2010–2015.

137 M. Mousavi, G. P. Jiang, J. Zhang, A. G. Kashkooli, H. Z. Dou, C. J. Silva, Z. P. Cano, Y. Niu, A. P. Yu and Z. W. Chen, *Energy Storage Mater.*, 2020, **32**, 465–476.

138 D. Kundu, P. Oberholzer, C. Glaros, A. Bouzid, E. Tervoort, A. Pasquarello and M. Niederberger, *Chem. Mater.*, 2018, **30**, 3874–3881.

139 Y. Lu, Q. Zhang, L. Li, Z. Q. Niu and J. Chen, *Chem*, 2018, **4**, 2786–2813.

140 K. W. Nam, H. Kim, Y. Beldjoudi, T. W. Kwon, D. J. Kim and J. F. Stoddart, *J. Am. Chem. Soc.*, 2020, **142**, 2541–2548.

141 H. Y. Shi, Y. J. Ye, K. Liu, Y. Song and X. Q. Sun, *Angew. Chem., Int. Ed.*, 2018, **57**, 16359–16363.

142 Z. W. Tie, L. J. Liu, S. Z. Deng, D. B. Zhao and Z. Q. Niu, *Angew. Chem., Int. Ed.*, 2020, **59**, 4920–4924.

143 N. Wang, X. L. Dong, B. L. Wang, Z. W. Guo, Z. Wang, R. H. Wang, X. Qiu and Y. G. Wang, *Angew. Chem., Int. Ed.*, 2020, **59**, 14577–14583.

144 Y. R. Wang, C. X. Wang, Z. G. Ni, Y. M. Gu, B. L. Wang, Z. W. Guo, Z. Wang, D. Bin, J. Ma and Y. G. Wang, *Adv. Mater.*, 2020, 32.

145 H. Z. Zhang, Y. B. Fang, F. Yang, X. Q. Liu and X. H. Lu, *Energy Environ. Sci.*, 2020, **13**, 2515–2523.

146 T. Sun, J. Xie, W. Guo, D. S. Li and Q. C. Zhang, *Adv. Energy Mater.*, 2020, **10**, 1904199.

147 Q. Zhao, W. W. Huang, Z. Q. Luo, L. J. Liu, Y. Lu, Y. X. Li, L. Li, J. Y. Hu, H. Ma and J. Chen, *Sci. Adv.*, 2018, **4**, eaao1761.

148 J. Park, M. Park, G. Nam, J. S. Lee and J. Cho, *Adv. Mater.*, 2015, **27**, 1396–1401.

149 Y. G. Li, M. Gong, Y. Y. Liang, J. Feng, J. E. Kim, H. L. Wang, G. S. Hong, B. Zhang and H. J. Dai, *Nat. Commun.*, 2013, **4**, 1805.

150 J. Pan, Y. Y. Xu, H. Yang, Z. H. Dong, H. F. Liu and B. Y. Xia, *Adv. Sci.*, 2018, **5**, 1700691.

151 H. F. Wang, C. Tang and Q. Zhang, *Adv. Funct. Mater.*, 2018, **28**, 1803329.

152 P. Yu, L. Wang, F. F. Sun, Y. Xie, X. Liu, J. Y. Ma, X. W. Wang, C. G. Tian, J. H. Li and H. G. Fu, *Adv. Mater.*, 2019, **31**, 1901666.

153 X. P. Han, X. F. Ling, Y. Wang, T. Y. Ma, C. Zhong, W. B. Hu and Y. D. Deng, *Angew. Chem., Int. Ed.*, 2019, **58**, 5359–5364.

154 H. F. Wang, C. Tang, B. Wang, B. Q. Li and Q. Zhang, *Adv. Mater.*, 2017, **29**, 1702327.

155 H. S. Shang, X. Y. Zhou, J. C. Dong, A. Li, X. Zhao, Q. H. Liu, Y. Lin, J. J. Pei, Z. Li, Z. L. Jiang, D. N. Zhou, L. R. Zheng, Y. Wang, J. Zhou, Z. K. Yang, R. Cao, R. Sarangi, T. T. Sun, X. Yang, X. S. Zheng, W. S. Yan, Z. B. Zhuang, J. Li, W. X. Chen, D. S. Wang, J. T. Zhang and Y. D. Li, *Nat. Commun.*, 2020, **11**, 3049.

156 P. Gu, M. B. Zheng, Q. X. Zhao, X. Xiao, H. G. Xue and H. Pang, *J. Mater. Chem. A*, 2017, **5**, 7651–7666.

157 J. Fu, Z. P. Cano, M. G. Park, A. P. Yu, M. Fowler and Z. W. Chen, *Adv. Mater.*, 2017, **29**, 1604685.

158 Z. Zhang, X. Huang, Z. Chen, J. J. Zhu, B. Endrödi, C. Janáky and D. H. Deng, *Angew. Chem., Int. Ed.*, 2023, **62**, e202302789.

159 L. Tang, S. B. Zhang, Q. L. Wu, X. R. Wang, H. Wu and Z. Y. Jiang, *J. Mater. Chem. A*, 2018, **6**, 2964–2973.

160 C. A. Trickett, A. Helal, B. A. Al-Maythalony, Z. H. Yamani, K. E. Cordova and O. M. Yaghi, *Nat. Rev. Mater.*, 2017, **2**, 17045.

161 S. I. Seneviratne, M. G. Donat, A. J. Pitman, R. Knutti and R. L. Wilby, *Nature*, 2016, **529**, 477–483.

162 G. A. Olah, G. K. S. Prakash and A. Goeppert, *J. Am. Chem. Soc.*, 2011, **133**, 12881–12898.

163 M. Mikkelsen, M. Jorgensen and F. C. Krebs, *Energy Environ. Sci.*, 2010, **3**, 43–81.

164 Z. J. Xie, X. Zhang, Z. Zhang and Z. Zhou, *Adv. Mater.*, 2017, **29**, 1605891.

165 F. Wang, Y. Li, X. H. Xia, W. Cai, Q. G. Chen and M. H. Chen, *Adv. Energy Mater.*, 2021, **11**, 2100667.

166 M. J. Wu, G. X. Zhang, H. M. Yang, X. H. Liu, M. Dubois, M. A. Gauthier and S. H. Sun, *InfoMat*, 2022, **4**, e12265.

167 J. F. Xie and Y. B. Wang, *Acc. Chem. Res.*, 2019, **52**, 1721–1729.

168 Y. Qiao, J. Yi, S. C. Wu, Y. Liu, S. X. Yang, P. He and H. S. Zhou, *Joule*, 2017, **1**, 359–370.

169 C. Yang, K. K. Guo, D. W. Yuan, J. L. Cheng and B. Wang, *J. Am. Chem. Soc.*, 2020, **142**, 6983–6990.

170 Y. Xiao, F. Du, C. G. Hu, Y. Ding, Z. L. Wang, A. Roy and L. M. Dai, *ACS Energy Lett.*, 2020, **5**, 916–921.

171 L. Song, C. G. Hu, Y. Xiao, J. P. He, Y. Lin, J. W. Connell and L. M. Dai, *Nano Energy*, 2020, **71**, 104595.

172 B. Liu, Y. L. Sun, L. Y. Liu, J. T. Chen, B. J. Yang, S. Xu and X. B. Yan, *Energy Environ. Sci.*, 2019, **12**, 887–922.

173 J. F. Xie, Z. Zhou and Y. B. Wang, *Adv. Funct. Mater.*, 2020, **30**, 1908285.

174 S. S. Gao, Y. F. Liu, Z. Y. Xie, Y. Qiu, L. C. Zhuo, Y. J. Qin, J. Q. Ren, S. S. Zhang, G. Z. Hu, J. Luo and X. J. Liu, *Small Methods*, 2021, **5**, 2001039.

175 W. T. Bi, C. Z. Wu and Y. Xie, *ACS Energy Lett.*, 2018, **3**, 624–633.

176 K. Wang, Y. Y. Wu, X. B. Cao, L. Gu and J. Hu, *Adv. Funct. Mater.*, 2020, **30**, 1908965.

177 J. Gu, C. S. Hsu, L. C. Bai, H. M. Chen and X. L. Hu, *Science*, 2019, **364**, 1091–1094.

178 T. T. Wang, X. H. Sang, W. Z. Zheng, B. Yang, S. Y. Yao, C. J. Lei, Z. J. Li, Q. G. He, J. G. Lu, L. C. Lei, L. M. Dai and Y. Hou, *Adv. Mater.*, 2020, **32**, 2002430.

179 J. F. Xie, X. Y. Wang, J. Q. Lv, Y. Y. Huang, M. X. Wu, Y. B. Wang and J. N. Yao, *Angew. Chem., Int. Ed.*, 2018, **57**, 16996–17001.

180 Y. Q. Yang, Y. Tang, G. Z. Fang, L. T. Shan, J. S. Guo, W. Y. Zhang, C. Wang, L. B. Wang, J. Zhou and S. Q. Liang, *Energy Environ. Sci.*, 2018, **11**, 3157–3162.

181 X. M. Ma, X. X. Cao, M. L. Yao, L. T. Shan, X. D. Shi, G. Z. Fang, A. Q. Pan, B. A. Lu, J. Zhou and S. Q. Liang, *Adv. Mater.*, 2022, **34**, 2105452.

182 Q. Zong, Q. Q. Wang, C. F. Liu, D. W. Tao, J. Y. Wang, J. J. Zhang, H. W. Du, J. F. Chen, Q. L. Zhang and G. Z. Cao, *ACS Nano*, 2022, **16**, 4588–4598.

183 X. Zhang, J. P. Hu, N. Fu, W. B. Zhou, B. Liu, Q. Deng and X. W. Wu, *InfoMat*, 2022, **4**, e12306.

184 X. Guo, J. Zhou, C. L. Bai, X. K. Li, G. Z. Fang and S. Q. Liang, *Mater. Today Energy*, 2020, **16**, 100396.

185 C. F. Liu, Z. Neale, J. Q. Zheng, X. X. Jia, J. J. Huang, M. Y. Yan, M. Tian, M. S. Wang, J. H. Yang and G. Z. Cao, *Energy Environ. Sci.*, 2019, **12**, 2273–2285.

186 F. W. Ming, H. F. Liang, Y. J. Lei, S. Kandambeth, M. Eddaoudi and H. N. Alshareef, *ACS Energy Lett.*, 2018, **3**, 2602–2609.

187 D. Selvakumaran, A. Q. Pan, S. Q. Liang and G. Z. Cao, *J. Mater. Chem. A*, 2019, **7**, 18209–18236.

188 B. Y. Tang, J. Zhou, G. Z. Fang, F. Liu, C. Y. Zhu, C. Wang, A. Q. Pan and S. Q. Liang, *J. Mater. Chem. A*, 2019, **7**, 940–945.

189 Y. Q. Yang, Y. Tang, S. Q. Liang, Z. X. Wu, G. Z. Fang, X. X. Cao, C. Wang, T. Q. Lin, A. Q. Pan and J. Zhou, *Nano Energy*, 2019, **61**, 617–625.

190 C. Y. Zhu, G. Z. Fang, S. Q. Liang, Z. X. Chen, Z. Q. Wang, J. Y. Ma, H. Wang, B. Y. Tang, X. S. Zheng and J. Zhou, *Energy Storage Mater.*, 2020, **24**, 394–401.

191 P. G. He, J. H. Liu, X. D. Zhao, Z. P. Ding, P. Gao and L. Z. Fan, *J. Mater. Chem. A*, 2020, **8**, 10370–10376.

192 S. Q. Wei, S. M. Chen, X. Z. Su, Z. H. Qi, C. D. Wang, B. B. Ganguli, P. J. Zhang, K. F. Zhu, Y. Y. Cao, Q. He, D. F. Cao, X. Guo, W. Wen, X. J. Wu, P. M. Ajayan and L. Song, *Energy Environ. Sci.*, 2021, **14**, 3954–3964.

193 J. W. Ding, Z. G. Du, B. Li, L. Z. Wang, S. W. Wang, Y. J. Gong and S. B. Yang, *Adv. Mater.*, 2019, **31**, 1904369.

194 H. Luo, B. Wang, F. Wang, J. Yang, F. D. Wu, Y. Ning, Y. Zhou, D. L. Wang, H. K. Liu and S. X. Dou, *ACS Nano*, 2020, **14**, 7328–7337.

195 J. W. Ding, H. Y. Zheng, H. G. Gao, Q. N. Liu, Z. Hu, L. F. Han, S. W. Wang, S. D. Wu, S. M. Fang and S. L. Chou, *Adv. Energy Mater.*, 2021, **11**, 2100973.

196 J. Cui, Z. W. Guo, J. Yi, X. Y. Liu, K. Wu, P. C. Liang, Q. Li, Y. Y. Liu, Y. G. Wang, Y. Y. Xia and J. J. Zhang, *ChemSusChem*, 2020, **13**, 2160–2185.

197 Z. H. Li, J. Tan, C. Y. Gao, Y. Wang, Y. G. Wang, M. X. Ye and J. F. Shen, *Energy Environ. Sci.*, 2023, **16**, 2398–2431.

198 Z. R. Lin, H. Y. Shi, L. Lin, X. P. Yang, W. L. Wu and X. Q. Sun, *Nat. Commun.*, 2021, **12**, 4424.

199 W. X. Wang, V. S. Kale, Z. Cao, Y. J. Lei, S. Kandambeth, G. D. Zou, Y. P. Zhu, E. Abouhamad, O. Shekhah, L. Cavallo, M. Eddaoudi and H. N. Alshareef, *Adv. Mater.*, 2021, **33**, 2103617.

200 Y. Zhao, Y. X. Huang, F. Wu, R. J. Chen and L. Li, *Adv. Mater.*, 2021, **33**, 2106469.

201 X. Y. Wu, A. Markir, L. Ma, Y. K. Xu, H. Jiang, D. P. Leonard, W. Shin, T. P. Wu, J. Lu and X. L. Ji, *Angew. Chem., Int. Ed.*, 2019, **58**, 12640–12645.

202 C. L. Dai, L. Y. Hu, X. T. Jin, H. Chen, X. Q. Zhang, S. H. Zhang, L. Song, H. Y. Ma, M. W. Xu, Y. Zhao, Z. P. Zhang, H. H. Cheng and L. T. Qu, *Adv. Mater.*, 2021, **33**, 2105480.

203 W. Li, K. L. Wang and K. Jiang, *Adv. Sci.*, 2020, **7**, 2000761.

204 C. L. Dai, X. T. Jin, H. Y. Ma, L. Y. Hu, G. Q. Sun, H. Chen, Q. J. Yang, M. W. Xu, Q. W. Liu, Y. K. Xiao, X. Q. Zhang, H. S. Yang, Q. Guo, Z. P. Zhang and L. T. Qu, *Adv. Energy Mater.*, 2021, **11**, 2003982.

205 W. Li, Y. S. Ma, P. Li, X. Y. Jing, K. Jiang and D. H. Wang, *Adv. Funct. Mater.*, 2021, **31**, 2101237.

206 Z. Chen, F. N. Mo, T. R. Wang, Q. Yang, Z. D. Huang, D. H. Wang, G. J. Liang, A. Chen, Q. Li, Y. Guo, X. L. Li, J. Fan and C. Y. Zhi, *Energy Environ. Sci.*, 2021, **14**, 2441–2450.

207 J. Shin, D. S. Choi, H. J. Lee, Y. Jung and J. W. Choi, *Adv. Energy Mater.*, 2019, **9**, 1900083.

208 N. Zhang, M. Jia, Y. Dong, Y. Y. Wang, J. Z. Xu, Y. C. Liu, L. F. Jiao and F. Y. Cheng, *Adv. Funct. Mater.*, 2019, **29**, 1807331.

209 D. Bin, Y. Liu, B. B. Yang, J. H. Huang, X. L. Dong, X. Zhang, Y. G. Wang and Y. Y. Xia, *ACS Appl. Mater. Interfaces*, 2019, **11**, 20796–20803.

210 T. J. Sun, Q. S. Nian, S. B. Zheng, X. M. Yuan and Z. L. Tao, *J. Power Sources*, 2020, **478**, 228758.

211 Y. X. Zeng, X. F. Lu, S. L. Zhang, D. Y. Luan, S. Li and X. W. Lou, *Angew. Chem., Int. Ed.*, 2021, **60**, 22189–22194.

212 D. Bin, W. C. Huo, Y. B. Yuan, J. H. Huang, Y. Liu, Y. X. Zhang, F. Dong, Y. G. Wang and Y. Y. Xia, *Chem*, 2020, **6**, 968–984.

213 H. L. Peng, C. H. Liu, N. N. Wang, C. G. Wang, D. D. Wang, Y. L. Li, B. Chen, J. Yang and Y. T. Qian, *Energy Environ. Sci.*, 2022, **15**, 1682–1693.

214 T. T. Lv, Y. Y. Liu, H. Wang, S. Y. Yang, C. S. Liu and H. Pang, *Chem. Eng. J.*, 2021, **411**, 128533.

215 M. S. Zhang, W. X. Wu, J. W. Luo, H. Z. Zhang, J. Liu, X. Q. Liu, Y. Y. Yang and X. H. Lu, *J. Mater. Chem. A*, 2020, **8**, 11642–11648.

216 T. Xiong, Z. G. Yu, H. J. Wu, Y. H. Du, Q. D. Xie, J. S. Chen, Y. W. Zhang, S. J. Pennycook, W. S. V. Lee and J. M. Xue, *Adv. Energy Mater.*, 2019, **9**, 1803815.

217 Z. Q. Li, Y. K. Ren, L. Mo, C. F. Liu, K. Hsu, Y. C. Ding, X. X. Zhang, X. L. Li, L. H. Hu, D. H. Ji and G. Z. Cao, *ACS Nano*, 2020, **14**, 5581–5589.

218 M. M. Han, J. W. Huang, S. Q. Liang, L. T. Shan, X. S. Xie, Z. Y. Yi, Y. R. Wang, S. Guo and J. Zhou, *Iscience*, 2020, **23**, 100797.

219 Y. Q. Zhang, L. Tao, C. Xie, D. D. Wang, Y. Q. Zou, R. Chen, Y. Y. Wang, C. K. Jia and S. Y. Wang, *Adv. Mater.*, 2020, **32**, 1905923.

4918 | *Chem. Soc. Rev.*, 2024, **53**, 4877–4925

This journal is © The Royal Society of Chemistry 2024

220 Z. C. Y. Zhang, B. J. Xi, X. Wang, X. J. Ma, W. H. Chen, J. K. Feng and S. L. Xiong, *Adv. Funct. Mater.*, 2021, **31**, 2103070.

221 X. L. Li, Z. D. Huang, C. E. Shuck, G. J. Liang, Y. Gogotsi and C. Y. Zhi, *Nat. Rev. Chem.*, 2022, **6**, 389–404.

222 W. Y. Du, L. Miao, Z. Y. Song, X. W. Zheng, Y. K. Lv, D. Z. Zhu, L. H. Gan and M. X. Liu, *J. Power Sources*, 2022, **536**, 231512.

223 N. Zhang, J. C. Wang, Y. F. Guo, P. F. Wang, Y. R. Zhu and T. F. Yi, *Coord. Chem. Rev.*, 2023, **479**, 215009.

224 Y. Z. Wu, M. C. Wang, Y. Tao, K. Zhang, M. L. Cai, Y. Ding, X. P. Liu, T. Hayat, A. Alsaedi and S. Y. Dai, *Adv. Funct. Mater.*, 2020, **30**, 1907120.

225 S. Z. Deng, Z. W. Tie, F. Yue, H. M. Cao, M. J. Yao and Z. Q. Niu, *Angew. Chem., Int. Ed.*, 2022, **61**, e202115877.

226 X. D. Zhu, Z. Y. Cao, W. J. Wang, H. J. Li, J. C. Dong, S. P. Gao, D. X. Xu, L. Li, J. F. Shen and M. X. Ye, *ACS Nano*, 2021, **15**, 2971–2983.

227 Y. X. Zeng, X. Y. Zhang, Y. Meng, M. H. Yu, J. N. Yi, Y. Q. Wu, X. H. Lu and Y. X. Tong, *Adv. Mater.*, 2017, **29**, 1700274.

228 Y. Q. Fu, Q. L. Wei, G. X. Zhang, X. M. Wang, J. H. Zhang, Y. F. Hu, D. N. Wang, L. C. Zuin, T. Zhou, Y. C. Wu and S. H. Sun, *Adv. Energy Mater.*, 2018, **8**, 1801445.

229 B. K. Wu, G. B. Zhang, M. Y. Yan, T. F. Xiong, P. He, L. He, X. Xu and L. Q. Mai, *Small*, 2018, **14**, 1703850.

230 J. J. Wang, J. G. Wang, H. Y. Liu, Z. Y. You, Z. Li, F. Y. Kang and B. Q. Wei, *Adv. Funct. Mater.*, 2021, **31**, 2007397.

231 Q. Ni, B. Kim, C. A. Wu and K. Kang, *Adv. Mater.*, 2022, **34**, 2108206.

232 J. Ji, H. Z. Wan, B. Zhang, C. Wang, Y. Gan, Q. Y. Tan, N. Z. Wang, J. Yao, Z. H. Zheng, P. Liang, J. Zhang, H. B. Wang, L. Tao, Y. Wang, D. L. Chao and H. Wang, *Adv. Energy Mater.*, 2021, **11**, 2003203.

233 Z. Q. Luo, S. L. Zheng, S. Zhao, X. Jiao, Z. S. Gong, F. S. Cai, Y. Q. Duan, F. J. Li and Z. H. Yuan, *J. Mater. Chem. A*, 2021, **9**, 6131–6138.

234 S. Wang, Z. S. Yuan, X. Zhang, S. S. Bi, Z. Zhou, J. L. Tian, Q. C. Zhang and Z. Q. Niu, *Angew. Chem., Int. Ed.*, 2021, **60**, 7056–7060.

235 Y. Q. Yang, S. Q. Liang, B. A. Lu and J. Zhou, *Energy Environ. Sci.*, 2022, **15**, 1192–1200.

236 Y. P. Zou, T. T. Liu, Q. J. Du, Y. Y. Li, H. B. Yi, X. Zhou, Z. X. Li, L. J. Gao, L. Zhang and X. Liang, *Nat. Commun.*, 2021, **12**, 170.

237 J. N. Hao, L. B. Yuan, B. Johannessen, Y. L. Zhu, Y. Jiao, C. Ye, F. X. Xie and S. Z. Qiao, *Angew. Chem., Int. Ed.*, 2021, **60**, 25114–25121.

238 H. Yang, T. S. Zhang, D. Chen, Y. C. Tan, W. H. Zhou, L. Li, W. Li, G. S. Li, W. Han, H. J. Fan and D. L. Chao, *Adv. Mater.*, 2023, **35**, 2300053.

239 Z. Chen, H. L. Cui, Y. Hou, X. Q. Wang, X. Jin, A. Chen, Q. Yang, D. H. Wang, Z. D. Huang and C. Y. Zhi, *Chem*, 2022, **8**, 2204–2216.

240 L. Y. Zhang, L. Chen, X. F. Zhou and Z. P. Liu, *Adv. Energy Mater.*, 2015, **5**, 1400930.

241 L. T. Ma, S. M. Chen, H. F. Li, Z. H. Ruan, Z. J. Tang, Z. X. Liu, Z. F. Wang, Y. Huang, Z. X. Pei, J. A. Zapien and C. Y. Zhi, *Energy Environ. Sci.*, 2018, **11**, 2521–2530.

242 Z. X. Liu, Q. Yang, D. H. Wang, G. J. Liang, Y. H. Zhu, F. N. Mo, Z. D. Huang, X. L. Li, L. T. Ma, T. C. Tang, Z. G. Lu and C. Y. Zhi, *Adv. Energy Mater.*, 2019, **9**, 1902473.

243 Z. G. Hou, X. Q. Zhang, X. N. Li, Y. C. Zhu, J. W. Liang and Y. T. Qian, *J. Mater. Chem. A*, 2017, **5**, 730–738.

244 F. Wan, Y. Zhang, L. L. Zhang, D. B. Liu, C. D. Wang, L. Song, Z. Q. Niu and J. Chen, *Angew. Chem., Int. Ed.*, 2019, **58**, 7062–7067.

245 N. Li, G. Q. Li, C. J. Li, H. C. Yang, G. W. Qin, X. D. Sun, F. Li and H. M. Cheng, *ACS Appl. Mater. Interfaces*, 2020, **12**, 13790–13796.

246 D. L. Chao, W. H. Zhou, C. Ye, Q. H. Zhang, Y. G. Chen, L. Gu, K. Davey and S. Z. Qiao, *Angew. Chem., Int. Ed.*, 2019, **58**, 7823–7828.

247 X. S. Xie, H. W. Fu, Y. Fang, B. A. Lu, J. Zhou and S. Q. Liang, *Adv. Energy Mater.*, 2022, **12**, 2102393.

248 C. Liu, X. W. Chi, Q. Han and Y. Liu, *Adv. Energy Mater.*, 2020, **10**, 1903589.

249 P. C. Ruan, S. Q. Liang, B. G. Lu, H. J. Fan and J. Zhou, *Angew. Chem., Int. Ed.*, 2022, **61**, e202200598.

250 P. C. Ruan, X. L. Xu, D. Zheng, X. H. Chen, X. Y. Yin, S. Q. Liang, X. W. Wu, W. H. Shi, X. H. Cao and J. Zhou, *ChemSusChem*, 2022, **15**, e202201118.

251 X. F. Shen, X. N. Wang, Y. R. Zhou, Y. H. Shi, L. M. Zhao, H. H. Jin, J. T. Di and Q. W. Li, *Adv. Funct. Mater.*, 2021, **31**, 2101579.

252 L. X. Dai, L. Wang, L. Sun, Y. Ding, Y. Q. Yao, L. D. Yao, N. E. Drewett, W. Zhang, J. Tang and W. T. Zheng, *Adv. Sci.*, 2021, **8**, 2004995.

253 C. X. Xie, T. Y. Li, C. Z. Deng, Y. Song, H. M. Zhang and X. F. Li, *Energy Environ. Sci.*, 2020, **13**, 135–143.

254 G. D. Li, W. Chen, H. Zhang, Y. J. Gong, F. F. Shi, J. Y. Wang, R. F. Zhang, G. X. Chen, Y. Jin, T. Wu, Z. Y. Tang and Y. Cui, *Adv. Energy Mater.*, 2020, **10**, 1902085.

255 J. F. Lei, Y. X. Yao, Z. Y. Wang and Y. C. Lu, *Energy Environ. Sci.*, 2021, **14**, 4418–4426.

256 Z. Chen, C. Li, Q. Yang, D. H. Wang, X. L. Li, Z. D. Huang, G. J. Liang, A. Chen and C. Y. Zhi, *Adv. Mater.*, 2021, **33**, 2105426.

257 Z. Chen, Q. Yang, F. N. Mo, N. Li, G. J. Liang, X. L. Li, Z. D. Huang, D. H. Wang, W. C. Huang, J. Fan and C. Y. Zhi, *Adv. Mater.*, 2020, **32**, 2001469.

258 X. L. Li, N. Li, Z. D. Huang, Z. Chen, Y. W. Zhao, G. J. Liang, Q. Yang, M. Li, Q. Huang, B. B. Dong, J. Fan and C. Y. Zhi, *ACS Nano*, 2021, **15**, 1718–1726.

259 X. L. Li, Y. L. Wang, Z. Chen, P. Li, G. J. Liang, Z. D. Huang, Q. Yang, A. Chen, H. L. Cui, B. B. Dong, H. Y. He and C. Y. Zhi, *Angew. Chem., Int. Ed.*, 2022, **61**, e202113576.

260 X. Y. Wu, Y. K. Xu, C. Zhang, D. P. Leonard, A. Markir, J. Lu and X. L. Ji, *J. Am. Chem. Soc.*, 2019, **141**, 6338–6344.

261 Z. Chen, Y. W. Zhao, F. N. Mo, Z. D. Huang, X. L. Li, D. H. Wang, G. J. Liang, Q. Yang, A. Chen, Q. Li, L. T. Ma, Y. Guo and C. Y. Zhi, *Small Struct.*, 2020, **1**, 2000005.

This journal is © The Royal Society of Chemistry 2024

Chem. Soc. Rev., 2024, **53**, 4877–4925 | 4919

262 J. Ibers, *Nat. Chem.*, 2009, **1**, 508.

263 X. F. Zhang, S. Q. Jiao, J. G. Tu, W. L. Song, X. Xiao, S. J. Li, M. Y. Wang, H. P. Lei, D. H. Tian, H. S. Chen and D. N. Fang, *Energy Environ. Sci.*, 2019, **12**, 1918–1927.

264 Z. Chen, S. N. Wang, Z. Q. Wei, Y. Q. Wang, Z. X. Wu, Y. Hou, J. X. Zhu, Y. B. Wang, G. J. Liang, Z. D. Huang, A. Chen, D. H. Wang and C. Y. Zhi, *J. Am. Chem. Soc.*, 2023, **145**, 20521–20529.

265 J. H. Huang, Y. H. Xie, L. Yan, B. L. Wang, T. Y. Kong, X. L. Dong, Y. G. Wang and Y. Y. Xia, *Energy Environ. Sci.*, 2021, **14**, 883–889.

266 Z. X. Zhu, T. L. Jiang, M. Ali, Y. H. Meng, Y. Jin, Y. Cui and W. Chen, *Chem. Rev.*, 2022, **122**, 16610–16751.

267 H. M. Tang, Y. Yin, Y. Huang, J. W. Wang, L. X. Liu, Z. Qu, H. Zhang, Y. Li, M. S. Zhu and O. G. Schmidt, *ACS Energy Lett.*, 2021, **6**, 1859–1868.

268 G. G. Yadav, D. Turney, J. C. Huang, X. Wei and S. Banerjee, *ACS Energy Lett.*, 2019, **4**, 2144–2146.

269 S. Gu, K. Gong, E. Z. Yan and Y. S. Yan, *Energy Environ. Sci.*, 2014, **7**, 2986–2998.

270 K. Gong, X. Y. Ma, K. M. Conforti, K. J. Kuttler, J. B. Grunewald, K. L. Yeager, M. Z. Bazant, S. Gu and Y. S. Yan, *Energy Environ. Sci.*, 2015, **8**, 2941–2945.

271 J. Winsberg, T. Hagemann, T. Janoschka, M. D. Hager and U. S. Schubert, *Angew. Chem., Int. Ed.*, 2017, **56**, 686–711.

272 C. X. Xie, H. M. Zhang, W. B. Xu, W. Wang and X. F. Li, *Angew. Chem., Int. Ed.*, 2018, **57**, 11171–11176.

273 D. G. Kwabi, Y. L. Ji and M. J. Aziz, *Chem. Rev.*, 2020, **120**, 6467–6489.

274 S. N. Wang, Z. Y. Wang, Y. B. Yin, T. Y. Li, N. N. Chang, F. T. Fan, H. M. Zhang and X. F. Li, *Energy Environ. Sci.*, 2021, **14**, 4077–4084.

275 Z. M. Zhao, X. H. Liu, M. Q. Zhang, L. Y. Zhang, C. K. Zhang, X. F. Li and G. H. Yu, *Chem. Soc. Rev.*, 2023, **52**, 6031–6074.

276 D. L. Yu, L. P. Zhi, F. F. Zhang, Y. Song, Q. Wang, Z. Z. Yuan and X. F. Li, *Adv. Mater.*, 2023, **35**, 2209390.

277 J. Wu, C. G. Yuan, T. Y. Li, Z. Z. Yuan, H. M. Zhang and X. F. Li, *J. Am. Chem. Soc.*, 2021, **143**, 13135–13144.

278 S. Q. Jiao, J. M. Fu, M. Z. Wu, T. Hua and H. B. Hu, *ACS Nano*, 2022, **16**, 1013–1024.

279 L. T. Ma, S. M. Chen, N. Li, Z. X. Liu, Z. J. Tang, J. A. Zapien, S. M. Chen, J. Fan and C. Y. Zhi, *Adv. Mater.*, 2020, **32**, 1908121.

280 F. Wang, O. Borodin, T. Gao, X. L. Fan, W. Sun, F. D. Han, A. Faraone, J. A. Dura, K. Xu and C. S. Wang, *Nat. Mater.*, 2018, **17**, 543–549.

281 D. Yuan, J. Zhao, H. Ren, Y. Q. Chen, R. Chua, E. T. J. Jie, Y. Cai, E. Edison, W. Manalastas, M. W. Wong and M. Srinivasan, *Angew. Chem., Int. Ed.*, 2021, **60**, 7213–7219.

282 Z. D. Zhao, R. Wang, C. X. Peng, W. J. Chen, T. Q. Wu, B. Hu, W. J. Weng, Y. Yao, J. X. Zeng, Z. H. Chen, P. Y. Liu, Y. C. Liu, G. S. Li, J. Guo, H. B. Lu and Z. P. Guo, *Nat. Commun.*, 2021, **12**, 6606.

283 Q. Zhang, Y. L. Ma, Y. Lu, X. Z. Zhou, L. Lin, L. Li, Z. H. Yan, Q. Zhao, K. Zhang and J. Chen, *Angew. Chem., Int. Ed.*, 2021, **60**, 23357–23364.

284 L. B. Yuan, J. N. Hao, C. C. Kao, C. Wu, H. K. Liu, S. X. Dou and S. Z. Qiao, *Energy Environ. Sci.*, 2021, **14**, 5669–5689.

285 D. E. Turney, J. W. Gallaway, G. G. Yadav, R. Ramirez, M. Nyce, S. Banerjee, Y. C. K. Chen-Wiegart, J. Wang, M. J. D'Ambrose, S. Kolhekar, J. C. Huang and X. Wei, *Chem. Mater.*, 2017, **29**, 4819–4832.

286 Z. F. Yang, C. Hu, Q. Zhang, T. Q. Wu, C. L. Xie, H. Wang, Y. G. Tang, X. B. Ji and H. Y. Wang, *Angew. Chem., Int. Ed.*, 2023, **62**, e202308017.

287 X. H. Zheng, T. Ahmad and W. Chen, *Energy Storage Mater.*, 2021, **39**, 365–394.

288 Y. M. Zhang, J. D. Howe, S. Ben-Yoseph, Y. T. Wu and N. Liu, *ACS Energy Lett.*, 2021, **6**, 404–412.

289 F. Moser, F. Fourgeot, R. Rouget, O. Crosnier and T. Brousse, *Electrochim. Acta*, 2013, **109**, 110–116.

290 H. F. Li, C. J. Xu, C. P. Han, Y. Y. Chen, C. G. Wei, B. H. Li and F. Y. Kang, *J. Electrochem. Soc.*, 2015, **162**, A1439–A1444.

291 L. S. Cao, D. Li, T. Deng, Q. Li and C. S. Wang, *Angew. Chem., Int. Ed.*, 2020, **59**, 19292–19296.

292 X. Wang, J. P. Meng, X. G. Lin, Y. D. Yang, S. Zhou, Y. P. Wang and A. Q. Pan, *Adv. Funct. Mater.*, 2021, **31**, 2106114.

293 J. L. Yang, J. Li, J. W. Zhao, K. Liu, P. H. Yang and H. J. Fan, *Adv. Mater.*, 2022, **34**, 2202382.

294 Y. Yang, C. Y. Liu, Z. H. Lv, H. Yang, Y. F. Zhang, M. H. Ye, L. B. Chen, J. B. Zhao and C. C. Li, *Adv. Mater.*, 2021, **33**, 2007388.

295 M. H. Yu, N. Chandrasekhar, R. K. M. Raghupathy, K. H. Ly, H. Z. Zhang, E. Dmitrieva, C. L. Liang, X. H. Lu, T. D. Kühne, H. Mirhosseini, I. M. Weidinger and X. L. Feng, *J. Am. Chem. Soc.*, 2020, **142**, 19570–19578.

296 M. S. Zhu, J. P. Hu, Q. Q. Lu, H. Y. Dong, D. D. Karnaushenko, C. Becker, D. Karnaushenko, Y. Li, H. M. Tang, Z. Qu, J. Ge and O. G. Schmidt, *Adv. Mater.*, 2021, **33**, 2007497.

297 P. Chen, X. H. Yuan, Y. B. Xia, Y. Zhang, L. J. Fu, L. L. Liu, N. F. Yu, Q. H. Huang, B. Wang, X. W. Hu, Y. P. Wu and T. van Ree, *Adv. Sci.*, 2021, **8**, 2100309.

298 Y. H. Cui, Q. H. Zhao, X. J. Wu, X. Chen, J. L. Yang, Y. T. Wang, R. Z. Qin, S. X. Ding, Y. L. Song, J. W. Wu, K. Yang, Z. J. Wang, Z. W. Mei, Z. B. Song, H. Wu, Z. Y. Jiang, G. Y. Qian, L. Y. Yang and F. Pan, *Angew. Chem., Int. Ed.*, 2020, **59**, 16594–16601.

299 Z. K. Guo, L. S. Fan, C. Y. Zhao, A. S. Chen, N. N. Liu, Y. Zhang and N. Q. Zhang, *Adv. Mater.*, 2022, **34**, 2105133.

300 H. B. He, H. Tong, X. Y. Song, X. P. Song and J. Liu, *J. Mater. Chem. A*, 2020, **8**, 7836–7846.

301 L. Hong, X. M. Wu, L. Y. Wang, M. Zhong, P. Y. Zhang, L. S. Jiang, W. Huang, Y. L. Wang, K. X. Wang and J. S. Chen, *ACS Nano*, 2022, **16**, 6906–6915.

302 C. Huang, X. Zhao, S. Liu, Y. S. Hao, Q. L. Tang, A. P. Hu, Z. X. Liu and X. H. Chen, *Adv. Mater.*, 2021, **33**, 2100445.

303 Q. Yang, Y. Guo, B. X. Yan, C. D. Wang, Z. X. Liu, Z. D. Huang, Y. K. Wang, Y. R. Li, H. F. Li, L. Song, J. Fan and C. Y. Zhi, *Adv. Mater.*, 2020, **32**, 2001755.

304 Q. Zhang, J. Y. Luan, X. B. Huang, Q. Wang, D. Sun, Y. G. Tang, X. B. Ji and H. Y. Wang, *Nat. Commun.*, 2020, **11**, 3961.

4920 | *Chem. Soc. Rev.*, 2024, **53**, 4877–4925

This journal is © The Royal Society of Chemistry 2024

305 J. H. Zhou, M. Xie, F. Wu, Y. Mei, Y. T. Hao, R. L. Huang, G. L. Wei, A. N. Liu, L. Li and R. J. Chen, *Adv. Mater.*, 2021, **33**, 2101649.

306 R. T. Guo, X. Liu, F. J. Xia, Y. L. Jiang, H. Z. Zhang, M. Huang, C. J. Niu, J. S. Wu, Y. Zhao, X. P. Wang, C. H. Han and L. Q. Mai, *Adv. Mater.*, 2022, **34**, 2202188.

307 L. T. Kang, M. W. Cui, F. Y. Jiang, Y. F. Gao, H. J. Luo, J. J. Liu, W. Liang and C. Y. Zhi, *Adv. Energy Mater.*, 2018, **8**, 1801090.

308 K. N. Zhao, C. X. Wang, Y. H. Yu, M. Y. Yan, Q. L. Wei, P. He, Y. F. Dong, Z. Y. Zhang, X. D. Wang and L. Q. Mai, *Adv. Mater. Interfaces*, 2018, **5**, 1800848.

309 H. Yu, Y. X. Zeng, N. W. Li, D. Y. Luan, L. Yu and X. W. Lou, *Sci. Adv.*, 2022, **8**, eabm5766.

310 S. B. Wang, Q. Ran, R. Q. Yao, H. Shi, Z. Wen, M. Zhao, X. Y. Lang and Q. Jiang, *Nat. Commun.*, 2020, **11**, 1634.

311 W. J. Lu, C. X. Xie, H. M. Zhang and X. F. Li, *ChemSusChem*, 2018, **11**, 3996–4006.

312 J. F. Parker, C. N. Chervin, E. S. Nelson, D. R. Rolison and J. W. Long, *Energy Environ. Sci.*, 2014, **7**, 1117–1124.

313 J. F. Parker, C. N. Chervin, I. R. Pala, M. Machler, M. F. Burz, J. W. Long and D. R. Rolison, *Science*, 2017, **356**, 414–417.

314 J. N. Hao, L. B. Yuan, C. Ye, D. L. Chao, K. Davey, Z. P. Guo and S. Z. Qiao, *Angew. Chem., Int. Ed.*, 2021, **60**, 7366–7375.

315 A. Naveed, H. J. Yang, J. Yang, Y. N. Nuli and J. L. Wang, *Angew. Chem., Int. Ed.*, 2019, **58**, 2760–2764.

316 X. H. Zeng, J. F. Mao, J. N. Hao, J. T. Liu, S. L. Liu, Z. J. Wang, Y. Y. Wang, S. L. Zhang, T. Zheng, J. W. Liu, P. H. Rao and Z. P. Guo, *Adv. Mater.*, 2021, **33**, 2007416.

317 C. Li, A. Shyamsunder, A. G. Hoane, D. M. Long, C. Y. Kwok, P. G. Kotula, K. R. Zavadil, A. A. Gewirth and L. F. Nazar, *Joule*, 2022, **6**, 1103–1120.

318 H. Y. Liu, J. G. Wang, W. Hua, L. B. Ren, H. H. Sun, Z. D. Hou, Y. Huyan, Y. J. Cao, C. G. Wei and F. Y. Kang, *Energy Environ. Sci.*, 2022, **15**, 1872–1881.

319 G. Q. Ma, L. C. Miao, Y. Dong, W. T. Yuan, X. Y. Nie, S. L. Di, Y. Y. Wang, L. B. Wang and N. Zhang, *Energy Storage Mater.*, 2022, **47**, 203–210.

320 L. C. Miao, R. H. Wang, S. L. Di, Z. F. Qian, L. Zhang, W. L. Xin, M. Y. Liu, Z. Q. Zhu, S. Q. Chu, Y. Du and N. Zhang, *ACS Nano*, 2022, **16**, 9667–9678.

321 X. H. Zeng, K. X. Xie, S. L. Liu, S. L. Zhang, J. N. Hao, J. T. Liu, W. K. Pang, J. W. Liu, P. H. Rao, Q. H. Wang, J. F. Mao and Z. P. Guo, *Energy Environ. Sci.*, 2021, **14**, 5947–5957.

322 S. W. Huang, L. Hou, T. Y. Li, Y. C. Jiao and P. Y. Wu, *Adv. Mater.*, 2022, **34**, 2110140.

323 T. C. Li, Y. Lim, X. L. Li, S. Z. Luo, C. J. Lin, D. L. Fang, S. W. Xia, Y. Wang and H. Y. Yang, *Adv. Energy Mater.*, 2022, **12**, 2103231.

324 S. L. Liu, J. F. Mao, W. K. Pang, J. Vongsvivut, X. H. Zeng, L. Thomsen, Y. Y. Wang, J. W. Liu, D. Li and Z. P. Guo, *Adv. Funct. Mater.*, 2021, **31**, 2104281.

325 S. L. Liu, R. Z. Zhang, J. F. Mao, Y. L. Zhao, Q. Cai and Z. P. Guo, *Sci. Adv.*, 2022, **8**, eabn5097.

326 Y. Q. Lv, Y. Xiao, L. T. Ma, C. Y. Zhi and S. M. Chen, *Adv. Mater.*, 2022, **34**, 2106409.

327 X. Y. Nie, L. C. Miao, W. T. Yuan, G. Q. Ma, S. L. Di, Y. Y. Wang, S. G. Shen and N. Zhang, *Adv. Funct. Mater.*, 2022, **32**, 2203905.

328 P. J. Wang, S. Q. Liang, C. Chen, X. S. Xie, J. W. Chen, Z. H. Liu, Y. Tang, B. A. Lu and J. Zhou, *Adv. Mater.*, 2022, **34**, 2202733.

329 Y. Y. Wang, Z. J. Wang, F. H. Yang, S. L. Liu, S. L. Zhang, J. F. Mao and Z. P. Guo, *Small*, 2022, **18**, 2107033.

330 H. J. Yang, Y. Qiao, Z. Chang, H. Deng, X. Y. Zhu, R. J. Zhu, Z. T. Xiong, P. He and H. S. Zhou, *Adv. Mater.*, 2021, **33**, 2102415.

331 M. Yang, J. C. Zhu, S. S. Bi, R. Wang and Z. Q. Niu, *Adv. Mater.*, 2022, **34**, 2201744.

332 W. N. Xu, K. N. Zhao, W. C. Huo, Y. Z. Wang, G. Yao, X. Gu, H. W. Cheng, L. Q. Mai, C. G. Hu and X. D. Wang, *Nano Energy*, 2019, **62**, 275–281.

333 Y. P. Zhu, J. Yin, X. L. Zheng, A. H. Emwas, Y. J. Lei, O. F. Mohammed, Y. Cui and H. N. Alshareef, *Energy Environ. Sci.*, 2021, **14**, 4463–4473.

334 Y. Tang, C. X. Liu, H. R. Zhu, X. S. Xie, J. W. Gao, C. B. Deng, M. M. Han, S. Q. Liang and J. Zhou, *Energy Storage Mater.*, 2020, **27**, 109–116.

335 H. J. Yang, Z. Chang, Y. Qiao, H. Deng, X. W. Mu, P. He and H. S. Zhou, *Angew. Chem., Int. Ed.*, 2020, **59**, 9377–9381.

336 H. Y. Lu, J. S. Hu, L. T. Wang, J. Z. Li, X. Ma, Z. C. Zhu, H. Q. Li, Y. J. Zhao, Y. J. Li, J. X. Zhao and B. G. Xu, *Adv. Funct. Mater.*, 2022, **32**, 2112540.

337 G. J. Liang, Z. J. Tang, B. Han, J. X. Zhu, A. Chen, Q. Li, Z. Chen, Z. D. Huang, X. L. Li, Q. Yang and C. Y. Zhi, *Adv. Mater.*, 2023, **35**, 2210051.

338 H. Jiang, L. T. Tang, Y. K. Fu, S. T. Wang, S. K. Sandstrom, A. M. Scida, G. X. Li, D. Hoang, J. Hong, N. C. Chiu, K. C. Stylianou, W. F. Stickle, D. H. Wang, J. Li, P. A. Greaney, C. Fang and X. L. Ji, *Nat. Sustain.*, 2023, **6**, 806–815.

339 Z. Liu, G. Pulletikurthi and F. Endres, *ACS Appl. Mater. Interfaces*, 2016, **8**, 12158–12164.

340 G. Kasiri, R. Trócoli, A. B. Hashemi and F. La Mantia, *Electrochim. Acta*, 2016, **222**, 74–83.

341 B. Sambandam, V. Soundharrajan, S. Kim, M. H. Alfaruqi, J. Jo, S. Kim, V. Mathew, Y. K. Sun and J. Kim, *J. Mater. Chem. A*, 2018, **6**, 3850–3856.

342 D. S. Liu, Z. Y. Zhang, Y. F. Zhang, M. H. Ye, S. Huang, S. Z. You, Z. J. Du, J. F. He, Z. P. Wen, Y. C. Tang, X. Q. Liu and C. C. Li, *Angew. Chem., Int. Ed.*, 2023, **62**, e202215385.

343 W. Zhang and G. J. He, *Angew. Chem., Int. Ed.*, 2023, **62**, e202218466.

344 H. F. Wang, W. Q. Ye, B. W. Yin, K. X. Wang, M. S. Riaz, B. B. Xie, Y. J. Zhong and Y. Hu, *Angew. Chem., Int. Ed.*, 2023, **62**, e202218872.

345 M. J. Qiu, P. Sun, Y. Wang, L. Ma, C. Y. Zhi and W. J. Mai, *Angew. Chem., Int. Ed.*, 2022, **61**, e202210979.

346 Y. Wang, T. R. Wang, S. Y. Bu, J. X. Zhu, Y. B. Wang, R. Zhang, H. Hong, W. J. Zhang, J. Fan and C. Y. Zhi, *Nat. Commun.*, 2023, **14**, 1828.

347 L. S. Cao, D. Li, E. Y. Hu, J. J. Xu, T. Deng, L. Ma, Y. Wang, X. Q. Yang and C. S. Wang, *J. Am. Chem. Soc.*, 2020, **142**, 21404–21409.

This journal is © The Royal Society of Chemistry 2024

Chem. Soc. Rev., 2024, **53**, 4877–4925 | 4921

348 X. M. Zeng, X. J. Meng, W. Jiang, M. Ling, L. J. Yan and C. D. Liang, *Electrochim. Acta*, 2021, **378**, 138106.

349 Z. H. Chen, H. Z. Chen, Y. C. Che, L. Cheng, H. Zhang, J. Chen, F. Y. Xie, N. Wang, Y. S. Jin and H. Meng, *ACS Sustainable Chem. Eng.*, 2021, **9**, 6855–6863.

350 M. D. Yan, C. L. Xu, Y. Sun, H. L. Pan and H. Li, *Nano Energy*, 2021, **82**, 105739.

351 Z. G. Hou, M. F. Dong, Y. L. Xiong, X. Q. Zhang, H. S. Ao, M. K. Liu, Y. C. Zhu and Y. T. Qian, *Small*, 2020, **16**, 2001228.

352 W. J. Zhou, M. F. Chen, Q. H. Tian, J. Z. Chen, X. W. Xu, X. Han and J. L. Xu, *J. Colloid Interface Sci.*, 2021, **601**, 486–494.

353 W. Zhang, Y. H. Dai, R. W. Chen, Z. M. Xu, J. W. Li, W. Zong, H. X. Li, Z. Li, Z. Y. Zhang, J. X. Zhu, F. Guo, X. Gao, Z. J. Du, J. T. Chen, T. L. Wang, G. J. He and I. P. Parkin, *Angew. Chem., Int. Ed.*, 2023, **62**, e202212695.

354 Y. Zhao, Y. N. Wang, Z. M. Zhao, J. W. Zhao, T. Xin, N. Wang and J. Z. Liu, *Energy Storage Mater.*, 2020, **28**, 64–72.

355 Z. Q. Luo, L. J. Liu, J. X. Ning, K. X. Lei, Y. Lu, F. J. Li and J. Chen, *Angew. Chem., Int. Ed.*, 2018, **57**, 9443–9446.

356 S. Gu, S. F. Wu, L. J. Cao, M. C. Li, N. Qin, J. Zhu, Z. Q. Wang, Y. Z. Li, Z. Q. Li, J. J. Chen and Z. G. Lu, *J. Am. Chem. Soc.*, 2019, **141**, 9623–9628.

357 X. J. Zhao, P. Pachfule and A. Thomas, *Chem. Soc. Rev.*, 2021, **50**, 6871–6913.

358 D. G. Wang, T. J. Qiu, W. H. Guo, Z. B. Liang, H. Tabassum, D. G. Xia and R. Q. Zou, *Energy Environ. Sci.*, 2021, **14**, 688–728.

359 L. J. Kong, M. Zhong, W. Shuang, Y. H. Xu and X. H. Bu, *Chem. Soc. Rev.*, 2020, **49**, 2378–2407.

360 X. X. Luo, W. H. Li, H. J. Liang, H. X. Zhang, K. D. Du, X. T. Wang, X. F. Liu, J. P. Zhang and X. L. Wu, *Angew. Chem., Int. Ed.*, 2022, **61**, e202117661.

361 M. A. Khayum, M. Ghosh, V. Vijayakumar, A. Halder, M. Nurhuda, S. Kumar, M. Addicoat, S. Kurungot and R. Banerjee, *Chem. Sci.*, 2019, **10**, 8889–8894.

362 B. J. Hopkins, C. N. Chervin, J. W. Long, D. R. Rolison and J. F. Parker, *ACS Energy Lett.*, 2020, **5**, 3405–3408.

363 K. W. Leong, Y. F. Wang, M. Ni, W. D. Pan, S. J. Luo and D. Y. C. Leung, *Renewable Sustainable Energy Rev.*, 2022, **154**, 111771.

364 L. T. Ma, S. M. Chen, Z. X. Pei, Y. Huang, G. J. Liang, F. N. Mo, Q. Yang, J. Su, Y. H. Gao, J. A. Zapien and C. Y. Zhi, *ACS Nano*, 2018, **12**, 1949–1958.

365 B. Q. Li, S. Y. Zhang, B. Wang, Z. J. Xia, C. Tang and Q. Zhang, *Energy Environ. Sci.*, 2018, **11**, 1723–1729.

366 W. J. Zang, A. Sumboja, Y. Y. Ma, H. Zhang, Y. Wu, S. S. Wu, H. J. Wu, Z. L. Liu, C. Guan, J. Wang and S. J. Pennycook, *ACS Catal.*, 2018, **8**, 8961–8969.

367 Y. Y. Guo, P. F. Yuan, J. N. Zhang, Y. F. Hu, I. S. Amiinu, X. Wang, J. G. Zhou, H. C. Xia, Z. B. Song, Q. Xu and S. C. Mu, *ACS Nano*, 2018, **12**, 1894–1901.

368 C. Guan, A. Sumboja, H. J. Wu, W. N. Ren, X. M. Liu, H. Zhang, Z. L. Liu, C. W. Cheng, S. J. Pennycook and J. Wang, *Adv. Mater.*, 2017, **29**, 1704117.

369 Y. Y. Guo, P. F. Yuan, J. A. Zhang, H. C. Xia, F. Y. Cheng, M. F. Zhou, J. Li, Y. Y. Qiao, S. C. Mu and Q. Xu, *Adv. Funct. Mater.*, 2018, **28**, 1805641.

370 D. X. Ji, L. Fan, L. L. Li, S. J. Peng, D. S. Yu, J. N. Song, S. Ramakrishna and S. J. Guo, *Adv. Mater.*, 2019, **31**, 1808267.

371 X. F. Lu, Y. Chen, S. B. Wang, S. Y. Gao and X. W. Lou, *Adv. Mater.*, 2019, **31**, 1902339.

372 C. Tang, B. Wang, H. F. Wang and Q. Zhang, *Adv. Mater.*, 2017, **29**, 1703185.

373 B. Q. Li, C. X. Zhao, S. M. Chen, J. N. Liu, X. Chen, L. Song and Q. Zhang, *Adv. Mater.*, 2019, **31**, 1900592.

374 Y. B. Li, C. Zhong, J. Liu, X. Q. Zeng, S. X. Qu, X. Han, Y. P. Deng, W. B. Hu and J. Lu, *Adv. Mater.*, 2018, **30**, 1703657.

375 C. X. Zhao, J. N. Liu, B. Q. Li, D. Ren, X. Chen, J. Yu and Q. Zhang, *Adv. Funct. Mater.*, 2020, **30**, 2003619.

376 C. X. Zhao, J. N. Liu, J. Wang, D. Ren, B. Q. Li and Q. Zhang, *Chem. Soc. Rev.*, 2021, **50**, 7745–7778.

377 D. H. Deng, K. S. Novoselov, Q. Fu, N. F. Zheng, Z. Q. Tian and X. H. Bao, *Nat. Nanotechnol.*, 2016, **11**, 218–230.

378 L. Tang, M. H. Xia, S. Y. Cao, X. Bo, S. B. Zhang, Y. L. Zhang, X. Liu, L. Z. Zhang, L. Yu and D. H. Deng, *Nano Energy*, 2022, **101**, 107562.

379 Z. W. Seh, J. Kibsgaard, C. F. Dickens, I. B. Chorkendorff, J. K. Norskov and T. F. Jaramillo, *Science*, 2017, **355**, eaad4998.

380 J. Y. Chen, H. Li, C. Fan, Q. W. Meng, Y. W. Tang, X. Y. Qiu, G. T. Fu and T. Y. Ma, *Adv. Mater.*, 2020, **32**, 2003134.

381 C. H. Zhou, X. Chen, S. Liu, Y. Han, H. B. Meng, Q. Y. Jiang, S. M. Zhao, F. Wei, J. Sun, T. Tan and R. F. Zhang, *J. Am. Chem. Soc.*, 2022, **144**, 2694–2704.

382 Y. S. Zhao, J. W. Wan, H. Y. Yao, L. J. Zhang, K. F. Lin, L. Wang, N. L. Yang, D. B. Liu, L. Song, J. Zhu, L. Gu, L. Liu, H. J. Zhao, Y. L. Li and D. Wang, *Nat. Chem.*, 2018, **10**, 924–931.

383 C. G. Hu, R. Paul, Q. B. Dai and L. M. Dai, *Chem. Soc. Rev.*, 2021, **50**, 11785.

384 Y. Jiang, Y. P. Deng, R. L. Liang, J. Fu, R. Gao, D. Luo, Z. Y. Bai, Y. F. Hu, A. P. Yu and Z. W. Chen, *Nat. Commun.*, 2020, **11**, 5858.

385 Y. Jiang, Y. P. Deng, R. L. Liang, N. Chen, G. King, A. P. Yu and Z. W. Chen, *J. Am. Chem. Soc.*, 2022, **144**, 4783–4791.

386 J. T. Zhang, Z. H. Zhao, Z. H. Xia and L. M. Dai, *Nat. Nanotechnol.*, 2015, **10**, 444–452.

387 J. Yin, Y. X. Li, F. Lv, Q. H. Fan, Y. Q. Zhao, Q. L. Zhang, W. Wang, F. Y. Cheng, P. X. Xi and S. J. Guo, *ACS Nano*, 2017, **11**, 2275–2283.

388 B. Y. Xia, Y. Yan, N. Li, H. B. Wu, X. W. Lou and X. Wang, *Nat. Energy*, 2016, **1**, 15006.

389 Q. C. Wang, Y. J. Ji, Y. P. Lei, Y. B. Wang, Y. D. Wang, Y. Y. Li and S. Y. Wang, *ACS Energy Lett.*, 2018, **3**, 1183.

390 Y. Tong, P. Z. Chen, T. P. Zhou, K. Xu, W. S. Chu, C. Z. Wu and Y. Xie, *Angew. Chem., Int. Ed.*, 2017, **56**, 7121–7125.

391 M. C. Luo, Z. L. Zhao, Y. L. Zhang, Y. J. Sun, Y. Xing, F. Lv, Y. Yang, X. Zhang, S. Hwang, Y. N. Qin, J. Y. Ma, F. Lin, D. Su, G. Lu and S. J. Guo, *Nature*, 2019, **574**, 81.

392 X. Liu, L. Wang, P. Yu, C. G. Tian, F. F. Sun, J. Y. Ma, W. Li and H. G. Fu, *Angew. Chem., Int. Ed.*, 2018, **57**, 16166–16170.

4922 | *Chem. Soc. Rev.*, 2024, **53**, 4877–4925

This journal is © The Royal Society of Chemistry 2024

393 Q. Liu, Y. B. Wang, L. M. Dai and J. N. Yao, *Adv. Mater.*, 2016, **28**, 3000–3006.

394 Y. J. Chen, S. F. Ji, S. Zhao, W. X. Chen, J. C. Dong, W. C. Cheong, R. A. Shen, X. D. Wen, L. R. Zheng, A. I. Rykov, S. C. Cai, H. L. Tang, Z. B. Zhuang, C. Chen, Q. Peng, D. S. Wang and Y. D. Li, *Nat. Commun.*, 2018, **9**, 5422.

395 J. Yin, Y. X. Li, F. Lv, M. Lu, K. Sun, W. Wang, L. Wang, F. Y. Cheng, Y. F. Li, P. X. Xi and S. J. Guo, *Adv. Mater.*, 2017, **29**, 1704681.

396 J. Zhang, Q. X. Zhou, Y. W. Tang, L. Zhang and Y. G. Li, *Chem. Sci.*, 2019, **10**, 8924–8929.

397 H. F. Wang and Q. Xu, *Matter*, 2019, **1**, 565–595.

398 S. S. Ren, X. D. Duan, S. Liang, M. D. Zhang and H. G. Zheng, *J. Mater. Chem. A*, 2020, **8**, 6144–6182.

399 S. S. Li, X. G. Hao, A. Abudula and G. Q. Guan, *J. Mater. Chem. A*, 2019, **7**, 18674–18707.

400 Z. F. Huang, J. J. Song, S. Dou, X. G. Li, J. Wang and X. Wang, *Matter*, 2019, **1**, 1494–1518.

401 G. T. Fu, Y. Wang, Y. W. Tang, K. Zhou, J. B. Goodenough and J. M. Lee, *ACS Mater. Lett.*, 2019, **1**, 123–131.

402 Y. Y. Huang, Y. Q. Wang, C. Tang, J. Wang, Q. Zhang, Y. B. Wang and J. T. Zhang, *Adv. Mater.*, 2019, **31**, 1803800.

403 L. Yan, Z. Y. Xu, W. K. Hu, J. Q. Ning, Y. J. Zhong and Y. Hu, *Nano Energy*, 2021, **82**, 105710.

404 Z. L. Wang, D. Xu, J. J. Xu and X. B. Zhang, *Chem. Soc. Rev.*, 2014, **43**, 7746–7786.

405 Z. Z. Liang, N. N. Kong, C. X. Yang, W. Zhang, H. Q. Zheng, H. P. Lin and R. Cao, *Angew. Chem., Int. Ed.*, 2021, **60**, 12759–12764.

406 H. Yang, S. Gao, D. W. Rao and X. H. Yan, *Energy Storage Mater.*, 2022, **46**, 553–562.

407 T. T. Cui, Y. P. Wang, T. Ye, J. Wu, Z. Q. Chen, J. Li, Y. P. Lei, D. S. Wang and Y. D. Li, *Angew. Chem., Int. Ed.*, 2022, **61**, e202115219.

408 Y. J. Li, L. Cui, P. F. Da, K. W. Qiu, W. J. Qin, W. B. Hu, X. W. Du, K. Davey, T. Ling and S. Z. Qiao, *Adv. Mater.*, 2018, **30**, 1804653.

409 G. G. Yang, J. W. Zhu, P. F. Yuan, Y. F. Hu, G. Qu, B. A. Lu, X. Y. Xue, H. B. Yin, W. Z. Cheng, J. Q. Cheng, W. J. Xu, J. Li, J. S. Hu, S. C. Mu and J. N. Zhang, *Nat. Commun.*, 2021, **12**, 1734.

410 H. J. Qiu, P. Du, K. L. Hu, J. J. Gao, H. L. Li, P. Liu, T. Ina, K. Ohara, Y. Ito and M. W. Chen, *Adv. Mater.*, 2019, **31**, 1900843.

411 X. Lei, Q. Y. Tang, Y. P. Zheng, P. Kidkhunthod, X. L. Zhou, B. F. Ji and Y. B. Tang, *Nat. Sustainable*, 2023, **6**, 816–826.

412 D. F. Yan, Y. X. Li, J. Huo, R. Chen, L. M. Dai and S. Y. Wang, *Adv. Mater.*, 2017, **29**, 1606459.

413 C. Xie, D. F. Yan, W. Chen, Y. Q. Zou, R. Chen, S. Q. Zang, Y. Y. Wang, X. D. Yao and S. Y. Wang, *Mater. Today*, 2019, **31**, 47–68.

414 X. C. Yan, Y. Jia and X. D. Yao, *Chem. Soc. Rev.*, 2018, **47**, 7628–7658.

415 H. J. Huang, A. M. Huang, D. Liu, W. T. Han, C. H. Kuo, H. Y. Chen, L. L. Li, H. Pan and S. J. Peng, *Adv. Mater.*, 2023, **35**, 2303109.

416 H. Tian, A. L. Song, P. Zhang, K. A. Sun, J. J. Wang, B. Sun, Q. H. Fan, G. J. Shao, C. Chen, H. Liu, Y. D. Li and G. X. Wang, *Adv. Mater.*, 2023, **35**, 2210714.

417 F. Liu and Z. X. Fan, *Chem. Soc. Rev.*, 2023, **52**, 1723–1772.

418 M. H. Luo, W. P. Sun, B. B. Xu, H. G. Pan and Y. Z. Jiang, *Adv. Energy Mater.*, 2021, **11**, 2002762.

419 Y. Yan, S. Liang, X. Wang, M. Y. Zhang, S. M. Hao, X. Cui, Z. W. Li and Z. Q. Lin, *Proc. Natl. Acad. Sci. U. S. A.*, 2021, **118**, e2110036118.

420 M. Jiao, Q. Zhang, C. Ye, Z. Liu, X. Zhong, J. Wang, C. Li, L. Dai, G. Zhou and H. M. Cheng, *Proc. Natl. Acad. Sci. U. S. A.*, 2022, **119**, e2202202119.

421 M. Jiao, Q. Zhang, C. Ye, R. Gao, L. Dai, G. Zhou and H. M. Cheng, *ACS Nano*, 2022, **16**, 13223–13231.

422 Z. H. Liu, Y. Du, R. H. Yu, M. B. Zheng, R. Hu, J. S. Wu, Y. Y. Xia, Z. C. Zhuang and D. S. Wang, *Angew. Chem., Int. Ed.*, 2023, **62**, e202212653.

423 W. Z. Li, L. K. Cheng, X. Y. Chen, Y. F. Liu, Y. Liu, Q. J. Liu and Y. Huang, *Nano Energy*, 2023, **106**, 108039.

424 J. Yu, B. Q. Li, C. X. Zhao, J. N. Liu and Q. Zhang, *Adv. Mater.*, 2020, **32**, 1908488.

425 C. X. Zhao, J. N. Liu, J. Wang, C. D. Wang, X. Guo, X. Y. Li, X. Chen, L. Song, B. Q. Li and Q. Zhang, *Sci. Adv.*, 2022, **8**, eabn5091.

426 J. Wang, C. X. Zhao, J. N. Liu, Y. W. Song, J. Q. Huang and B. Q. Li, *Nano Energy*, 2022, **104**, 107927.

427 P. Z. Chen, T. P. Zhou, L. L. Xing, K. Xu, Y. Tong, H. Xie, L. D. Zhang, W. S. Yan, W. S. Chu, C. Z. Wu and Y. Xie, *Angew. Chem., Int. Ed.*, 2017, **56**, 610–614.

428 X. N. Li, L. H. Liu, X. Y. Ren, J. J. Gao, Y. Q. Huang and B. Liu, *Sci. Adv.*, 2020, **6**, eabb6833.

429 J. Wang, H. H. Wu, D. F. Gao, S. Miao, G. X. Wang and X. H. Bao, *Nano Energy*, 2015, **13**, 387–396.

430 Y. L. Zhao, L. Xu, L. Q. Mai, C. H. Han, Q. Y. An, X. Xu, X. Liu and Q. J. Zhang, *Proc. Natl. Acad. Sci. U. S. A.*, 2012, **109**, 19569–19574.

431 R. Cepitis, N. Kongi, J. Rossmeisl and V. Ivanistsev, *ACS Energy Lett.*, 2023, **8**, 1330–1335.

432 Q. Liu, L. Wang and H. G. Fu, *J. Mater. Chem. A*, 2023, **11**, 4400–4427.

433 P. Zhang, K. Chen, J. Y. Li, M. M. Wang, M. Li, Y. Q. Liu and Y. Pan, *Adv. Mater.*, 2023, **35**, 2303243.

434 Y. Gao, B. Z. Liu and D. S. Wang, *Adv. Mater.*, 2023, **35**, 2209654.

435 Z. J. Li, S. Q. Ji, C. Wang, H. X. Liu, L. P. Leng, L. Du, J. C. Gao, M. Qiao, J. H. Horton and Y. Wang, *Adv. Mater.*, 2023, **35**, 2300905.

436 B. Chen, X. W. Zhong, G. M. Zhou, N. Q. Zhao and H. M. Cheng, *Adv. Mater.*, 2022, **34**, 2105812.

437 G. Yasin, S. Ali, S. Ibraheem, A. Kumar, M. Tabish, M. A. Mushtaq, S. Ajmal, M. Arif, M. A. Khan, A. Saad, L. Qiao and W. Zhao, *ACS Catal.*, 2023, **13**, 2313–2325.

438 B. Y. Lu, B. Chen, D. S. Wang, C. Li, R. H. Gao, Y. Q. Liu, R. Mao, J. L. Yang and G. M. Zhou, *Proc. Natl. Acad. Sci. U. S. A.*, 2023, **120**, e2216933120.

This journal is © The Royal Society of Chemistry 2024

Chem. Soc. Rev., 2024, **53**, 4877–4925 | **4923**

439 R. C. Iwata, L. N. Zhang, K. L. Wilke, S. Gong, M. F. He, B. M. Gallant and E. N. Wang, *Joule*, 2021, **5**, 887–900.

440 L. Tang, L. Yu, C. Ma, Y. Song, Y. C. Tu, Y. L. Zhang, X. Bo and D. H. Deng, *J. Mater. Chem. A*, 2022, **10**, 6242–6250.

441 L. K. Gao, X. Cui, C. D. Sewell, J. Li and Z. Q. Lin, *Chem. Soc. Rev.*, 2021, **50**, 8428–8469.

442 L. K. Gao, X. Cui, Z. W. Wang, C. D. Sewell, Z. L. Li, S. Liang, M. Y. Zhang, J. Li, Y. J. Hu and Z. Q. Lin, *Proc. Natl. Acad. Sci. U. S. A.*, 2021, **118**, e2023421118.

443 T. Wang, Y. He, Y. J. Liu, F. J. Guo, X. F. Li, H. B. A. Chen, H. M. Li and Z. Q. Lin, *Nano Energy*, 2021, **79**, 105487.

444 J. T. Fan, M. Chen, Z. L. Zhao, Z. Zhang, S. Y. Ye, S. Y. Xu, H. J. Wang and H. Li, *Nat. Energy*, 2021, **6**, 475–486.

445 W. D. Xue, Q. X. Zhou, X. Cui, J. W. Zhang, S. J. Zuo, F. Mo, J. W. Jiang, X. Y. Zhu and Z. Q. Lin, *Angew. Chem., Int. Ed.*, 2023, **62**, e2023075.

446 R. Ma, X. Cui, X. X. Xu, Y. L. Wang, G. Q. Xiang, L. K. Gao, Z. Q. Lin and Y. K. Yang, *Nano Energy*, 2023, **108**, 108179.

447 B. F. Ji, J. L. Gou, Y. P. Zheng, X. H. Pu, Y. H. Wang, P. Kidkhunthod and Y. B. Tang, *Adv. Mater.*, 2023, **35**, 2300381.

448 B. F. Ji, J. L. Gou, Y. P. Zheng, X. L. Zhou, P. Kidkhunthod, Y. H. Wang, Q. Y. Tang and Y. B. Tang, *Adv. Mater.*, 2022, **34**, 2202714.

449 T. Meng, P. P. Sun, F. Yang, J. Zhu, B. G. Mao, L. R. Zheng and M. H. Cao, *Proc. Natl. Acad. Sci. U. S. A.*, 2022, **119**, 2214089119.

450 Z. J. Li, S. Q. Ji, C. Xu, L. P. Leng, H. X. Liu, J. H. Horton, L. Du, J. C. Gao, C. He, X. Y. Qi, Q. Xu and J. F. Zhu, *Adv. Mater.*, 2023, **35**, 2209644.

451 W. J. Lu, C. K. Zhang, H. M. Zhang and X. F. Li, *ACS Energy Lett.*, 2021, **6**, 2765–2785.

452 C. Y. Yang, J. L. Xia, C. Y. Cui, T. P. Pollard, J. Vatamanu, A. Faraone, J. A. Dura, M. Tyagi, A. Kattan, E. Thimsen, J. J. Xu, W. T. Song, E. Y. Hu, X. Ji, S. Y. Hou, X. Y. Zhang, M. S. Ding, S. Hwang, D. Su, Y. Ren, X. Q. Yang, H. Wang, O. Borodin and C. S. Wang, *Nat. Sustain.*, 2023, **6**, 325–335.

453 Y. X. Zeng, P. X. Sun, Z. H. Pei, Q. Jin, X. T. Zhang, L. Yu and X. W. Lou, *Adv. Mater.*, 2022, **34**, 2200342.

454 Y. H. Zou, X. Z. Yang, L. Shen, Y. W. Su, Z. Y. Chen, X. Gao, J. Zhou and J. Y. Sun, *Energy Environ. Sci.*, 2022, **15**, 5017–5038.

455 J. F. Parker, J. S. Ko, D. R. Rolison and J. W. Long, *Joule*, 2018, **2**, 2519–2527.

456 X. W. Zhong, Y. F. Shao, B. Chen, C. Li, J. Z. Sheng, X. Xiao, B. M. Xu, J. Li, H. M. Cheng and G. M. Zhou, *Adv. Mater.*, 2023, **35**, 2301952.

457 J. S. Lee, S. T. Kim, R. Cao, N. S. Choi, M. Liu, K. T. Lee and J. Cho, *Adv. Energy Mater.*, 2011, **1**, 34–50.

458 D. U. Lee, J. Y. Choi, K. Feng, H. W. Park and Z. W. Chen, *Adv. Energy Mater.*, 2014, **4**, 1301389.

459 T. Zhang, N. Imanishi, Y. Shimonishi, A. Hirano, Y. Takeda, O. Yamamoto and N. Sammes, *Chem. Commun.*, 2010, **46**, 1661–1663.

460 L. J. Li, Y. Z. Fu and A. Manthiram, *Electrochem. Commun.*, 2014, **47**, 67–70.

461 L. J. Li and A. Manthiram, *Adv. Energy Mater.*, 2016, **6**, 1502054.

462 L. J. Li, S. H. Chai, S. Dai and A. Manthiram, *Energy Environ. Sci.*, 2014, **7**, 2630–2636.

463 J. X. Li, K. Zhang, B. J. Wang and H. S. Peng, *Angew. Chem., Int. Ed.*, 2022, **61**, e202213026.

464 J. Q. Lv, S. C. Abbas, Y. Y. Huang, Q. Liu, M. X. Wu, Y. B. Wang and L. M. Dai, *Nano Energy*, 2018, **43**, 130–137.

465 X. R. Liu, Y. F. Yuan, J. Liu, B. Liu, X. Chen, J. Ding, X. P. Han, Y. D. Deng, C. Zhong and W. B. Hu, *Nat. Commun.*, 2019, **10**, 4767.

466 D. F. Du, S. Zhao, Z. Zhu, F. J. Li and J. Chen, *Angew. Chem., Int. Ed.*, 2020, **59**, 18140–18144.

467 W. X. Shang, W. T. Yu, P. Tan, B. Chen, Z. Wu, H. R. Xu and M. Ni, *J. Mater. Chem. A*, 2019, **7**, 15564–15574.

468 X. W. Wang, F. X. Wang, L. Y. Wang, M. X. Li, Y. F. Wang, B. W. Chen, Y. S. Zhu, L. J. Fu, L. S. Zha, L. X. Zhang, Y. P. Wu and W. Huang, *Adv. Mater.*, 2016, **28**, 4904–4911.

469 L. T. Ma, S. M. Chen, Z. X. Pei, H. F. Li, Z. F. Wang, Z. X. Liu, Z. J. Tang, J. A. Zapien and C. Y. Zhi, *ACS Nano*, 2018, **12**, 8597–8605.

470 D. U. Lee, J. Fu, M. G. Park, H. Liu, A. G. Kashkooli and Z. W. Chen, *Nano Lett.*, 2016, **16**, 1794–1802.

471 C. C. Chang, Y. C. Lee, H. J. Liao, Y. T. Kao, J. Y. An and D. Y. Wang, *ACS Sustainable Chem. Eng.*, 2019, **7**, 2860–2866.

472 B. Li, X. M. Ge, F. W. T. Goh, T. S. A. Hor, D. S. Geng, G. J. Du, Z. L. Liu, J. Zhang, X. G. Liu and Y. Zong, *Nanoscale*, 2015, **7**, 1830–1838.

473 P. Tan, B. Chen, H. R. Xu, W. Z. Cai, W. He and M. Ni, *Electrochim. Acta*, 2018, **283**, 1028–1036.

474 P. Tan, B. Chen, H. R. Xu, W. Z. Cai, W. He and M. Ni, *Appl. Catal., B*, 2019, **241**, 104–112.

475 K. L. Wang, P. C. Pei, Z. Ma, H. C. Chen, H. C. Xu, D. F. Chen and X. Z. Wang, *J. Mater. Chem. A*, 2015, **3**, 22648–22655.

476 J. F. Parker, E. S. Nelson, M. D. Wattendorf, C. N. Chervin, J. W. Long and D. R. Rolison, *ACS Appl. Mater. Interfaces*, 2014, **6**, 19471–19476.

477 X. C. Chen, Z. Zhou, H. E. Karahan, Q. Shao, L. Wei and Y. Chen, *Small*, 2018, **14**, 1801929.

478 J. X. Zheng, D. C. Bock, T. Tang, Q. Zhao, J. F. Yin, K. R. Tallman, G. Wheeler, X. T. Liu, Y. Deng, S. Jin, A. C. Marschilok, E. S. Takeuchi, K. J. Takeuchi and L. A. Archer, *Nat. Energy*, 2021, **6**, 398.

479 J. N. Hao, X. L. Li, X. H. Zeng, D. Li, J. F. Mao and Z. P. Guo, *Energy Environ. Sci.*, 2020, **13**, 3917–3949.

480 L. An, Z. Y. Zhang, J. R. Feng, F. Lv, Y. X. Li, R. Wang, M. Lu, R. B. Gupta, P. X. Xi and S. Zhang, *J. Am. Chem. Soc.*, 2018, **140**, 17624–17631.

481 Y. F. Cui, Y. H. Zhu, J. Y. Du, Y. L. Zhang, K. Li, W. Q. Liu, G. Huang and X. B. Zhang, *Joule*, 2022, **6**, 1617–1631.

482 M. L. Jiao, L. X. Dai, H. R. Ren, M. T. Zhang, X. Xiao, B. R. Wang, J. L. Yang, B. L. Liu, G. M. Zhou and H. M. Cheng, *Angew. Chem., Int. Ed.*, 2023, **62**, e202301114.

483 J. Park, M. Park, G. Nam, J. S. Lee and J. Cho, *Adv. Mater.*, 2015, **27**, 1396.

484 S. S. Shinde, J. Y. Jung, N. K. Wagh, C. H. Lee, D. H. Kim, S. H. Kim, S. U. Lee and J. H. Lee, *Nat. Energy*, 2021, **6**, 592–604.

4924 | *Chem. Soc. Rev.*, 2024, **53**, 4877–4925

This journal is © The Royal Society of Chemistry 2024

485 J. Yin, Y. Z. Wang, Y. P. Zhu, J. J. Jin, C. L. Chen, Y. Y. Yuan, Z. Bayhan, N. Salah, N. A. Alhebshi, W. L. Zhang, U. Schwingenschlogl and H. N. Alshareef, *Nano Energy*, 2022, **99**, 107331.

486 P. Xiong, Y. Zhang, J. R. Zhang, S. Ha Baek, L. X. Zeng, Y. Yao and H. S. Park, *Energychem*, 2022, **4**, 100076.

487 S. X. Qu, B. Liu, X. Y. Fan, X. R. Liu, J. Liu, J. Ding, X. P. Han, Y. D. Deng, W. B. Hu and C. Zhong, *ChemistrySelect*, 2020, **5**, 8305–8310.

488 L. Y. Li, Y. C. A. Tsang, D. W. Xiao, G. Y. Zhu, C. Y. Zhi and Q. Chen, *Nat. Commun.*, 2022, **13**, 2870.

489 D. Yang, J. S. Li, C. P. Liu, W. Xing and J. B. Zhu, *J. Energy Chem.*, 2023, **82**, 122–138.

490 W. X. Shang, W. T. Yu, Y. F. Liu, R. X. Li, Y. W. Dai, C. Cheng, P. Tan and M. Ni, *Energy Storage Mater.*, 2020, **31**, 44–57.

491 L. P. Wang, N. W. Li, T. S. Wang, Y. X. Yin, Y. G. Guo and C. R. Wang, *Electrochim. Acta*, 2017, **244**, 172–177.

492 X. X. Yang, X. C. Zheng, H. X. Li, B. C. Luo, Y. K. He, Y. Yao, H. H. Zhou, Z. H. Yan, Y. F. Kuang and Z. Y. Huang, *Adv. Funct. Mater.*, 2022, **32**, 2200397.

493 W. Sun, M. M. Ma, M. G. Zhu, K. L. Xu, T. Xu, Y. C. Zhu and Y. T. Qian, *Small*, 2022, **18**, 2106604.

494 P. Thakur, K. Alam, A. Roy, C. Downing, V. Nicolosi, P. Sen and T. N. Narayanan, *ACS Appl. Mater. Interfaces*, 2021, **13**, 33112–33122.

495 D. J. Dong, T. R. Wang, Y. Sun, J. Fan and Y. C. Lu, *Nat. Sustain.*, 2023, **6**, 1474–1484.

496 Y. Yamada, J. H. Wang, S. Ko, E. Watanabe and A. Yamada, *Nat. Energy*, 2019, **4**, 269–280.

497 N. K. Wagh, D. H. Kim, S. H. Kim, S. S. Shinde and J. H. Lee, *ACS Nano*, 2021, **15**, 14683–14696.

498 W. Sun, V. Küpers, F. Wang, P. Bieker and M. Winter, *Angew. Chem., Int. Ed.*, 2022, **61**, e202207353.

499 C. Wang, Z. X. Pei, Q. Q. Meng, C. M. Zhang, X. Sui, Z. W. Yuan, S. J. Wang and Y. Chen, *Angew. Chem., Int. Ed.*, 2021, **60**, 990–997.

500 Y. A. Zhang, D. S. Wu, F. L. Huang, Y. B. Cai, Y. G. Li, H. Z. Ke, P. F. Lv and Q. F. Wei, *Adv. Funct. Mater.*, 2022, **32**, 2203204.

501 C. Y. Chen, K. Matsumoto, K. Kubota, R. Hagiwara and Q. Xu, *Adv. Energy Mater.*, 2019, **9**, 1900196.

502 W. Sun, F. Wang, B. Zhang, M. Y. Zhang, V. Küpers, X. Ji, C. Theile, P. Bieker, K. Xu, C. S. Wang and M. Winter, *Science*, 2021, **371**, 46–51.

503 L. S. Cao, D. Li, T. Pollard, T. Deng, B. Zhang, C. Y. Yang, L. Chen, J. Vatamanu, E. Y. Hu, M. J. Hourwitz, L. Ma, M. Ding, Q. Li, S. Y. Hou, K. Gaskell, J. T. Fourkas, X. Q. Yang, K. Xu, O. Borodin and C. S. Wang, *Nat. Nanotechnol.*, 2021, **16**, 902–910.

504 X. P. Han, X. Y. Wu, C. Zhong, Y. D. Deng, N. Q. Zhao and W. B. Hu, *Nano Energy*, 2017, **31**, 541–550.

505 X. Zhong, Z. Zheng, J. Xu, X. Xiao, C. Sun, M. Zhang, J. Ma, B. Xu, K. Yu, X. Zhang, H. M. Cheng and G. Zhou, *Adv. Mater.*, 2023, **35**, 2209980.

506 M. Jiao, L. Dai, H. R. Ren, M. Zhang, X. Xiao, B. Wang, J. Yang, B. Liu, G. Zhou and H. M. Cheng, *Angew. Chem., Int. Ed.*, 2023, **62**, e202301114.

507 X. Y. Fan, H. Z. Wang, X. R. Liu, J. Liu, N. Q. Zhao, C. Zhong, W. B. Hu and J. Lu, *Adv. Mater.*, 2023, **35**, 2209290.

508 Y. Huang, M. Zhong, F. K. Shi, X. Y. Liu, Z. J. Tang, Y. K. Wang, Y. Huang, H. Q. Hou, X. M. Xie and C. Y. Zhi, *Angew. Chem., Int. Ed.*, 2017, **56**, 9141–9145.

509 M. Wang, N. N. Xu, J. Fu, Y. Y. Liu and J. L. Qiao, *J. Mater. Chem. A*, 2019, **7**, 11257–11264.

510 C. Lin, S. S. Shinde, X. P. Li, D. H. Kim, N. W. Li, Y. Sun, X. K. Song, H. J. Zhang, C. H. Lee, S. U. Lee and J. H. Lee, *ChemSusChem*, 2018, **11**, 3215–3224.

511 T. N. T. Tran, H. J. Chung and D. G. Ivey, *Electrochim. Acta*, 2019, **327**, 135021.

512 H. F. Li, C. P. Han, Y. Huang, Y. Huang, M. S. Zhu, Z. X. Pei, Q. Xue, Z. F. Wang, Z. X. Liu, Z. J. Tang, Y. K. Wang, F. Y. Kang, B. H. Li and C. Y. Zhi, *Energy Environ. Sci.*, 2018, **11**, 941–951.

513 Z. S. Song, J. Ding, B. Liu, X. R. Liu, X. P. Han, Y. D. Deng, W. B. Hu and C. Zhong, *Adv. Mater.*, 2020, **32**, 1908127.

514 K. Takechi, T. Shiga and T. Asaoka, *Chem. Commun.*, 2011, **47**, 3463–3465.

515 X. Y. Wang, J. F. Xie, M. A. Ghausi, J. Q. Lv, Y. Y. Huang, M. X. Wu, Y. B. Wang and J. N. Yao, *Adv. Mater.*, 2019, **31**, 1807807.

516 Z. P. Zeng, L. Y. Gan, H. B. Yang, X. Z. Su, J. J. Gao, W. Liu, H. Matsumoto, J. Gong, J. M. Zhang, W. Z. Cai, Z. Y. Zhang, Y. B. Yan, B. Liu and P. Chen, *Nat. Commun.*, 2021, **12**, 4088.

517 L. L. Han, X. Y. Peng, H. T. Wang, P. F. Ou, Y. Y. Mi, C. W. Pao, J. G. Zhou, J. Wang, X. J. Liu, W. F. Pong, J. Song, Z. Lin, J. Luo and H. L. L. Xin, *Proc. Natl. Acad. Sci. U. S. A.*, 2022, **119**, e2207326119.

518 W. Wang, Y. Wu, X. Cao, L. Gu and J. Hu, *Adv. Funct. Mater.*, 2020, **30**, 1908965.

519 R. Zhang, S. C. Zhang, Y. Guo, C. Li, J. H. Liu, Z. D. Huang, Y. W. Zhao, Y. Y. Li and C. Y. Zhi, *Energy Environ. Sci.*, 2022, **15**, 3024–3032.

520 Z. L. Li, S. L. Ning, J. C. Xu, J. M. Zhu, Z. X. Yuan, Y. L. Wu, J. Chen, F. Y. Xie, Y. S. Jin, N. Wang, H. Meng and S. H. Sun, *Energy Environ. Sci.*, 2022, **15**, 5300–5312.

521 S. Y. An, Z. P. Liu, J. Bu, J. Lin, Y. Yao, C. Yan, W. Tian and J. Zhang, *Angew. Chem., Int. Ed.*, 2022, **61**, e202116370.

522 Q. Q. Liu, C. F. Xia, C. H. He, W. Guo, Z. P. Wu, Z. Li, Q. Zhao and B. Y. Xia, *Angew. Chem., Int. Ed.*, 2022, **61**, e202210567.

This journal is © The Royal Society of Chemistry 2024

Chem. Soc. Rev., 2024, **53**, 4877–4925 | **4925**